Title
Characterization of Biogenesis of Lysosome-related Organelle Complex 1 in Mouse Brain and in vitro

Author
Lee, Frank Y.

Publication Date
2017

Peer reviewed|Thesis/dissertation

UNIVERSITY OF CALIFORNIA

Los Angeles

Characterization of Biogenesis of Lysosome-related Organelle Complex 1 in Mouse Brain and *in vitro*

A dissertation submitted in partial satisfaction of the

requirements for the degree Doctor of Philosophy

in Human Genetics

by

Frank Lee

2017

ABSTRACT OF THE DISSERTATION

Characterization of Biogenesis of Lysosome-related

Organelles Complex 1 in Mouse brain and *in vitro*

by

Frank Lee

Doctor of Philosophy in Human Genetics

University of California, Los Angeles, 2017

Professor Esteban C Dell'Angelica, Co-Chair

Professor Cristina A Ghiani, Co-Chair

Biogenesis of Lysosome-related Organelles Complex 1 (BLOC-1) is a multimeric protein complex composed of eight subunits and involved in the intracellular trafficking of integral membrane proteins from early endosomes to lysosomes and lysosome-related organelles. The overall goal of this dissertation was to characterize BLOC-1 in the mouse brain and *in vitro*. Previous behavioral and electrophysiological studies of BLOC-1-deficient mice had suggested that BLOC-1 has a physiological function in the brain. The BLOC-1-deficient mouse brain was analyzed at postnatal day (P)1 and the brains of BLOC-1-deficient mice displayed subtle cytoarchitectural abnormalities specific to the hippocampus. Previous *in vitro* studies have shown that BLOC-1-deficient neurons have abnormalities in the development of their neurites. The brains from wild-type and BLOC-1-deficient mice were analyzed at P60, using the Golgi

method. BLOC-1-deficient neurons from some of the hippocampal neurons had defects in their dendritic arborization. Two of the BLOC-1 subunits, dysbindin and pallidin, have alternatively spliced variants that are expressed in brain. In addition to these subunit variants, the genomes of humans and other mammals contain an uncharacterized gene encoding a paralog of the cappuccino subunit. Some of the alternative subunits were found to replace the full-length form and form a stable complex with the other BLOC-1 subunits. BLOC-1 is well described to have a physical interaction with another multimeric protein complex, Adaptor Protein (AP)-3. The minimal region within dysbindin to bind AP-3 was delineated and critical residues were identified.

The dissertation of Frank Lee is approved.

Deborah Krakow

Karen Reue

Michael S Levine

Esteban C Dell'Angelica, Committee Co-Chair

Cristina A Ghiani, Committee Co-Chair

University of California, Los Angeles

2017

For Megan and Edith Lee

TABLE OF CONTENTS

LIST OF FIGURES

Chapter 2

Chapter 3

Chapter 4

Chapter 5

Chapter 6

LIST OF TABLES

Chapter 2

LIST OF ABBREVIATIONS

ANOVA: Analysis Of variance

AP-3: Adaptor protein-3

BLAST: Basic local alignment search tool

BLOC-1: Biogenesis of lysosome-related organelles-1

CA: Cornus Ammonis

CH: Cortical hem

DAPI: 4'-6-diamidino-2-phenylinodole

DNE: Dentate neuroepithelium

DPX: Distyrene plasticizer toluene-xylene

GLAST: Glutamate aspartate transporter

GST: Glutathione S-transferase

GWAS: Genome-wide

HNE: Hippocampal neuroepithelium

HPS: Hermansky-Pudlak Syndrome

IHC: Immunohisotochemistry

IPTG: Isopropyl-beta-D-thiogalactopyranoside

LRO: Lysosome-related organelles

ORF: Open reading frame

Pa: Pallid

PBS: Phosphate-buffered saline

PFA: Paraformaldehyde

P: Postnatal day

SDS-PAGE: Ssodium dodecyl sulfate polyacrylamide gel electrophoresis

SNP: Single nucleotide polymorphism

TEV: Tobacco etch virus

WB: Western blot

WT: Wild type

Y2H: Yeast two-hybrid

ACKNOWLEDGMENTS

I would like to thank my two advisors, Cristina Ghiani and Esteban Dell'Angelica for their support both in and out of the lab. Both have taught me so much and have even taken their time to sit down at the bench with me to teach me any laboratory techniques that I needed help with.

I would also like to thank my committee members, Deborah Krakow, Karen Reue, and Michael Levine, for all their advice and and support throughout my graduate career. They have given me invaluable advise that has expanded my project.

I would also like to thank current and former lab members, Marta Starcevic, Veronica Cheli, Imilce Rodriguez-Fernandez, Kelly Chan, Christina Falcone, Achilles Aiken, Linh Linh Mikutowicz, Diana Nguyen, Sonia Zaheer, Olivia Hitchcock, and Collette Kokikian. I would like to especially thank Marta and Veronica for constructing some of the constructs that I have used in the project presented in Chapter 6. I would also like to thank the lab members who have helped me with the data analysis in the project presented in Chapter 2 and 4.

I would like to thank the Genomic Analysis and Interpretation Training program for supporting me and my research.

A special thank you to my wife, Megan Lee, who has been there with me from the very beginning. She has motivated and spurred me on especially when times were hard. This dissertation would not have been possible without you.

VITA

2007-2011	B.S. Physiological Science Cum Laude University of California, Los Angeles
2013-2015	Pre-doctoral training grant UCLA Human Genetics Genomic Analysis Training Program (GATP)
Fall 2013	Teaching Assistant, Introduction to Laboratory & Scientific Methodology Department of Life Sciences Core Education Laboratories University of California, Los Angeles
Spring 2014	Teaching Assistant, Introduction to Laboratory & Scientific Methodology Department of Life Sciences Core Education Laboratories University of California, Los Angeles
2015-2016	Graduate Student Mentor Undergraduate Research Center University of California, Los Angeles
Summer 2016	Amgen Writing Tutor, Amgen Scholars Summer Program Undergraduate Research Center University of California, Los Angeles

SELECTED PRESENTATIONS

Frank Y Lee, Achilles Aiken, Esteban C Dell'Angelica, Cristina A Ghiani. "Evidence for a role of BLOC-1 in mouse brain development". Annual American Society for Neurochemistry (ASN) Meeting. March 14-18, 2015. Atlanta, GA.

Frank Y Lee, Achilles Aiken, Olivia N Hitchcock, Collette Y Kokikian, Robin S Fisher, Giovanni Coppola, Esteban C Dell' Angelica, Cristina A Ghiani. "Evidence for a role of BLOC-1 in mouse brain development". Annual American Society of Cell Biology (ASCB) Meeting. December 3-6, 2016. San Francisco, CA.

CHAPTER 1

INTRODUCTION

BLOC-1

Biogenesis of Lysosome-related Organelles Complex 1 (BLOC-1) is a multimeric protein complex composed of eight subunits. The first subunits identified as part of this complex were pallidin and muted, followed few years later by cappuccino and dysbindin [1-4]. Mutant mouse models for these four subunits are available and arose from spontaneous mutations [4-7]. The other four subunits of BLOC-1 were identified by mass spectrometry of the purified complex [8]. It has been proposed that BLOC-1 has a role in the biogenesis of lysosome-related organelles (LROs) based on the presence of abnormal LROs, such as melanosomes and platelet dense granules in the pallid and muted mutant mice [1,2]. LROs are cell-type specific, membrane-bound compartments, which share common characteristics with lysosomes such as low lumenal pH and presence of lysosome-associated membrane proteins (reviewed in [9]). Later, BLOC-1 was reported to be involved in the intracellular trafficking of integral membrane proteins from early endosomes to lysosomes and LROs in primary melanocytes [10], immortalized melanocytes [11], and fibroblasts [10,12], but the exact mechanism was and is still largely unknown. More recently, because BLOC-1 was shown to form a flexible linear chain with a substantial bend [13], and localize to tubular endosomes [10], it was investigated whether BLOC-1 could act as molecular scaffold for the formation of tubules. It was found that BLOC-1 plays a role in the formation of recycling endosomes from sorting endosomes by interacting with the kinesin KIF13A and stabilizing the interaction between KIF13A and a phospholipid binding protein, Annexin A2 [14].

Hermansky-Pudlak Syndrome

In humans, mutations in some BLOC-1 subunits are associated with Hermansky-Pudlak syndrome (HPS), a rare autosomal recessive disorder [7,15-17], which was first characterized by two Czech physicians in 1959 [18]. Two patients were characterized to have seemingly unrelated symptoms of oculocutaneous albinism, prolong bleeding and lung abnormalities [18]. These symptoms were later attributed to defective LROs, i.e. melanosomes, and platelet-dense granules (reviewed in [19]). Since the first description of HPS, nine other types of HPS have been reported (reviewed in [20]). Three of which, HPS types, HPS-7, HPS-8, and HPS-9, have mutations in the BLOC-1 subunits, dysbindin [7,17], BLOS3 [15], and pallidin [16], respectively. The other HPS types were described to have mutations in other protein complexes also involved in the biogenesis of LROs. Analysis of the HPS affected individuals and mutant mice, with HPS-like phenotypes led to the identification of four complexes (AP-3, BLOC-1, BLOC-2, and BLOC-3), all of which are involved in the biogenesis of LROs (reviewed in [21]).

BLOC-1 in Brain

The gene encoding one of the BLOC-1 subunits, *DTNBP1*, has also been associated with another disorder, schizophrenia. Schizophrenia is a psychiatric disorder with a neurodevelopmental origin and is estimated to affect more than 25 million people worldwide, and is predominant in males (reviewed in [22]). The estimated heritability is almost 80%, but no single gene with strong effect size is known. In a systematic linkage-disequilbrium mapping study across a previously linked schizophrenia susceptibility region, single nucleotide polymorphisms (SNPs) within the dysbindin-encoding gene, *DTNBP1*, were found associated

with increased risk of developing schizophrenia in an Irish population [23]. As a result, a number of studies followed to replicate this association in different populations, although with mixed results. According to the Schizophrenia Research Forum website, www.szgene.org, there have been 37 case-control studies and 15 family-based studies, in populations from 22 different countries. Twenty-two studies found a positive association and thirty studies found no association. Even among the studies that found a positive association, the specific markers and haplotypes reported in *DTNBP1* reported to increase risk of developing schizophrenia were found to be inconsistent between studies (reviewed in [24]). Different meta-analyses have been done to deal with the issues of inconsistent use of SNPs [25] and to integrate the genetics studies with functional studies from humans and animal models [26], and the conclusion was that *DTNBP1* was still a top candidate. Additionally, the protein levels of dysbindin were decreased in the postmortem brains of patients with schizophrenia [27,28]. Despite all these initial studies supporting the association between *DTNBP1* and schizophrenia, to date, no genome-wide association study (GWAS) has found genome-wide significance for a *DTNBP1* susceptibility variant. Additionally, no neuropsychiatric phenotypes have been reported in individuals with HPS caused by mutations in *DTNBP1* [17]. It should be noted that *DTNBP1* is one of 25 genes once considered strong candidates for schizophrenia that leading researchers in schizophrenia no longer consider to be so [29].

Although the genetic association between *DTNBP1* and schizophrenia has not panned out, ironically, studies using the sandy mice, which carries an in-frame deletion in the dysbindin-encoding gene, have shown behavioral and electrophysiological abnormalities. Because the mutation in the *Dtnbp1* gene in the sandy mouse arose spontaneously in the DBA/2J mouse

strain [7], initial studies were carried out in this background [30-33]. However, the DBA/2J mouse strain itself is known to have electrophysiological and behavior abnormalities [34], and for this reason, the sandy allele was transferred into the C57BL/6J background [35-38]. In the new background, only certain abnormalities previously observed were still consistently seen in the sandy mice (reviewed in [35]), suggesting a role for dysbindin in brain function. Moreover it is worthy to mention that behavioral and electrophysiological phenotypes described in the sandy mouse were detected in both homozygous and heterozygous mutants. Since the sandy mouse has an in-frame deletion in the gene encoding dysbindin, it was suggested that it may not be a true null, and express an abnormal form of dysbindin, leading to a semi-dominant or dominant allele for some of the behavioral or electrophysiological phenotypes (reviewed in [35]).

In my work, I studied the function of BLOC-1 deficient mouse, namely, the pallid mouse, which carries a non-sense mutation in the *Bloc1s6* gene encoding pallidin [5]. The transcript levels of *Bloc1s6* have been shown to be drastically reduced due to nonsense-mediated mRNA decay, and subsequently the protein it encodes is undetectable by immunoblot [3]. It was later described that the lack of pallidin in the pallid mouse leads to destabilization of BLOC-1 and reduced steady-state protein levels of the other BLOC-1 subunits [1], essentially making the pallid mouse not only a null for pallidin, but also for BLOC-1. Thus, this mouse is a good model to study the effects of lack of BLOC-1.

The behavior and electrophysiological analyses mentioned above were all carried out in adult mice and it was assumed that the abnormalities observed were due to absences of BLOC-1 in an otherwise normally developed brain. Analysis of the protein levels of the BLOC-1 subunits, dysbindin and pallidin, showed that BLOC-1 in the brain is expressed at higher levels during

embryonic and early postnatal periods than in young adulthood, suggesting that BLOC-1 might play a role during brain development [40]. However, it is unclear how BLOC-1 deficiency affects the developing brain. This issue will be discussed in Chapters 2 and 3 of this dissertation. One of the reported functions of BLOC-1 is in the neurites outgrowth. Cultured hippocampal neurons from pallid and sandy mice were shown to have deficits in neurite outgrowth [40,41]. Additionally, RNAi-mediated knockdown of dysbindin in cultured hippocampal neurons from rats affected proper development of their dendritic spines [42]. Since these analyses were done *in vitro*, I set out to determine whether lack of BLOC-1 affects neuronal morphology in the hippocampus, which will be discussed in Chapter 4.

BLOC-1 and alternative subunits

Analysis of some of the BLOC-1 subunits in the brain also led to the discovery that different splice variants of two of the BLOC-1 subunits seemed to be expressed in the brain. One study examined the expression pattern of dysbindin splice variants in human postmortem brains and reported that the splice variants were expressed in different areas of the brain in a isoform-dependent manner [28]. A second study showed that in human brains, only the mRNA of a splice variant of pallidin was expressed [16]. In addition to these variants, the cappuccino subunit was reported to have a paralog encoded by the gene *BCAS4* [4]. Proteomic analysis of the BCAS4 protein showed that this protein interacts with all BLOC-1 subunits except cappuccino [43]. Altogether these findings led me to ask the following question: can these alternative splice variants and paralogs replace the full-length subunits to form a complex like BLOC-1? This question will be addressed in Chapter 5.

BLOC-1 and AP-3

Adaptor Protein (AP)-3 is a heterotetrameric protein complex composed of four subunits, δ, β3, μ3, and σ3 [44]. Various animal models with mutations in AP-3 have helped illuminate the function of this complex (reviewed in [45]). Two mouse models (mocha [46] and pearl [47]) and two patients (HPS-2 [48]), with mutations in the genes encoding AP-3 subunits present with hypopigmentation and prolonged bleeding, suggesting that AP-3 plays a role in the biogenesis of lysosome-related organelles. Analysis of cultured cells from AP-3-deficient mammals have shown major missorting of lysosomal membrane proteins [48]. Because of the similar characteristics of BLOC-1 and AP-3 mutants, it was hypothesized that these two complexes worked in the same machinery that controls protein sorting from endosomes to lysosomes and LROs. In fact, a physical interaction between BLOC-1 and AP-3 has been well characterized in different tissues and cell lines [10,50-53]. However, the critical residues for this interaction are not known and will be addressed in Chapter 6.

REFERENCES

1. Falcón-Pérez JM, Starcevic M, Gautam R, Dell'Angelica EC. BLOC-1, a novel complex containing the pallidin and muted proteins involved in the biogenesis of melanosomes and platelet-dense granules. J Biol Chem. 2002 Aug 2;277(31):28191-9.
2. Moriyama K, Bonifacino JS. Pallidin is a component of a multi-protein complex involved in the biogenesis of lysosome-related organelles. Traffic. 2002 Sep;3(9):666-77.
3. Li W, Zhang Q, Oiso N, Novak EK, Gautam R, O'Brien EP, Tinsley CL, Blake DJ, Spritz RA, Copeland NG, Jenkins NA, Amato D, Roe BA, Starcevic M, Dell'Angelica EC, Elliott RW, Mishra V, Kingsmore SF, Paylor RE, Swank RT. Hermansky-Pudlak syndrome type 7 (HPS-7) results from mutant dysbindin, a member of the biogenesis of lysosome-related organelles complex 1 (BLOC-1). Nat Genet. 2003 Sep;35(1):84-9.
4. Ciciotte SL, Gwynn B, Moriyama K, Huizing M, Gahl WA, Bonifacino JS, Peters LL. Cappuccino, a mouse model of Hermansky-Pudlak syndrome, encodes a novel protein that is part of the pallidin-muted complex (BLOC-1). Blood. 2003 Jun 1;101(11):4402-7.
5. Huang L, Kuo YM, Gitschier J. The pallid gene encodes a novel, syntaxin13-interacting protein involved in platelet storage pool deficiency. Nat Genet. 1999 Nov;23(3):329-32.
6. Zhang Q, Li W, Novak EK, Karim A, Mishra VS, Kingsmore SF, Roe BA, Suzuki T, Swank RT. The gene for the muted (mu) mouse, a model for Hermansky-Pudlak syndrome, defines a novel protein which regulates vesicle trafficking. Hum Mol Genet. 2002 Mar 15;11(6): 697-706.

7. Swank RT, Sweet HO, Davisson MT, Reddington M, Novak EK. Sandy: a new mouse model for platelet storage pool deficiency. Genet Res. 1991 Aug;58(1):51-62.
8. Starcevic M, Dell'Angelica EC. Identification of snapin and three novel proteins (BLOS1, BLOS2, and BLOS3/reduced pigmentation) as subunits of biogenesis of lysosome-related organelles complex-1 (BLOC-1). J Biol Chem. 2004 Jul 2;279(27):28393-401.
9. Dell'Angelica EC, Mullins C, Caplan S, Bonifacino JS. Lysosome-related organelles. FASEB J. 2000 Jul;14(10):1265-78.
10. Di Pietro SM, Falcón-Pérez JM, Tenza D, Setty SR, Marks MS, Raposo G, Dell'Angelica EC. BLOC-1 interacts with BLOC-2 and the AP-3 complex to facilitate protein trafficking on endosomes. Mol Biol Cell. 2006 Sep;17(9):4027-38.
11. Setty SR, Tenza D, Truschel ST, Chou E, Sviderskaya EV, Theos AC, Lamoreux ML, Di Pietro SM, Starcevic M, Bennett DC, Dell'Angelica EC, Raposo G, Marks MS. BLOC-1 is required for cargo-specific sorting from vacuolar early endosomes toward lysosome-related organelles. Mol Biol Cell. 2007 Mar;18(3):768-80.
12. Salazar G, Craige B, Styers ML, Newell-Litwa KA, Doucette MM, Wainer BH, Falcon-Perez JM, Dell'Angelica EC, Peden AA, Werner E, Faundez V. BLOC-1 complex deficiency alters the targeting of adaptor protein complex-3 cargoes. Mol Biol Cell. 2006 Sep;17(9): 4014-26.
13. Lee HH, Nemecek D, Schindler C, Smith WJ, Ghirlando R, Steven AC, Bonifacino JS, Hurley JH. Assembly and architecture of biogenesis of lysosome-related organelles complex-1 (BLOC-1). J Biol Chem. 2012 Feb 17;287(8):5882-90.

14. Delevoye C, Heiligenstein X, Ripoll L, Gilles-Marsens F, Dennis MK, Linares RA, Derman L, Gokhale A, Morel E, Faundez V, Marks MS, Raposo G. BLOC-1 Brings Together the Actin and Microtubule Cytoskeletons to Generate Recycling Endosomes. Curr Biol. 2016 Jan 11;26(1):1-13.
15. Morgan NV, Pasha S, Johnson CA, Ainsworth JR, Eady RA, Dawood B, McKeown C, Trembath RC, Wilde J, Watson SP, Maher ER. A germline mutation in BLOC1S3/reduced pigmentation causes a novel variant of Hermansky-Pudlak syndrome (HPS8). Am J Hum Genet. 2006 Jan;78(1):160-6.
16. Cullinane AR, Curry JA, Carmona-Rivera C, Summers CG, Ciccone C, Cardillo ND, Dorward H, Hess RA, White JG, Adams D, Huizing M, Gahl WA. A BLOC-1 mutation screen reveals that PLDN is mutated in Hermansky-Pudlak Syndrome type 9. Am J Hum Genet. 2011 Jun 10;88(6):778-87.
17. Lowe GC, Sánchez Guiu I, Chapman O, Rivera J, Lordkipanidzé M, Dovlatova N, Wilde J, Watson SP, Morgan NV; UK GAPP collaborative.. Microsatellite markers as a rapid approach for autozygosity mapping in Hermansky-Pudlak syndrome: identification of the second HPS7 mutation in a patient presenting late in life. Thromb Haemost. 2013 Apr; 109(4):766-8.
18. Hermansky F, Pudlak P. Albinism associated with hemorrhagic diathesis and unusual pigmented reticular cells in the bone marrow: report of two cases with histochemical studies. Blood. 1959 Feb;14(2):162-9.
19. Huizing M, Anikster Y, Gahl WA. Hermansky-Pudlak syndrome and related disorders of organelle formation. Traffic. 2000 Nov;1(11):823-35.

20. Schneier AJ, Fulton AB. The hermansky-pudlak syndrome: clinical features and imperatives from an ophthalmic perspective. Semin Ophthalmol. 2013 Sep-Nov;28(5-6):387-91.
21. Di Pietro SM, Dell'Angelica EC. The cell biology of Hermansky-Pudlak syndrome: recent advances. Traffic. 2005 Jul;6(7):525-33.
22. Rapoport JL, Addington AM, Frangou S, Psych MR. The neurodevelopmental model of schizophrenia: update 2005. Mol Psychiatry. 2005 May;10(5):434-49.
23. Straub RE, Jiang Y, MacLean CJ, Ma Y, Webb BT, Myakishev MV, Harris-Kerr C, Wormley B, Sadek H, Kadambi B, Cesare AJ, Gibberman A, Wang X, O'Neill FA, Walsh D, Kendler KS. Genetic variation in the 6p22.3 gene DTNBP1, the human ortholog of the mouse dysbindin gene, is associated with schizophrenia. Am J Hum Genet. 2002 Aug;71(2):337-48. Erratum in: Am J Hum Genet 2002 Oct;72(4):1007.
24. Mutsuddi M, Morris DW, Waggoner SG, Daly MJ, Scolnick EM, Sklar P. Analysis of high-resolution HapMap of DTNBP1 (Dysbindin) suggests no consistency between reported common variant associations and schizophrenia. Am J Hum Genet. 2006 Nov;79(5):903-9.
25. Allen NC, Bagade S, McQueen MB, Ioannidis JP, Kavvoura FK, Khoury MJ, Tanzi RE, Bertram L. Systematic meta-analyses and field synopsis of genetic association studies in schizophrenia: the SzGene database. Nat Genet. 2008 Jul;40(7):827-34.
26. Ayalew M, Le-Niculescu H, Levey DF, Jain N, Changala B, Patel SD, Winiger E, Breier A, Shekhar A, Amdur R, Koller D, Nurnberger JI, Corvin A, Geyer M, Tsuang MT, Salomon D, Schork NJ, Fanous AH, O'Donovan MC, Niculescu AB. Convergent functional genomics of schizophrenia: from comprehensive understanding to genetic risk prediction. Mol Psychiatry. 2012 Sep;17(9):887-905.

27. Talbot K, Eidem WL, Tinsley CL, Benson MA, Thompson EW, Smith RJ, Hahn CG, Siegel SJ, Trojanowski JQ, Gur RE, Blake DJ, Arnold SE. Dysbindin-1 is reduced in intrinsic, glutamatergic terminals of the hippocampal formation in schizophrenia. J Clin Invest. 2004 May;113(9):1353-63.

28. Talbot K, Louneva N, Cohen JW, Kazi H, Blake DJ, Arnold SE. Synaptic dysbindin-1 reductions in schizophrenia occur in an isoform-specific manner indicating their subsynaptic location. PLoS One. 2011 Mar 1;6(3):e16886.

29. Farrell MS, Werge T, Sklar P, Owen MJ, Ophoff RA, O'Donovan MC, Corvin A, Cichon S, Sullivan PF. Evaluating historical candidate genes for schizophrenia. Mol Psychiatry. 2015 May;20(5):555-62.

30. Hattori S, Murotani T, Matsuzaki S, Ishizuka T, Kumamoto N, Takeda M, Tohyama M, Yamatodani A, Kunugi H, Hashimoto R. Behavioral abnormalities and dopamine reductions in sdy mutant mice with a deletion in Dtnbp1, a susceptibility gene for schizophrenia. Biochem Biophys Res Commun. 2008 Aug 22;373(2):298-302.

31. Takao K, Toyama K, Nakanishi K, Hattori S, Takamura H, Takeda M, Miyakawa T, Hashimoto R. Impaired long-term memory retention and working memory in sdy mutant mice with a deletion in Dtnbp1, a susceptibility gene for schizophrenia. Mol Brain. 2008 Oct 22;1:11.

32. Chen XW, Feng YQ, Hao CJ, Guo XL, He X, Zhou ZY, Guo N, Huang HP, Xiong W, Zheng H, Zuo PL, Zhang CX, Li W, Zhou Z. DTNBP1, a schizophrenia susceptibility gene, affects kinetics of transmitter release. J Cell Biol. 2008 Jun 2;181(5):791-801.

33. Jentsch JD, Trantham-Davidson H, Jairl C, Tinsley M, Cannon TD, Lavin A. Dysbindin modulates prefrontal cortical glutamatergic circuits and working memory function in mice. Neuropsychopharmacology. 2009 Nov;34(12):2601-8.
34. Bothe GW, Bolivar VJ, Vedder MJ, Geistfeld JG. Behavioral differences among fourteen inbred mouse strains commonly used as disease models. Comp Med. 2005
35. Aug;55(4):326-34.Cox MM, Tucker AM, Tang J, Talbot K, Richer DC, Yeh L, Arnold SE. Neurobehavioral abnormalities in the dysbindin-1 mutant, sandy, on a C57BL/6J genetic background. Genes Brain Behav. 2009 Jun;8(4):390-7.
36. Ji Y, Yang F, Papaleo F, Wang HX, Gao WJ, Weinberger DR, Lu B. Role of dysbindin in dopamine receptor trafficking and cortical GABA function. Proc Natl Acad Sci U S A. 2009 Nov 17;106(46):19593-8.
37. Papaleo F, Yang F, Garcia S, Chen J, Lu B, Crawley JN, Weinberger DR. Dysbindin-1 modulates prefrontal cortical activity and schizophrenia-like behaviors via dopamine/D2 pathways. Mol Psychiatry. 2012 Jan;17(1):85-98.
38. Karlsgodt KH, Robleto K, Trantham-Davidson H, Jairl C, Cannon TD, Lavin A, Jentsch JD. Reduced dysbindin expression mediates N-methyl-D-aspartate receptor hypofunction and impaired working memory performance. Biol Psychiatry. 2011 Jan 1;69(1):28-34.
39. Ghiani CA, Dell'Angelica EC. Dysbindin-containing complexes and their proposed functions in brain: from zero to (too) many in a decade. ASN Neuro. 2011 May 27;3(2).
40. Ghiani CA, Starcevic M, Rodriguez-Fernandez IA, Nazarian R, Cheli VT, Chan LN, Malvar JS, de Vellis J, Sabatti C, Dell'Angelica EC. The dysbindin-containing complex (BLOC-1) in

brain: developmental regulation, interaction with SNARE proteins and role in neurite outgrowth. Mol Psychiatry. 2010 Feb;15(2):115, 204-15.

41. Ma X, Fei E, Fu C, Ren H, Wang G. Dysbindin-1, a schizophrenia-related protein, facilitates neurite outgrowth by promoting the transcriptional activity of p53. Mol Psychiatry. 2011 Nov;16(11):1105-16.
42. Ito H, Morishita R, Shinoda T, Iwamoto I, Sudo K, Okamoto K, Nagata K. Dysbindin-1, WAVE2 and Abi-1 form a complex that regulates dendritic spine formation. Mol Psychiatry. 2010 Oct;15(10):976-86.
43. Huttlin EL, Ting L, Bruckner RJ, Gebreab F, Gygi MP, Szpyt J, Tam S, Zarraga G, Colby G, Baltier K, Dong R, Guarani V, Vaites LP, Ordureau A, Rad R, Erickson BK, Wühr M, Chick J, Zhai B, Kolippakkam D, Mintseris J, Obar RA, Harris T, Artavanis-Tsakonas S, Sowa ME, De Camilli P, Paulo JA, Harper JW, Gygi SP. The BioPlex Network: A Systematic Exploration of the Human Interactome. Cell. 2015 Jul 16;162(2):425-40.
44. Pevsner J, Volknandt W, Wong BR, Scheller RH. Two rat homologs of clathrin-associated adaptor proteins. Gene. 1994 Sep 2;146(2):279-83.
45. Dell'Angelica EC. AP-3-dependent trafficking and disease: the first decade. Curr Opin Cell Biol. 2009 Aug;21(4):552-9.
46. Kantheti P, Qiao X, Diaz ME, Peden AA, Meyer GE, Carskadon SL, Kapfhamer D, Sufalko D, Robinson MS, Noebels JL, Burmeister M. Mutation in AP-3 delta in the mocha mouse links endosomal transport to storage deficiency in platelets, melanosomes, and synaptic vesicles. Neuron. 1998 Jul;21(1):111-22.

47. Feng L, Seymour AB, Jiang S, To A, Peden AA, Novak EK, Zhen L, Rusiniak ME, Eicher EM, Robinson MS, Gorin MB, Swank RT. The beta3A subunit gene (Ap3b1) of the AP-3 adaptor complex is altered in the mouse hypopigmentation mutant pearl, a model for Hermansky-Pudlak syndrome and night blindness. Hum Mol Genet. 1999 Feb;8(2):323-30.
48. Dell'Angelica EC, Shotelersuk V, Aguilar RC, Gahl WA, Bonifacino JS. Altered trafficking of lysosomal proteins in Hermansky-Pudlak syndrome due to mutations in the beta 3A subunit of the AP-3 adaptor. Mol Cell. 1999 Jan;3(1):11-21.
49. Newell-Litwa K, Seong E, Burmeister M, Faundez V. Neuronal and non-neuronal functions of the AP-3 sorting machinery. J Cell Sci. 2007 Feb 15;120(Pt 4):531-41.
50. Salazar G, Zlatic S, Craige B, Peden AA, Pohl J, Faundez V. Hermansky-Pudlak syndrome protein complexes associate with phosphatidylinositol 4-kinase type II alpha in neuronal and non-neuronal cells. J Biol Chem. 2009 Jan 16;284(3):1790-802.
51. Mead CL, Kuzyk MA, Moradian A, Wilson GM, Holt RA, Morin GB. Cytosolic protein interactions of the schizophrenia susceptibility gene dysbindin. J Neurochem. 2010 Jun; 113(6):1491-503.
52. Taneichi-Kuroda S, Taya S, Hikita T, Fujino Y, Kaibuchi K. Direct interaction of Dysbindin with the AP-3 complex via its mu subunit. Neurochem Int. 2009 Jun;54(7):431-8.
53. Han MH, Hu Z, Chen CY, Chen Y, Gucek M, Li Z, Markey SP. Dysbindin-associated proteome in the p2 synaptosome fraction of mouse brain. J Proteome Res. 2014 Nov 7;13(11):4567-80.

CHAPTER 2

Morphological analysis of BLOC-1-deficient mouse brain

ABSTRACT

Previous behavioral and electrophysiological studies of BLOC-1-deficient mice had suggested that BLOC-1 has a physiological function in the brain. In this chapter, the morphology of the BLOC-1-deficient brain was analyzed in mice at different developmental ages. I have found that at postnatal day 1 the brains of BLOC-1-deficient male, but not females, displayed decreased weight and cytoarchitectural abnormalities specific to the hippocampus.

INTRODUCTION

After the initial studies that linked single nucleotide polymorphisms in *DTNBP1* with schizophrenia, several behavioral and electrophysiological studies were carried out using mouse models to test whether dysbindin has a physiological function in brain. Most studies were done using the BLOC-1-deficient sandy mouse, which carries a mutation in the *Dtnbp1* gene. Electrophysiological analyses conducted in the sandy mice found that dysbindin deficiencies caused both pre- and postsynaptic abnormalities [4-9]. These mice were also reported to have increased dopamine release and over-expression of D2 dopamine receptors at the cell surface [10,11]. Multiple behavioral studies consistently observed that sandy mice have impaired memory [8,9,13]. As mentioned in the previous chapter, dysbindin was found to be part of BLOC-1 in mouse liver [1] and it was later determined that its longest form is part of BLOC-1 in brain [2]. Consistent with this idea, impaired memory was also reported the pallid mice, which carry a mutation in another subunit of BLOC-1 [14]. From the behavior and electrophysiological studies, it is evident that BLOC-1 has a physiological role in brain.

In the previously mentioned studies, it was predominantly assumed that the behavioral and electrophysiological phenotypes observed in the sandy and pallid mice were due to deficiency of BLOC-1 in an otherwise normally developing brain. However, it was also reported that protein expression levels of some of the BLOC-1 subunits (dysbindin and pallidin) in the cerebral cortex, hippocampus, and cerebellum were higher during embryonic and early postnatal periods than in young adulthood, suggesting that

BLOC-1 might play a role during brain development [2]. Hence, to examine the possible role of BLOC-1 during brain development, I have analyzed the gross morphology of the BLOC-1-deficient mouse brain. In particular, I examined the brain wet-weight at various postnatal ages and then the cytohistopathology of two brain regions (cerebral cortex and hippocampus) of relevance to the behavioral defects shown in BLOC-1-deficient mice.

EXPERIMENTAL PROCEDURES

Animals

The BLOC-1-deficient mutant "pallid" mice, B6.Cg-*Bloc1s6*^{pa}/J, and the "wild type" control strain (WT), C57BL/6J, were from our breeding colony maintained at the University of California, Los Angeles (UCLA). Euthanasia prior to tissue dissection was performed in accordance to procedures approved by the UCLA Chancellor's Animal Research Committee.

Brain weight

The whole brains of WT and pallid male mice at three difference ages [postnatal day (P)1, P14, and P45] as well as from P1 pallid females and age-matching WT, were dissected out and rapidly weighted on an analytical balance. A minimum of five animals was used for each age per gender per genotype. For the P1 WT and pallid males and females, the overall body mass was also measured before euthanasia.

Specimen preparation for Nissl Staining

Whole brains of P1 WT and pallid male (5 animals per genotype) and female (5 animals per genotype) mice were rapidly dissected out and fixed overnight in 4% (w/v) paraformaldehyde (PFA) at 4°C. P45 WT and pallid male mice (4 animals per genotype) were anesthetized with isoflurane and transcardially perfused with saline solution (NaCl 0.15 M) followed by phosphate buffered saline containing 4% (w/v) PFA. The brains were rapidly dissected out and post-fixed

overnight in 4% (w/v) PFA at 4°C and then cryoprotected in 15% (w/v) sucrose. Sequential Coronal sections (40 μm) cut on a Lecia cryostat were collected.

Nissl staining

The coronal sections were processed with the following protocol: sections were dehydrated and rehydrated using increasing and decreasing concentration of ethanol (70% (v/v) ethanol for 5 mins; 95% (v/v) ethanol for 5 mins; absolute ethanol for 5 mins; 95% (v/v) ethanol for 5 mins; 70% (v/v) ethanol for 5 mins; 50% (v/v) ethanol for 5 mins). After rinsing in water, sections were incubated with cresyl violet acetate stain [1% (w/v) cresyl violet in acetate buffer] for 5 mins. After rinsing in water three times, sections were dehydrated (70% (v/v) ethanol for 5 mins; 95% (v/v) ethanol for 5 mins) and placed in the differentiation solution [6 drops of glacial acetic acid in 100 mL of 95% (v/v) ethanol] for up to 1 hour, until the structures of interest were clearly defined. After incubation in 95% (v/v) ethanol for 1 min, absolute ethanol for 1 min, and xylene for 5 mins three times, coverslips were then mounted using DPX (distyrene plasticizer toluene-xylene; Sigma) mounting medium.

Imaging/Analysis

Images of Nissl-stained sections were acquired on a Zeiss Axioskop microscope with an Axiocam using the AxioVision software (Zeiss). The cross-sectional area and perimeter of the hippocampus, and the thickness of the cerebral cortex (layers I-VI), both in rostral and caudal sections were measured from the images of the stained sections using the Axiovision software by two independent investigators masked to the genotype and age of the animals. The cell density of

the Cornus Ammonis (CA)1 region was analyzed by measuring the staining intensity of the Nissl-stained sections using the National Institutes of Health Image ImageJ Software (http://rsb.info.nih.gov/ij/) [15]. We determined that staining intensity using the "profile plot analysis" as follow: a grid was over-imposed on each image using the "Grid Setting" ("Area Per Point" set to 16000 pixel^2) as shown in blue in Figure 2.2, and then three identical rectangular boxes were drawn with the following criteria: width of the box was the same as that of one column of the grid, while the height of the box encompassed the cell layer of the hippocampus (magenta box in figure 2.2) about two of the grid squares. A rectangular box was set in the third, fifth, and seventh columns of the grid at fixed distance from the lateral ventricle. The "profile plot analysis" was then performed for each box. This analysis measures the average pixel intensity per row of pixels within the matrix of the rectangular box. Values from the three plots were averaged to produce an average plot per brain section, and 8-12 sections were analyzed per animal. A polynomial curve (order: 6^{th}) was fit to each average plot, the peaks of the average plots per section were aligned to then calculate a single averaged plot per animal. A total of five P1 animals per genotype per gender were analyzed and a total of four P45 animals per genotype were analyzed.

RESULTS

The wet-weight of pallid male brains is less than that of the WT male brains at P1

As a first crude approximation, brain wet-weight was measured to determine if lack of BLOC-1 affects brain development in mice. At P1, the pallid male brains displayed a significant decrease in wet-weight (10%) as compared to WT male brains and the difference was not due to differences in body weight (Fig. 2.1). More importantly, there was no significant difference in the brain wet-weight of female mice at P1. In addition, the brain wet-weight of older (P14 and P45) pallid male mice were not different from age-matching WT (Fig. 2.1). To identify if such differences were due to abnormalities in a specific brain region, individual brain areas (forebrain, hindbrain, and cerebellum) were dissected and weighed. However, I was unable to obtain a clear result. Because of the brain size, the dissection had to be done in PBS, under a stereoscope, and as a result, the samples had differing amounts of PBS, producing a high variability.

Anomalous distribution of the hippocampal cell layer in pallid male mice at P1

Next, the cross-sectional area and perimeter of the hippocampus as well as the thickness of the cerebral cortex (rostral and caudal) were measured in Nissl-stained brain sections to identify any gross morphological differences. No differences were seen in either brain regions between pallid and WT male mice at either P1 or P45 (Table 2.1). However, an anomalous distribution was observed in the CA1 cell layer of P1 pallid males. More in particular, the cell bodies were not as compact as in the WT hippocampus, but appeared dispersed, covering a wider area (Fig. 2.2A-D). This phenotype was less evident in pallid females, in which the distribution

of cell bodies was closer to that of the WT (Fig. 2.2E,F). To quantify cell body dispersion, staining intensity of Nissl-stained sections was measured across the cell layer. The pallid males displayed a signficantly wider cell layer along with a decrease in staining intensity compared to the WT (Fig. 2.3A). Even though the P1 pallid females showed a slightly wider peak, this differences was not as much as the pallid males, and there was no apparent differences in levels of staining intensity compared to the plot of WT cell layer (Fig. 2.3B). Lastly, the cell layer of the P45 WT and pallid males had no differences (Fig. 2.3C). These findings suggest that the hippocampal cytoarchitecture in females is less affected by lack of BLOC-1 compared to males and in the latter, this phenotype is recovered with time.

DISCUSSION

Analysis of the BLOC-1-deficient brains at early postnatal ages showed clear abnormalities in males supporting the hypothesis that BLOC-1 has a function during brain development and, more importantly suggesting that its deficiency has sexual dimorphic effects. At P1, BLOC-1-deficient male brains weighed less than WT male brains and displayed an anomalous cell distribution in CA1. Cell distribution in CA1 appeared to be dispersed and lack compaction. Such phenomenon could be due to the lack of BLOC-1 interfering with cell migration, delayed or slower, and mis-positioning of the neurons or changes in cell number. This question will be further discussed in Chapter 3.

Interestingly, the abnormalities observed in P1 BLOC-1-deficient male mice were less pronounced in the BLOC-1-deficient P1 female mice, suggesting that they are somehow "protected" from the deleterious effects of BLOC-1 deficiency on brain development. It has been well documented that some neurological and developmental neuropsychiatric disorders (Alzheimer's disease, multiple sclerosis, schizophrenia) present sex differences, either in disease prevalence or in the presentation of the symptoms, where they may appear earlier in one gender or with greater severity (reviewed in reference 16). Although the mechanism is not well understood, experimental and clinical evidence suggests that estrogen may have a protective effect on the brain atrophy and dysfunction (reviewed in references 17,18). Thus, it is possible that these similar neuroprotective effects are acting in the BLOC-1-deficient female brain. Lastly, since the abnormalities seen at P1 were absent at later postnatal ages, we could speculate that a

possible compensatory mechanism(s) occurs, and further work is required to identify these underlying compensatory mechanism(s) and or factors.

		Rostral Cerebral Cortex Thickness (μm)	Genotype	Age	Interaction Effect (genotype x age)
P1	WT	2228 ± 92 ; n=5	*F* = 2.02; P=0.177	*F* = 520; P<0.0001	*F* = 0.23; P=0.635
	Pa	2072 ± 81 ; n=5			
P45	WT	4060 ± 72 ; n=4			
	Pa	3983 ± 64 ; n=4			
		Caudal Cerebral Cortex Thickness (μm)			
P1	WT	1849 ± 66 ; n=5	*F* = 0.25; P=0.625	*F* = 298; P<0.0001	*F* = 1.13; P=0.305
	Pa	1815 ± 31; n=5			
P45	WT	2838 ± 89 ; n=4			
	Pa	2933 ± 47 ; n=4			
		Hippocampal Perimeter (μm)			
P1	WT	12401 ± 332 ; n=5	*F* = 0.68; P=0.421	*F* = 699; P<0.0001	*F* = 0.47; P=0.504
	Pa	12034 ± 128 ; n=5			
P45	WT	18643 ± 212 ; n=4			
	Pa	18609 ± 219 ; n=4			
		Hippocampal Area (mm^2)			
P1	WT	7.582 ± 0.53 ; n=5	*F* = 0.07; P=0.788	*F* = 841; P<0.0001	*F* = 3.18; P=0.096
	Pa	8.213 ± 0.14 ; n=5			
P45	WT	20.45 ± 0.53 ; n=4			
	Pa	19.59 ± 0.34 ; n=4			

Table 2.1 No differences in cerebral cortical thickness and hippocampal area between wild-type and pallid brains at postnatal day (P)1 and P45. Nissl-stained wild-type (WT) and pallid (Pa) brain sections were used to measure cerebral cortical thickness (rostral and caudal), hippocampal area and hippocampal perimeter. Measurement values are in their corresponding units as labeled and the errors are the SEM. Statistical significance was assessed using a two-way ANOVA (Analysis of Variance) model.

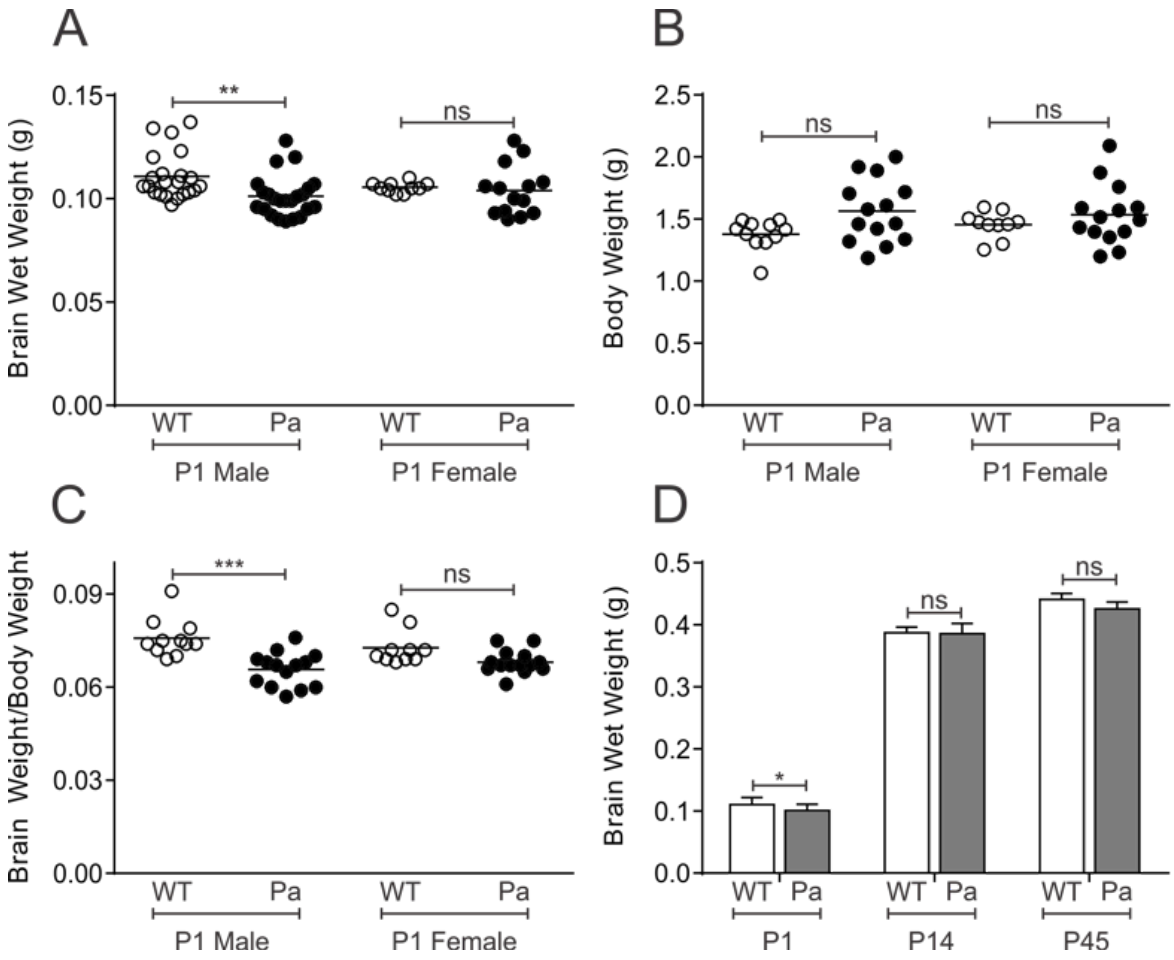

Figure 2.1 Pallid male mice have smaller brains than wild-type mice at postnatal day (P)1. (A) Whole brains of male and female wild-type (WT) and pallid (Pa) mice at P1 were dissected and weighed. Each dot represents the brain wet-weight of one animal and each line represents the mean. (B) Before dissecting the brains from the bodies, the whole body of the P1 mice was weighed. Each dot represents the body weight of one animal and each line represents the mean. (C) The brain wet-weight of each animal was divided by its body weight to calculate the brain to body weight ratio. Each dot represents the brain weight to body weight ratio of one animal and each line represents the mean. (D) Whole-wet brains of male WT and Pa mice were also dissected and measured in older mice. Bars and error bars represent the mean ± SEM of the brain wet-weight at P1 (WT: n=22, Pa: n=23), P14 (WT: n=13, Pa: n=11) and P45 (WT: n=7, Pa: n=6). Statistical significance was assessed using a one-way ANOVA (Analysis of Variance) model followed by Bonferroni's multiple comparison tests. **p<0.01, *p<0.05, ns, not significant.

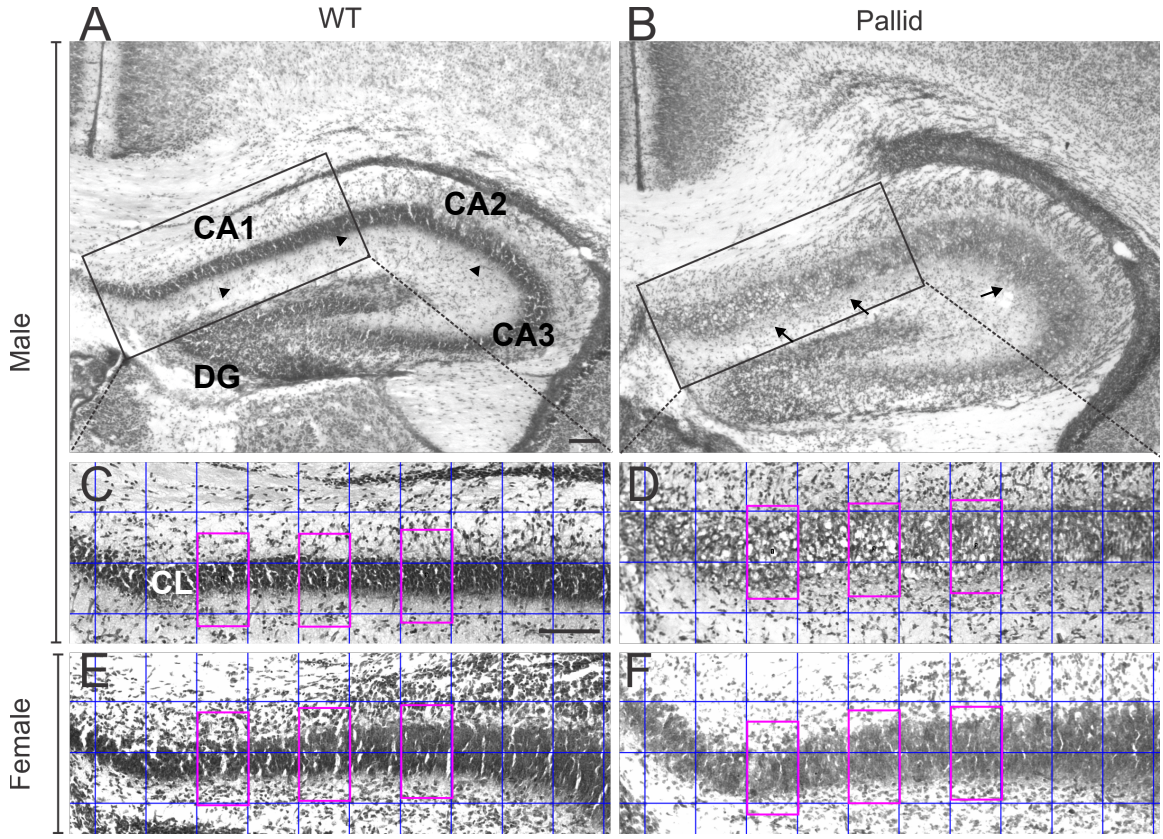

Figure 2.2 Cellular arrangement of the hippocampal cell layer is abnormal in the pallid mice at postnatal day (P)1. Nissl-stained male wild-type (WT) (A) and pallid (B) hippocampi. The hippocampal cell layer in the P1 male pallid mouse appears to have a diffused cellular distribution (arrows) compared to that of P1 male WT mouse (arrowheads), particularly in the cornus ammonis (CA)1 area. DG, dentate gyrus. The black boxes in panels A and B indicate regions shown at higher magnification in panels C and D respectively. CL, cell layer. (E,F) High magnification of the CA1 area in female WT and pallid hippocampi. In panels C-F, blue lines represent the grid and magenta lines represent the rectangular boxes used for the analysis of the CA1 cell layer as described under Experimental Procedures. Scale bar, 100µm.

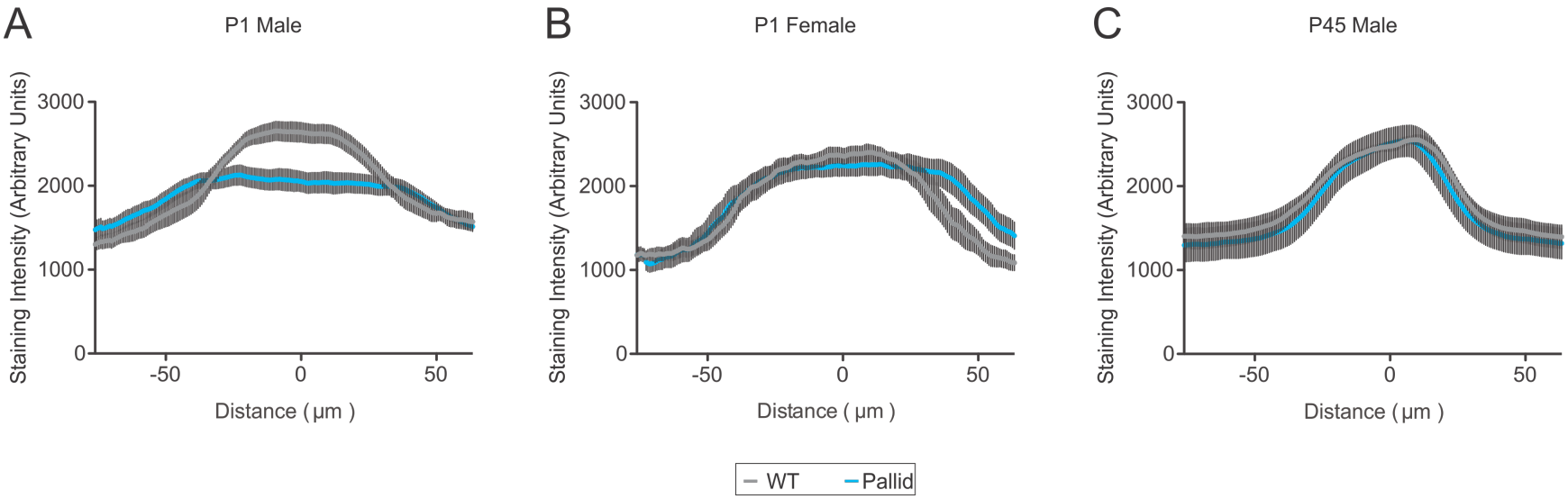

Figure 2.3 Staining intensity plot of the Cornus Ammonis (CA)1 cell layer. The staining intensity of Nissl-stained hippocampal sections was measured in the CA1 area of the hippocampus. Rectangular boxes, as shown in Figure 2.2, were used to perform a profile plot analysis, which measures the average pixel intensity per row of pixels within the matrix of the rectangular box. Three of these measurements were taken from each section and values were averaged. 8-12 sections were analyzed per animal. For each animal, the peaks of the average plots per section were aligned and the values were averaged to obtain a single plot per animal. A total of five P1 animals per genotype per gender were analyzed and a total of four P45 animals per genotype were analyzed. The gray lines represent the mean staining intensity of wild-type (WT) sections, the blue lines represent the mean staining intensity of pallid (Pa) sections, and the black lines represent the SEM.

REFERENCE

1. Li W, Zhang Q, Oiso N, Novak EK, Gautam R, O'Brien EP, Tinsley CL, Blake DJ, Spritz RA, Copeland NG, Jenkins NA, Amato D, Roe BA, Starcevic M, Dell'Angelica EC, Elliott RW, Mishra V, Kingsmore SF, Paylor RE, Swank RT. Hermansky-Pudlak syndrome type 7 (HPS-7) results from mutant dysbindin, a member of the biogenesis of lysosome-related organelles complex 1 (BLOC-1). Nat Genet. 2003 Sep;35(1):84-9.
2. Ghiani CA, Starcevic M, Rodriguez-Fernandez IA, Nazarian R, Cheli VT, Chan LN, Malvar JS, de Vellis J, Sabatti C, Dell'Angelica EC. The dysbindin-containing complex (BLOC-1) in brain: developmental regulation, interaction with SNARE proteins and role in neurite outgrowth. Mol Psychiatry. 2010 Feb;15(2):115, 204-15.
3. Swank RT, Sweet HO, Davisson MT, Reddington M, Novak EK. Sandy: a new mouse model for platelet storage pool deficiency. Genet Res. 1991 Aug;58(1):51-62.
4. Chen XW, Feng YQ, Hao CJ, Guo XL, He X, Zhou ZY, Guo N, Huang HP, Xiong W, Zheng H, Zuo PL, Zhang CX, Li W, Zhou Z. DTNBP1, a schizophrenia susceptibility gene, affects kinetics of transmitter release. J Cell Biol. 2008 Jun 2;181(5):791-801.
5. Jentsch JD, Trantham-Davidson H, Jairl C, Tinsley M, Cannon TD, Lavin A. Dysbindin modulates prefrontal cortical glutamatergic circuits and working memory function in mice. Neuropsychopharmacology. 2009 Nov;34(12):2601-8.
6. Ji Y, Yang F, Papaleo F, Wang HX, Gao WJ, Weinberger DR, Lu B. Role of dysbindin in dopamine receptor trafficking and cortical GABA function. Proc Natl Acad Sci U S A. 2009 Nov 17;106(46):19593-8.

7. Tang TT, Yang F, Chen BS, Lu Y, Ji Y, Roche KW, Lu B. Dysbindin regulates hippocampal LTP by controlling NMDA receptor surface expression. Proc Natl Acad Sci U S A. 2009 Dec 15;106(50):21395-400. doi: 10.1073/pnas.0910499106.
8. Karlsgodt KH, Robleto K, Trantham-Davidson H, Jairl C, Cannon TD, Lavin A, Jentsch JD. Reduced dysbindin expression mediates N-methyl-D-aspartate receptor hypofunction and impaired working memory performance. Biol Psychiatry. 2011 Jan 1;69(1):28-34.
9. Papaleo F, Yang F, Garcia S, Chen J, Lu B, Crawley JN, Weinberger DR. Dysbindin-1 modulates prefrontal cortical activity and schizophrenia-like behaviors via dopamine/D2 pathways. Mol Psychiatry. 2012 Jan;17(1):85-98.
10. Murotani T, Ishizuka T, Hattori S, Hashimoto R, Matsuzaki S, Yamatodani A. High dopamine turnover in the brains of Sandy mice. Neurosci Lett. 2007 Jun 21;421(1):47-51.
11. Iizuka Y, Sei Y, Weinberger DR, Straub RE. Evidence that the BLOC-1 protein dysbindin modulates dopamine D2 receptor internalization and signaling but not D1 internalization. J Neurosci. 2007 Nov 7;27(45):12390-5.
12. Ghiani CA, Dell'Angelica EC. Dysbindin-containing complexes and their proposed functions in brain: from zero to (too) many in a decade. ASN Neuro. 2011 May 27;3(2).
13. Takao K, Toyama K, Nakanishi K, Hattori S, Takamura H, Takeda M, Miyakawa T, Hashimoto R. Impaired long-term memory retention and working memory in sdy mutant mice with a deletion in Dtnbp1, a susceptibility gene for schizophrenia. Mol Brain. 2008 Oct 22;1:11.

14. Spiegel S, Chiu A, James AS, Jentsch JD, Karlsgodt KH. Recognition deficits in mice carrying mutations of genes encoding BLOC-1 subunits pallidin or dysbindin. Genes Brain Behav. 2015 Nov;14(8):618-24.
15. Mullen BR, Khialeeva E, Hoffman DB, Ghiani CA, Carpenter EM. Decreased reelin expression and organophosphate pesticide exposure alters mouse behaviour and brain morphology. ASN Neuro. 2012 Feb 18;5(1):e00106.
16. Cahill L. Why sex matters for neuroscience. Nat Rev Neurosci. 2006 Jun;7(6):477-84.
17. Engler-Chiurazzi EB, Singh M, Simpkins JW. From the 90's to now: A brief historical perspective on more than two decades of estrogen neuroprotection. Brain Res. 2016 Feb 15;1633:96-100.
18. Peri A. Neuroprotective effects of estrogens: the role of cholesterol. J Endocrinol Invest. 2016 Jan;39(1):11-8.

CHAPTER 3

BLOC-1 deficiency hinders radial glial cells in the hippocampus of newborn mice

ABSTRACT

Neural cell maturation is a timely process tightly regulated, which terminates with the cell migrating to its final location and becoming fully differentiated. In this chapter, I investigated whether the atypical cell distribution observed in BLOC-1 deficient CA1 of hippocampus at postnatal day 1 was due to an abnormality in some of the cells and factors involved in migration. The protein levels of GLAST and nestin, which are markers for radial glia, a cell type critically involved in neuronal migration, were greatly reduced in pallid male mice, and fewer fiber tracts could be seen in male pallid CA1. This phenotype was much less severe in age-matching pallid females. In agreement with lack of a well-assembled radial glia scaffold, the expression pattern of immature neuronal markers in pallid CA1 was also in disarray, while the protein levels were unaltered. These results suggest that BLOC-1-deficient immature neurons are mal-positioned due to the defects in the fiber tracts of radial glial cells.

INTRODUCTION

In mouse, hippocampal development begins around embryonic day (E)12.5, when the dorsal telecephalnon gives rise to three areas: the hippocampal neuroepithelium (HNE), dentate neuroepithelium (DNE), and cortical hem (CH). Cajal Retzinus cells are located along the pial side of the HNE, which later develops into the CA1-3 areas. These cells secrete a large glycoprotein, called reelin, which plays a critical role in the regulation of neuronal migration and positioning. At E14.5, radial glial cells appear in the ventricular zone of the HNE, and extend their processes toward CA1, forming the tracts along which pyramidal neurons will migrate to reach their final location. By E17.5, the development of the hippocampus is nearly complete. At this stage, pyramidal neurons born in the ventricular zone migrate along the processes of the radial glia, towards their location in the hippocampal areas. Cajal-Retzinus cells continue to be present and to secret reelin. By birth, most of the CA1 pyramidal neurons have migrated (reviewed in reference 1).

Perinatally, CA1-3 are composed of 6 to 10 rows of neuronal somata. However, this number decreases as hippocampal development progresses and eventually the cell layer has 2 to 3 rows of cells [2]. It has been suggested that this change in thickness is unlikely to be a passive effect. Perinatal X-ray irradiation has been shown to preferential affect radial glia and cause an anomalous distribution of neuronal cell bodies in the hippocampal cell layer, suggesting that these cells also play role in the perinatal maturation and refinement of the cell layers [3]. Another factor that likely plays a pivotal role in this process is reelin. This glycoprotein is involved in the

maintenance of the radial glial scaffold and considered a stop signal for the migratory neurons. In its absence, the hippocampal cell layer has an unusual lamination and is malformed [2].

In the previous chapter, I reported that BLOC-1-deficient mice at postnatal day (P)1 displayed an abnormal distribution of CA1 neurons. One possible explanation for this phenomenon stems from the proposed role of BLOC-1 in membrane biogenesis and secretion [4]. Thus, I hypothesize that BLOC-1 could interfere with the neuronal migration process, pathways, and players during which long processes need to be extended and "go and stop" signaling cues are released into the extracellular space. In line with this hypothesis, I analyzed the expression levels of radial glial markers as well as its morphology in BLOC-1-deficient hippocampi, and the protein levels of the different forms of reelin in comparison with wild-type (WT) mice. In addition, I analyzed the protein levels and expression pattern of several immature neuronal markers in BLOC-1-deficient hippocampi and compared to WT, to rule out that the observed effect could be cause by loss or "gain" of neurons.

EXPERIMENTAL PROCEDURES

Animals

Mouse strains were used maintained as previously described in chapter 2.

Antibodies

Primary antibodies were used at the following concentrations for immunohistochemistry (IHC) or western blot (WB): rabbit anti-α-Internexin (Millipore, Cat.# AB5354) IHC = 1:250, WB = 1:500; rabbit anti-βIII-Tubulin (Covance, Clone: Tuj1) IHC = 1:200, WB = 1:10,000; rabbit anti-doublecortin (Cell Signaling, Cat.# 4604) IHC = 1:300, WB = 1:1000; guinea pig anti-GLAST (Millipore, Cat.# AB1782) IHC = 1:250, WB = 1:1000; mouse anti-GLAST (Millipore, Clone: 8C11.1); Mouse anti-nestin (BD Biosciences, Clone: Rat401) IHC = 1:100, WB = 1:1000; rabbit anti-reelin (Millipore, Clone: 142) WB = 1:1000; mouse anti-β-actin (Sigma, Clone: AC-15) WB = 1:10,000

Immunohistochemistry

The brains of P1 wild-type (WT) and pallid mice were rapidly dissected out, fixed overnight in 4% (w/v) paraformaldehyde at 4°C, and then cryoprotected in 15% (w/v) sucrose. Coronal sections (40 μm) were cut on a Lecia cryostat Leica, collected sequentially. Sections (40 μm) were blocked for 1 h in carrier solution [1% BSA (w/v) and 0.3% (w/v) Triton X-100 in phosphate-buffered saline (PBS)] containing 20% (v/v) normal donkey serum then incubated for 24h or 48h at 4°C with primary antibodies diluted in carrier solution containing 5% (v/v) normal

donkey serum. Following incubation with primary antibodies, tissue sections were washed 3 times for 10 min each with carrier solution, incubated with the appropriate secondary antibodies conjugated to Cy3 (Jackson ImmunoResearch Laboratories) or AlexaFluor 488 (Molecular Probes) diluted in carrier solution, and washed again 3 times for 10 min each in carrier solution. Tissue sections were mounted with Vectashield mounting medium with DAPI (4'-6-diamidino-2-phenylinodole; Vector Laboratories). Immunostained sections were visualized and images taken on a Zeiss Axio Imager 2 microscope equipped with an AxioCam MRm and the ApoTome imaging system (Zeiss) using the Axiovision software.

Immunoblot analysis

Hippocampi from P1 WT and pallid mice were rapidly dissected and frozen. WT and pallid samples were prepared and run in pairs. Hippocampi were homogenized in lysis buffer [50 mM Tris-HCl (pH 7.5), 1% (w/v) Triton X-100, 0.25% (w/v) sodium deoxycholate, 0.1% (w/v) sodium dodecyl sulfate (SDS), 0.15 M NaCl, 1 mM EDTA] containing a protease inhibitor mixture consisting of 1 mM 4-(2-aminoethyl)-benzenesulfonyl fluoride, 10 mg/l leupeptin, 5 mg/l aprotinin and 1 mg/l pepstatin A, as previously reported [4]. Samples were incubated on ice for 30 min. The crude extracts were then cleared by centrifugation for 10 min at 14,000 rpm. Total protein concentration of cleared extracts was estimated using the Pierce™ BCA Protein Assay Kit (Thermo Fisher Scientific) with bovine serum albumin as a standard. Based on the resulting total protein concentrations of the samples, appropriate amounts of lysis buffer and SDS polyacrylamide gel electrophoresis (SDS-PAGE) sample buffer [50 mM Tris-HCl, pH 6.8, 15.6 g/l dithiothreitol, 0.1 g/l bromophenol blue, 4% (w/v) SDS, 12% (w/v) glycerol] were added in

order to equalize the total volume of all samples. Samples were then heated up at 95°C for 3 mins, spun down, and stored at -80°C.

Thirty μg of total proteins were resolved by SDS-PAGE on a 4–20% Tris-Glycine gel (Invitrogen). The proteins were transferred onto polyvinylidene difluoride membranes (BioRad) overnight (35 V) at 4°C in transfer buffer [25 mM Tris base, 192 mM glycine, 20% (v/v) methanol]. Equal protein loading was verified by Ponceau S solution (Sigma) reversible staining of the membranes. The membranes were incubated in blocking buffer [5% (w/v) non-fat dry milk and 0.5% (w/v) Tween® 20 in PBS] for at least 1 hour at room temperature. Membranes were then incubated overnight at 4°C with primary antibody diluted in blocking buffer. After washing 3 times for 10 min in PBST (0.5% (w/v) Tween® 20 in PBS), then membranes were incubated for 30 min at room temperature with the appropriate HRP horseradish peroxidase-conjugated secondary antibodies (Cell Signaling) in blocking buffer, and again washed 3 times for 10 min in PBST. Protein bands were detected by chemiluminescence using the Thermo Scientific™ Pierce™ ECL 2 Western Blotting Substrate or the Amersham ECL kit (GE Healthcare). For quantitative analysis of protein expression levels, enhanced chemiluminescence signals were captured on X-ray films, scanned at a resolution of 720 dots per inch and 8 bits per pixel, and digitally integrated using the National Institutes of Health ImageJ Software (http://rsb.info.nih.gov/ij/). For the comparison of relative protein levels, the mean pixel intensity was measured for each band using the same area for both WT and pallid samples lanes. The pixel intensity of the background was then subtracted from that of each sample band. Background-corrected values of each sample were then divided by the background-correct values of the

respective β-actin. For each WT and pallid pair, the normalized values were divided by the normalized value of the WT. Because WT values were divide by itself, all WT values equaled one. Therefore, pallid ratios were analyzed using one sample t-test comparing pallid ratios to the theoretical value of one using GraphPad Prism 5.0b (GraphPad Software).

RESULTS

Radial glia processes are disrupted in the male pallid hippocampus

In a normally developing murine brain, radial glia processes extend across the hippocampal cell layer and form a scaffold along which neurons migrate. To determine if the extension of these tracks was affected by the lack of BLOC-1, the expression of GLutamate ASpartate Transporter (GLAST), a marker of radial glia, was examined at P1. In the WT male hippocampus, the GLAST-positive radial glial processes were observed nicely aligned throughout the entire cell layer (Fig. 3.1A). In contrast, in the pallid male hippocampus, the immunoreactivity of GLAST was drastically reduced and the radial glia tracks almost completely absent (Fig. 3.1A). In the female hippocampus of WT and pallid mice, there was no apparent difference in immunostaining of GLAST (Fig. 3.1B) Next, the total protein levels of GLAST were measured by immunoblot. In males, the total protein levels of GLAST were significantly decreased in the pallid hippocampi compared to the WT hippocampi, and in the females, the protein levels of GLAST in pallid and WT hippocampi had no differences (Fig 3.2). These findings were further confirmed by using nestin, a marker for radial glia as well as neural progenitor cells. The immunoreactivity of nestin was also greatly reduced in the pallid male hippocampus and again the tracts of the radial glia were not visible (Fig 3.3A). No apparent differences in nestin expression was observed in the female hippocampus of WT and pallid mice (Fig. 3.3B).The total protein levels of nestin displayed a striking decrease in the pallid male, but not female hippocampi as compared to age-matching WT (Fig. 3.4) These results suggest that

lack of BLOC-1 elicits a weakening of the radial glia scaffold in male mice hampering hippocampal development.

Next, the expression of reelin was examined. This large extracellular protein is a crucial regulator of neuronal migration, and it is involved in stabilizing the radial glial scaffold. It is known that there are three cleavage sites on reelin, which produce multiple fragments with different molecular weights. Among them, the 180 kDa fragment is considered able to be excreted in the extracellular space and to diffuse far enough from the Cajal Retzius cell layer to regulate cell migration in the different layers. It is accepted that any change in its levels will greatly affect cell migration. The identity or role(s) of the even smaller fragments is still controversial. I used an antibody that detects the full-length 400 kDa, the 300 kDa, and the 180 kDa forms and no differences were found in males or females pallid and WT (Fig. 3.5).

Subtle alterations in the staining pattern of immature neuronal markers

Neurons are derived from neuroepithelial multiple potential progenitor cells, and they express markers at different developmental stages. The expression of some of these markers overlap and do no clearly define a maturation stage or a type of neuron, hence more than one marker must be used to thoroughly examine normal maldevelopment. The expression of doublecortin, a microtubule-associated protein expressed in neuroblasts and immature neurons, in P1 male and female pallid CA1 did not differ from that of gender or age-matching WT, although it seemed to be slightly decreased in pallid males (Fig 3.6A, arrows). The neuronal intermediate filament protein, α-internexin, is highly expressed during embryogenesis and in immature neurons. In male pallid hippocampus at P1, the α-internexin-positive neurons appeared

to be in disarray, particularly near the subiculum compared to those of matching age and gender WT (Fig. 3.7A arrows). Conversely, the organization of immature pallid females did not appear to be different from WT (Fig. 3.7B). This result suggests that the immature neurons are "malpositioned" in the male pallid hippocampus during early postnatal development. At this stage of maturation, immature neurons also express βIII-tubulin and as expected the layout of the CA1 neurons in pallid males appeared disorganized around the subiculum, although such effect was more subtle than seen with α-internexin (Fig 3.8A). In addition, some βIII-tubulin-positive neurons displayed a strong and more defined staining especially of a long leading process, characteristic of migrating neurons (Fig 3.8A, arrows). The expression pattern of βIII-tubulin did not show any abnormalities in pallid females (Fig 3.8B). The total protein levels of these immature neuronal markers, doublecortin (Fig. 3.9), α-internexin (Fig. 3.10), and βIII-tubulin (Fig. 3.11), were not different between genotypes in both males and females at P1.

DISCUSSION

Here, I further investigated and characterized the abnormal cytoarchitecture observed in CA1 in P1 pallid males, but absent in females. Markers for immature neurons displayed normal total protein levels, but an atypical expression pattern in pallid males. This effect was accompanied by a dramatic reduction in the presence of radial glia tracts, as shown by the drastic decrease in GLAST and nestin immunoreactivity and total protein levels. These findings suggest that a weakening of the glial scaffold might be hampering or delaying neuronal migration to the cell layer of CA1 and causing the aberrant neuronal distribution seen in BLOC-1-deficient hippocampi early postnatally. This aberrant cyto-organization was not accompanied by changes in the protein levels of the different reelin forms. As shown in the previous chapter, these abnormalities were absent at a later postnatal age, P45, suggesting that not all the components of the signaling pathways involved in these process are disrupted by lack of BLOC-1, for instance reelin secretion into the extracellular space.

Although the functional role of BLOC-1 in the the central nervous system is not yet fully understood, our group and others have previously reported that BLOC-1 in brain may be involved in neurite elongation [4,6]. Although the mechanism is not fully understood, it has been suggested that impairment of the cargo delivery by BLOC-1 could disturb neurite outgrowth. Thus, it is plausible to speculate that lack of BLOC-1 also negatively affects the extension of the radial glia fibers. Further analysis is required to address this point.

As discussed in Chapter 2, the alternation in cell distribution seen in BLOC-1-deficient CA1 at P1 was absent in P45 pallid mice, suggesting that other pathways and players involved in cell migration are not affected and the phenotype is somehow compensated. For instance, protein

levels of reelin were not found to be different in pallid and WT. In addition, previous studies have demonstrated that mice lacking glutamate transporters GLAST, GLT1, and EAAC1, have seemingly normal brain development, suggesting that glutamate transporter subtypes may functionally compensate for one another during brain development [7,8,9]. Only in mice lacking two of the glutamate transporters (GLAST -/- and GLT1 -/-) displayed multiple brain defects [10]. Strikingly, one of the phenotypes reported in these double mutants is less densely packed pyramidal neurons in the hippocampus [10]. Thus, it could be that in BLOC-1-deficient brains, normal levels of reelin and other proteins, such as GLT1 and EAAC1, cooperate to rescue the P1 phenotype, and although delayed, the neurons will eventually reach their final position or at least appear to.

The effects described above were absent or much less pronounced in BLOC-1-deficient females, further suggesting that BLOC-1-deficient females are protected from the effects of BLOC-1-deficiency.

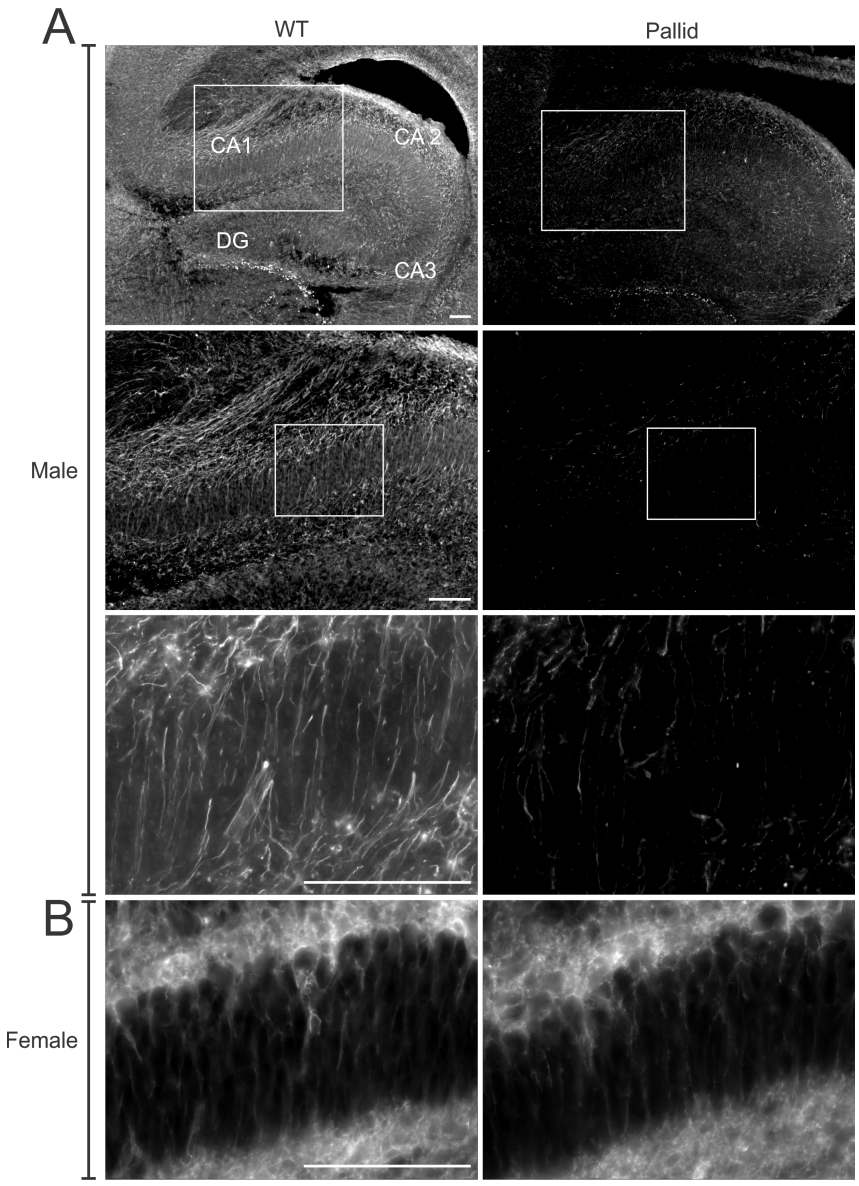

Figure 3.1 The expression of the radial glia marker, GLAST, is altered in postnatal day (P)1 male pallid CA1, but not in females. (A) Left panels, in wild-type (WT) CA1, radial glia processes were observed throughout the entire width of the CA1, while (right panels) pallid hippocampi displayed a dramatic decrease in GLAST immunopositive processes. (B) Right bottom panel, pallid females were less affected than males by lack of BLOC-1. Well organized GLAST- positive radial glia fibers could be seen across CA1 in pallid females similarly to WT females and males. Sections (40 μm) from male mice in A were stained using a guinea pig polyclonal anti-GLAST antibody, whereas, those from females in B, using a mouse monoclonal anti-GLAST. White boxes in top panels indicate regions shown at higher magnification. Left and right panels in B are representative higher magnification images taken as shown by the white boxed area in A. CA: Cornus Ammonis; DG: dentate gyrus. Scale bars, 100 μm.

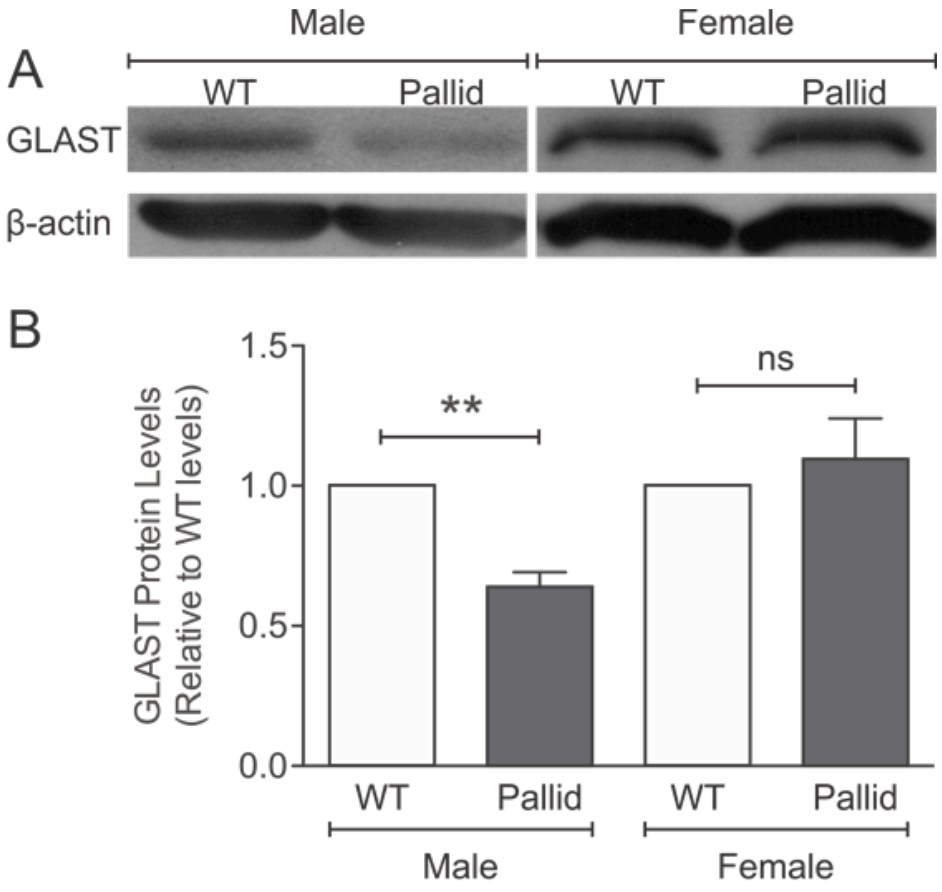

Figure 3.2 GLAST total protein levels are drastically reduced in the male pallid hippocampi at postnatal day (P)1. (A) Representative immunoblots of hippocampal extracts from both males and females wild-type (WT) and pallid mice at P1. β-actin was used as a loading control. (B) Each band was analyzed by densitometry corrected for background, normalized to β-actin levels. Data are shown as the mean ± S.E.M. of the ratio of each pallid and its respective WT, n = 5 animals per genotype per gender. Statistical significance was assessed using a one-sample t-test. **$p<0.01$, ns, not significant.

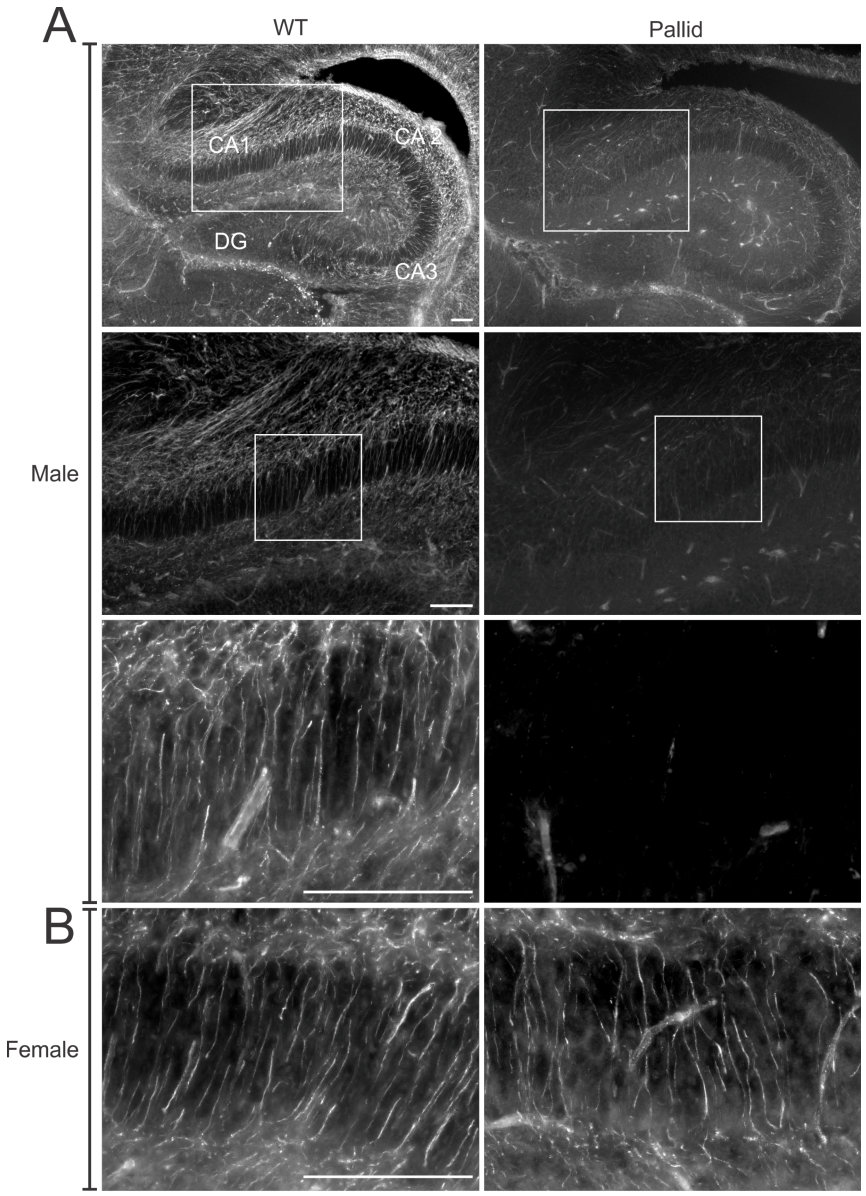

Figure 3.3 Nestin expression in CA1 is impacted by lack of BLOC-1 at postnatal day (P)1 in pallid males, but not females. (A) Left panels, in wild-type (WT) CA1, radial glia processes, immunopositive for nestin were observed throughout the entire width of the CA1, whilst (right panels) pallid hippocampi displayed a drastic decrease in nestin immunopositive processes. (B) Right panel, pallid females were less affected than males by lack of BLOC-1. Well organized nestin-positive radial glia fibers could be seen across CA1 in pallid females similarly to WT females and males. Sections (40 μm) from male and female mice in A and B were stained using a mouse monoclonal anti-nestin antibody. White boxes indicate regions shown at higher magnification. Left and right panels in B are representative higher magnification images taken as shown by the white boxed area in A. CA: Cornus Ammonis; DG: dentate gyrus. Scale bars, 100 μm.

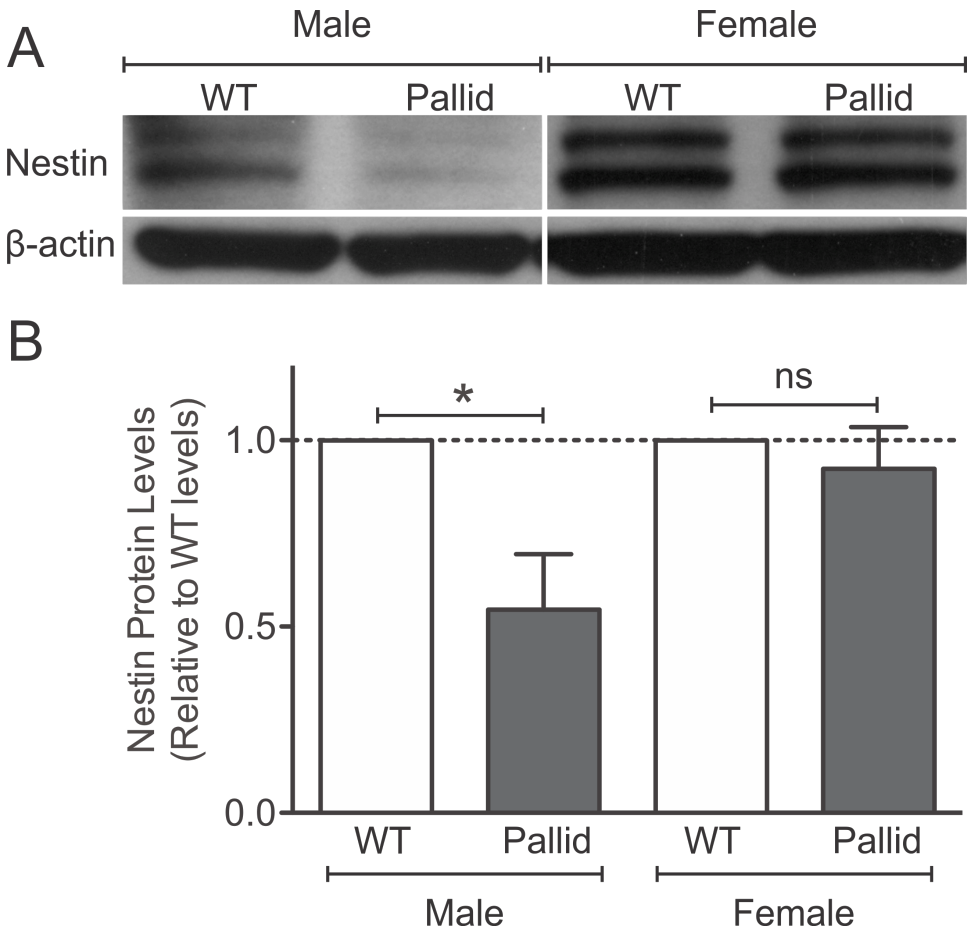

Figure 3.4 Decreased nestin total protein levels in male pallid hippocampi at postnatal day (P)1. (A) Representative immunoblots of hippocampal extracts from both males and females wild-type (WT) and pallid mice at P1. β-actin was used as a loading control. (B) Each band was analyzed by densitometry corrected for background, normalized to β-actin levels. Data are shown as the mean ± S.E.M. of the ratio of each pallid and its respective WT, n = 5 animals per genotype per gender. Statistical significance was assessed using a one-sample t-test. **$p<0.01$, ns, not significant.

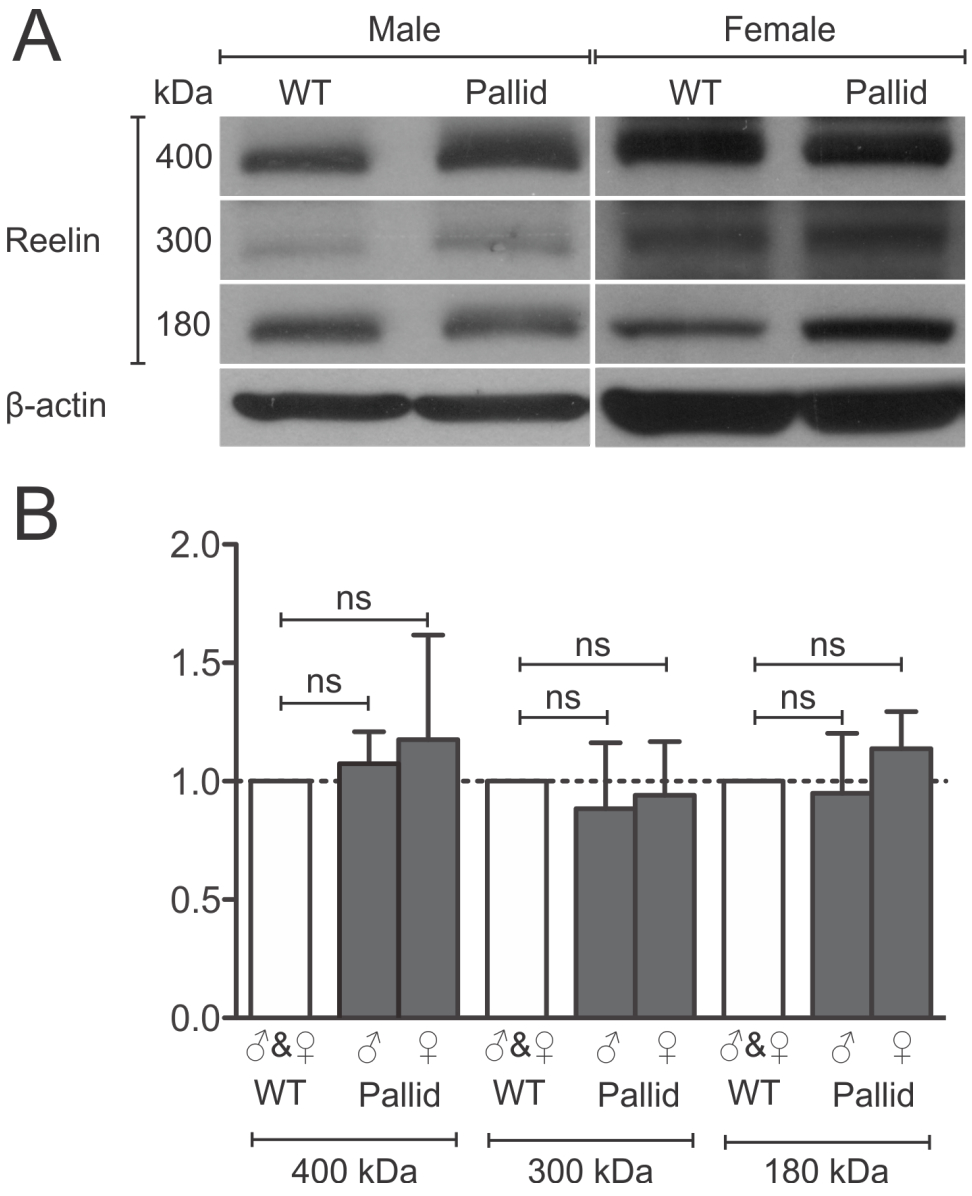

Figure 3.5 Reelin protein expression levels are not altered by the lack of BLOC-1 at postnatal day (P)1. (A) Representative immunoblots of hippocampal extracts showing no differences in the total protein of the three main forms of reelin, (full-length, 400 kDa, plus two cleaved fragments, 300 kDa, and 180 kDa) in males and females wild-type (WT) and pallid mice. β-actin was used as a loading control. (B) Each band was analyzed by densitometry, corrected for the background, normalized to β-actin levels. Data are shown as the mean ± S.E.M. of the ratio of each pallid and its respective WT, n = 5 animals per genotype per gender. Statistical significance was assessed using a one-sample t-test. ns, not significant.

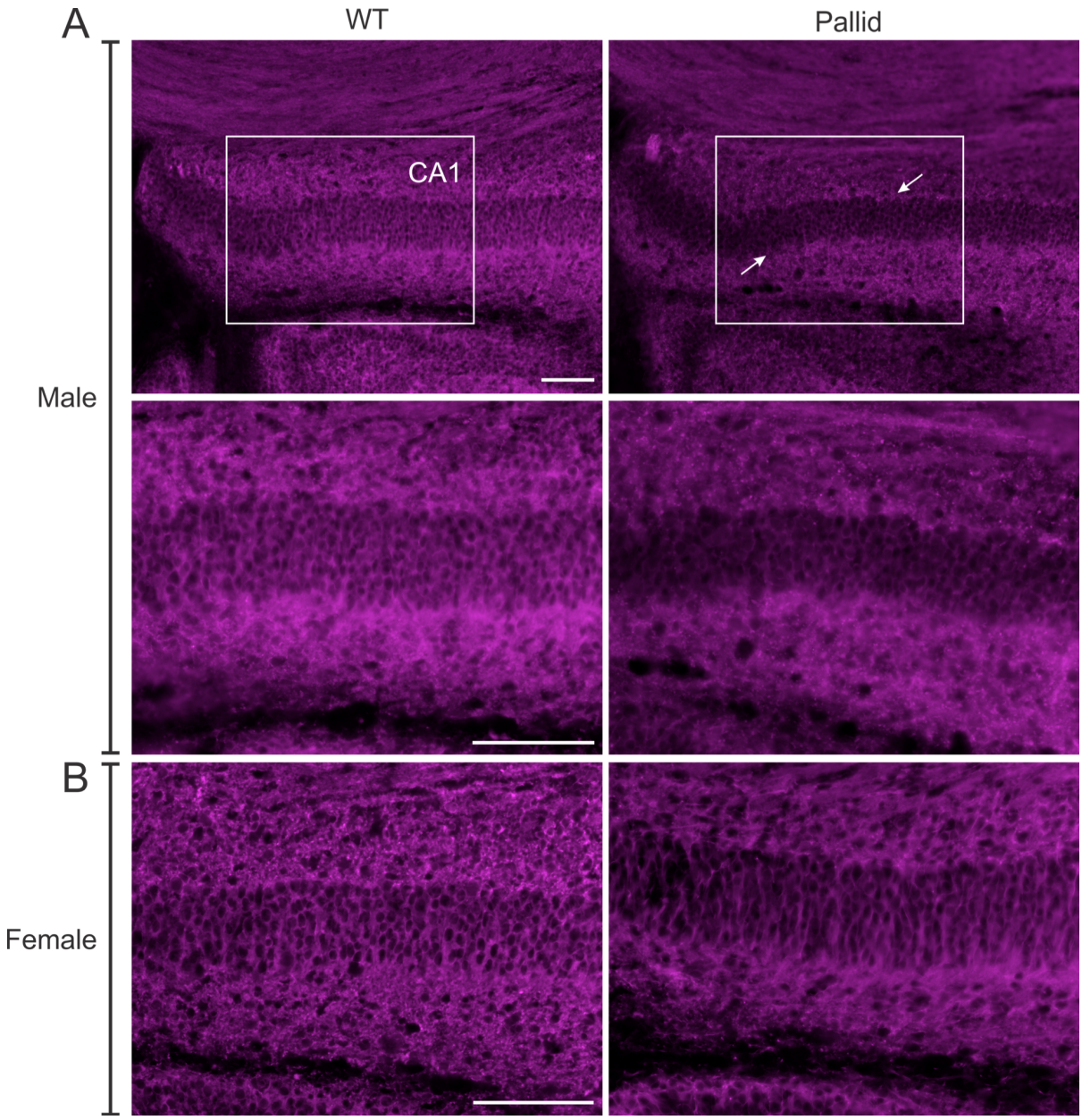

Figure 3.6 The expression levels of the immature neuronal marker, doublecortin, are marginally altered in postnatal day (P)1 male pallid CA1, but not in females. (A) Left panels, in WT CA1, doublecortin-positive neuronal cells appeared well organized throughout the entire CA1 cell layer. Right panels, in pallid hippocampi, the expression level of doublecortin appeared to be slightly decreased in the CA1 cell layer (arrows). (B) This phenotype is less apparent in pallid females. Sections (40 μm) from male and female mice in A and B were stained using a rabbit polyclonal anti-doublecortin antibody. White boxes indicate regions shown at higher magnification. Left and right panels in B are representative higher magnification images taken as shown by the white boxed area in A. CA: Cornus Ammonis; DG: dentate gyrus. Scale bars, 100 μm.

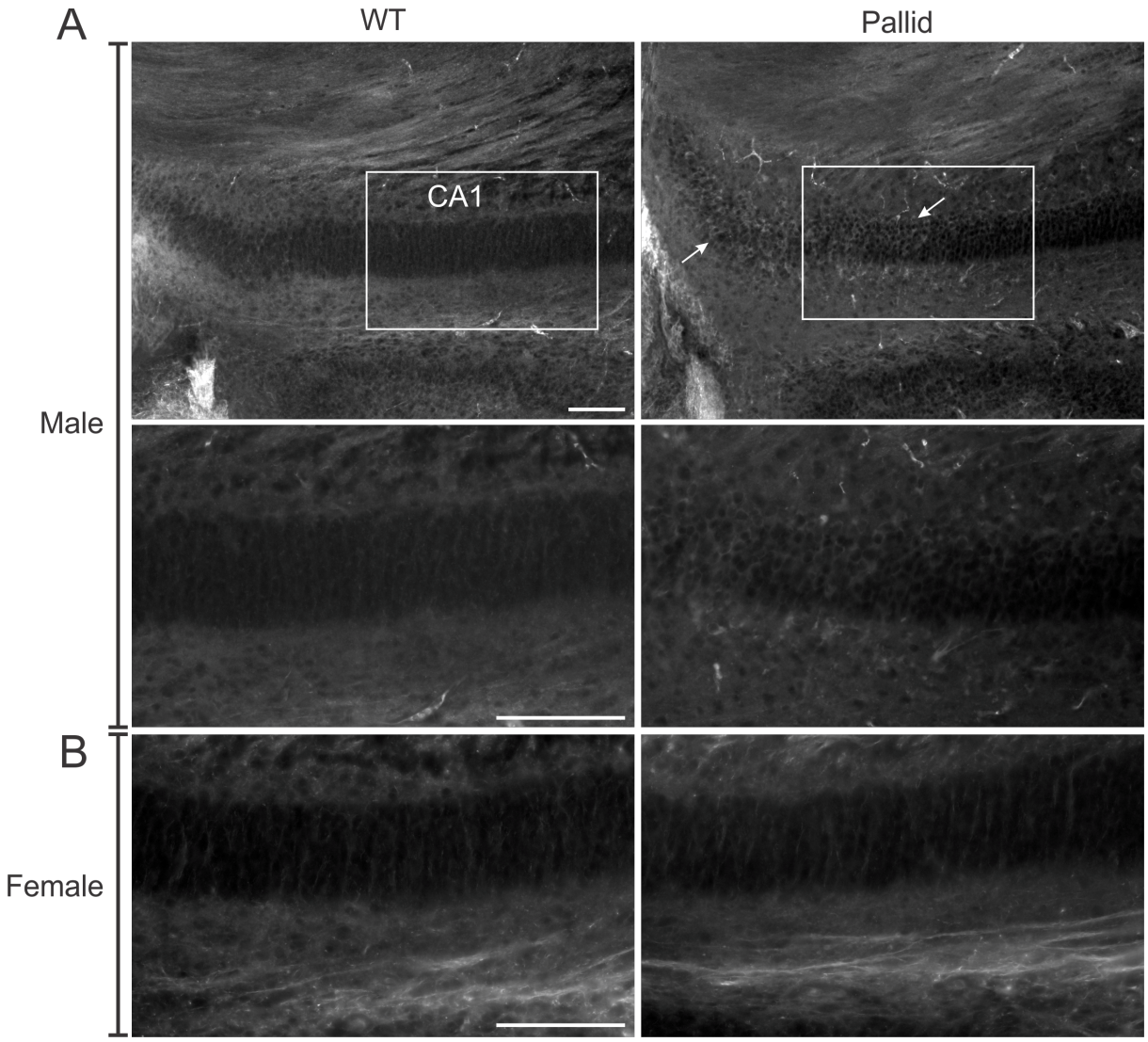

Figure 3.7 The expression pattern of the immature neuronal marker, α-internexin, is altered in postnatal day (P)1 male pallid CA1, but not in females. (A) Left panels, in WT CA1, immature neurons immunopositive for α-internexin appeared well organized throughout the entire CA1 cell layer. Right panels, in pallid hippocampi, the distribution pattern of α-internexin-positive neurons, appear malpositioned, especially around the subiculum (arrows). (B) Pallid females displayed well distributed α-internexin-positive neurons as seen in the WT females and males. Sections (40 μm) from male and female mice in A and B were stained using a rabbit polyclonal anti-α-internexin antibody. White boxes indicate regions shown at higher magnification. Left and right panels in B are representative higher magnification images taken as shown by the white boxed area in A. CA: Cornus Ammonis; DG: dentate gyrus. Scale bars, 100 μm.

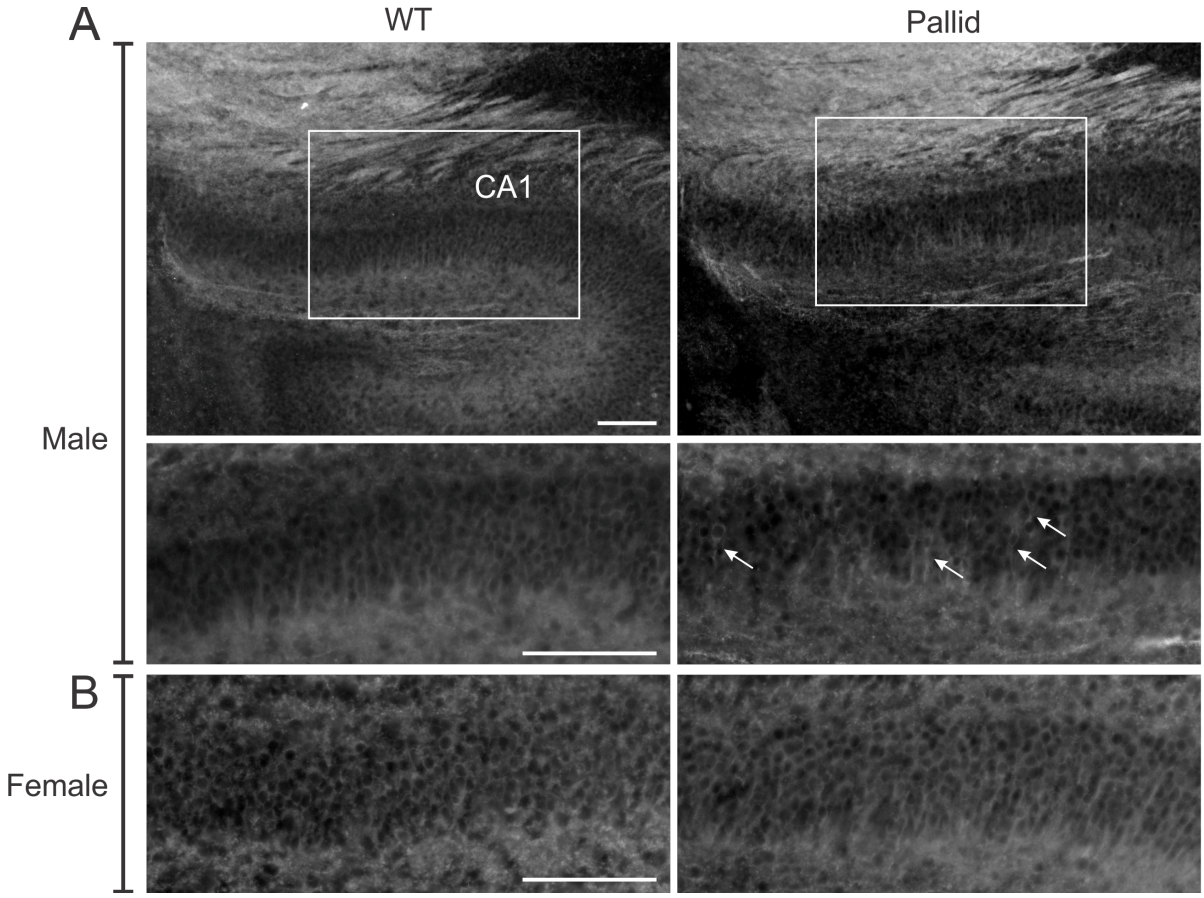

Figure 3.8 The expression pattern of the immature neuronal marker, βIII-tubulin, is altered in postnatal day (P)1 male pallid CA1, but not in females. (A) Left panels, in WT displayed well distributed βIII-tubulin-positive neurons throughout CA1. Right panels, in pallid hippocampi, the expression pattern of βIII-tubulin-positive neurons was disorganized (arrows). (B) Pallid females were not impacted by lack of BLOC-1 and their CA1 was not different from WT. Sections (40 μm) from male and female mice in A and B were stained using a rabbit polyclonal anti-βIII-tubulin antibody. White boxes indicate regions shown at higher magnification. Left and right panels in B are representative higher magnification images taken as shown by the white boxed area in A. CA: Cornus Ammonis; DG: dentate gyrus. Scale bars, 100 μm.

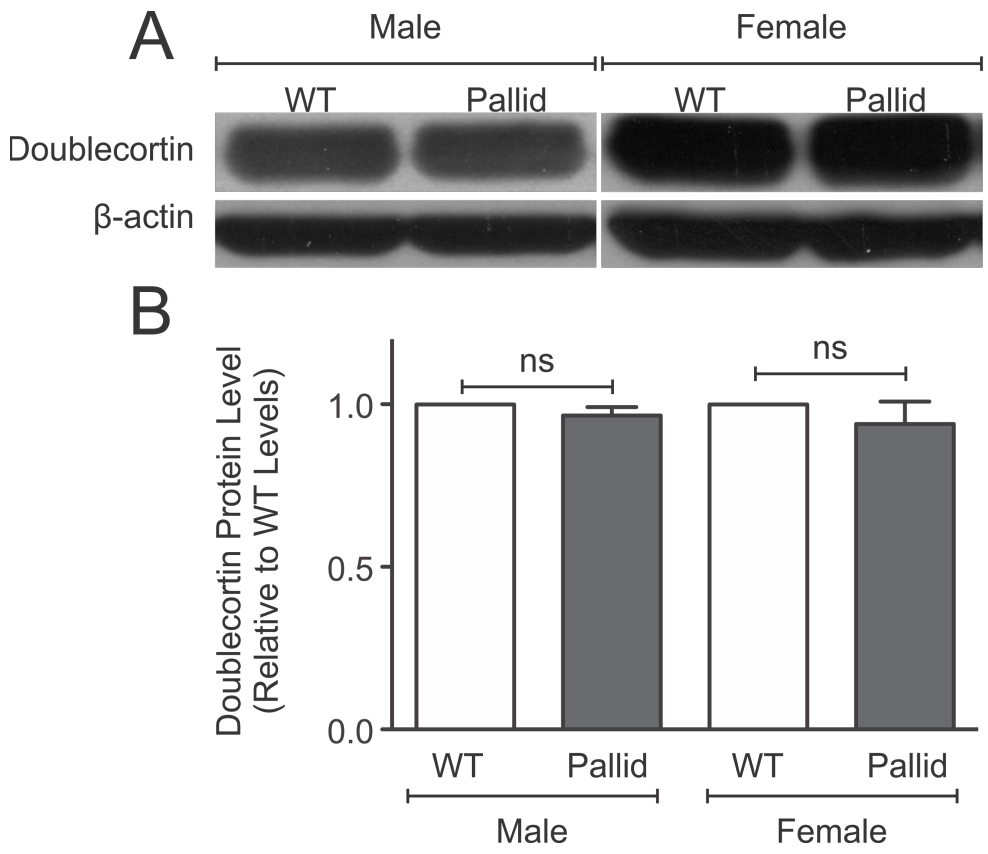

Figure 3.9 The total protein levels of immature neuronal marker doublecortin are not impacted by lack of BLOC-1. (A) Representative immunoblots of hippocampal extracts from both males and females wild-type (WT) and pallid mice at P1. β-actin was used as a loading control. (B) Each band was analyzed by densitometry corrected for background, normalized to β-actin levels. Data are shown as the mean ± S.E.M. of the ratio of each pallid and its respective WT, n = 5 animals per genotype per gender. Statistical significance was assessed using a one-sample t-test. ns, not significant.

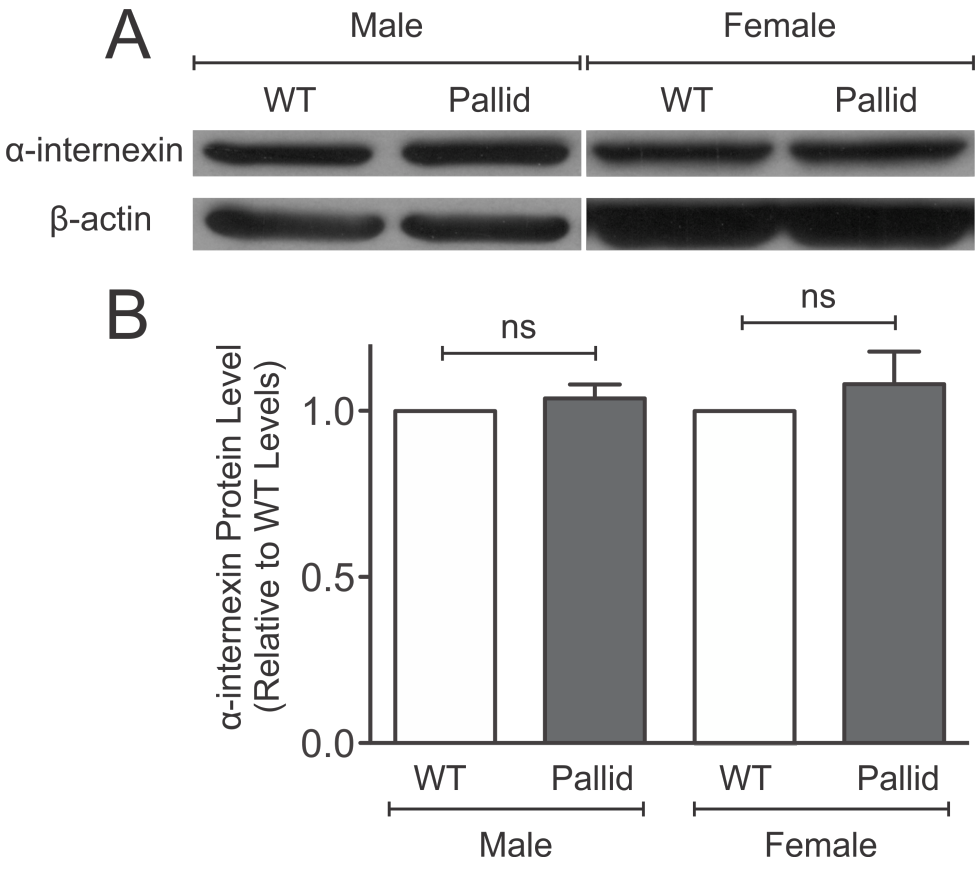

Figure 3.10 The total protein levels of immature neuronal marker α-internexin are not affected by lack of BLOC-1. (A) Representative immunoblots of hippocampal extracts from both males and females wild-type (WT) and pallid mice at P1. β-actin was used as a loading control. (B) Each band was analyzed by densitometry corrected for background, normalized to β-actin levels. Data are shown as the mean ± S.E.M. of the ratio of each pallid and its respective WT, n = 5 animals per genotype per gender. Statistical significance was assessed using a one-sample t-test. ns, not significant.

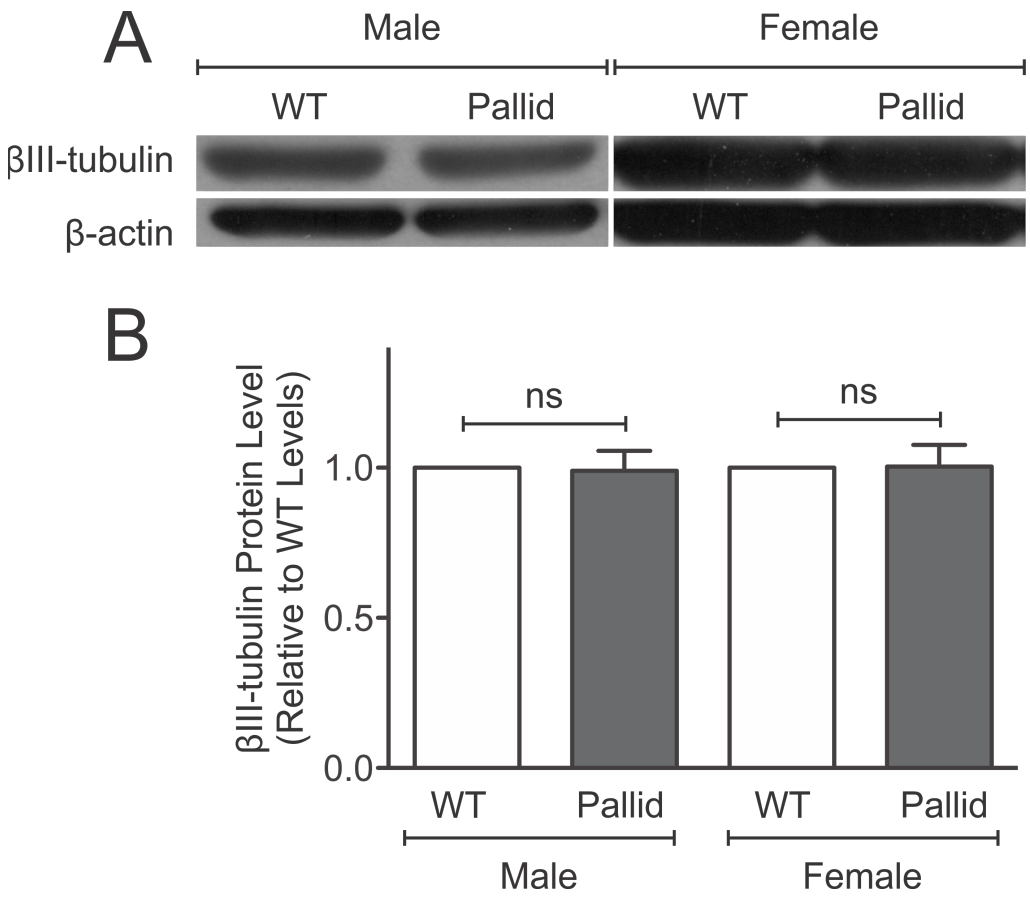

Figure 3.11 Lack of BLOC-1 does not affect the total protein elevs of immture neuronal marker βIII-tubulin. (A) Representative immunoblots of hippocampal extracts from both males and females wild-type (WT) and pallid mice at P1. β-actin was used as a loading control. (B) Each band was analyzed by densitometry corrected for background, normalized to β-actin levels. Data are shown as the mean ± S.E.M. of the ratio of each pallid and its respective WT, n = 5 animals per genotype per gender. Statistical significance was assessed using a one-sample t-test. ns, not significant.

REFERENCES

1. Urbán N, Guillemot F. Neurogenesis in the embryonic and adult brain: same regulators, different roles. Front Cell Neurosci. 2014 Nov 27;8:396.
2. Andersen P, Morris R, Amaral D, Bliss T, O'Keefe J. The Hippocampus Book. Oxford University Press. 2007. Chapter 4.
3. Czurkó A, Czéh B, Seress L, Nadel L, Bures J. Severe spatial navigation deficit in the Morris water maze after single high dose of neonatal x-ray irradiation in the rat. Proc Natl Acad Sci USA. 1997 Mar 18;94(6):2766-71.
4. Ghiani CA, Starcevic M, Rodriguez-Fernandez IA, Nazarian R, Cheli VT, Chan LN, Malvar JS, de Vellis J, Sabatti C, Dell'Angelica EC. The dysbindin-containing complex (BLOC-1) in brain: developmental regulation, interaction with SNARE proteins and role in neurite outgrowth. Mol Psychiatry. 2010 Feb;15(2):115, 204-15.
5. Matteucci A, Gaddini L, Macchia G, Varano M, Petrucci TC, Macioce P, Malchiodi-Albedi F, Ceccarini M. Developmental expression of dysbindin in Muller cells of rat retina. Exp Eye Res. 2013 Nov;116:1-8.
6. Ma X, Fei E, Fu C, Ren H, Wang G. Dysbindin-1, a schizophrenia-related protein, facilitates neurite outgrowth by promoting the transcriptional activity of p53. Mol Psychiatry. 2011 Nov;16(11):1105-16.
7. Tanaka K, Watase K, Manabe T, Yamada K, Watanabe M, Takahashi K, Iwama H, Nishikawa T, Ichihara N, Kikuchi T, Okuyama S, Kawashima N, Hori S, Takimoto M, Wada K.

Epilepsy and exacerbation of brain injury in mice lacking the glutamate transporter GLT-1. Science. 1997 Jun 13;276(5319):1699-702.

8. Peghini P, Janzen J, Stoffel W. Glutamate transporter EAAC-1-deficient mice develop dicarboxylic aminoaciduria and behavioral abnormalities but no neurodegeneration. EMBO J. 1997 Jul 1;16(13):3822-32.
9. Watase K, Hashimoto K, Kano M, Yamada K, Watanabe M, Inoue Y, Okuyama S, Sakagawa T, Ogawa S, Kawashima N, Hori S, Takimoto M, Wada K, Tanaka K. Motor discoordination and increased susceptibility to cerebellar injury in GLAST mutant mice. Eur J Neurosci. 1998 Mar;10(3):976-88.
10. Matsugami TR, Tanemura K, Mieda M, Nakatomi R, Yamada K, Kondo T, Ogawa M, Obata K, Watanabe M, Hashikawa T, Tanaka K. Indispensability of the glutamate transporters GLAST and GLT1 to brain development. Proc Natl Acad Sci USA. 2006 Aug 8;103(32): 12161-6.

CHAPTER 4

Dendritic arborization abnormalities in hippocampal neurons deficient in BLOC-1

ABSTRACT

Previous *in vitro* studies had shown that BLOC-1-deficient hippocampal neurons have deficient neurite elongation. To examine whether such abnormality is present *in vivo* as well, I have analyzed the cytoarchitecture of hippocampal neurons in wild-type and BLOC-1-deficient mice, at postnatal day 60 using the Golgi method. Neurons in two hippocampal areas known to involved in cognitive and behavioral deficits, the Dentate Gyrus and Cornus Ammonis (CA)1, were examined. Morphological analyses revealed a significant decrease in the number of dendrites in the granule cells of the Dentate Gyrus, but no changes in the length. Conversely, I did not find any deficiencies in CA1 pyramidal neurons. These results reinforce the likelihood of a prosed function for BLOC-1 in brain development and its involvement in process elongation.

INTRODUCTION

Published studies suggest a role for BLOC-1 in brain development, and more particularly, in membrane trafficking and neurite elongation. Our lab previously reported that primary hippocampal neurons from newborn pallid mice, deficient in BLOC-1, display decreased number of neurites when grown for three days, and, sum of the lengths of all neurites per cell [1]. In agreement, similar findings were shown in neurons cultured from the sandy mice, another model of BLOC-1 deficiency [2]. Additionally, siRNA-mediated knockdown of dysbindin in a mouse neuroblastoma cell lines caused a decrease in the neurite length in cultured neuroblastoma cells [2]. Lastly, in cultured rat hippocampal neurons, RNA interference-mediated knockdown of endogenous dysbindin resulted in abnormal dendritic spine formation [3].

Altogether these findings point to a role for BLOC-1 in neurite development, but they were all performed *in vitro*, where the growth conditions do not completely recapitulate the brain environment. Thus, I have analyzed the cytoarchitecture of hippocampal neurons from postnatal day (P)60 wild-type and pallid brains using the Golgi method followed by Sholl analysis to determine if lack of BLOC-1 affect the dendritic arborization of hippocampal neurons in the Dentate Gyrus, and Cornus Ammonis (CA)1. Furthermore, it was important to determine whether the alternations seen early in postnatal development but absent in young adult, had caused any abnormality in young brains.

EXPERIMENTAL PROCEDURES

Animals

Mouse strains were used and maintained as described in Chapter 2.

Golgi

Whole brains were rapidly dissected from P60 wild-type (WT) and pallid mice (n = 5 animals per genotype) and then processed following the FD Rapid GolgiStain Kit manufacturer's instructions (FD NeuroTechnologies). Briefly, the brains were placed into the Golgi-Cox solution (provided in the kit) for 2 weeks at room temperature in the dark. Golgi stained brains were then sectioned (100 μm) coronally on a vibratome (Electron Microscopy Sciences). Sections were collected in phosphate-buffer saline (PBS) and mounted on gelatin-coated glass microscope slides and developed with the silver-mercury solutions provided in the kit. Cover-slips were mounted using Permount mounting media.

Image collection and analysis

Pyramidal neurons from the CA1 and granule cells from the Dentate Gyrus of the hippocampus were selected based on their dark impregnation, projected, and traced. An upright microscope (Leica) equipped with a camera lucida was used. A minimum of 15 neurons were selected from each brain region per animal, and 5 animals per genotype were analyzed. Two quantitative analyses were used to examine the complexity of the dendritic arbor. 1) The Sholl analysis: a template of equally spaced concentric circles (15 μm) was overimposed to each traced neuron paying extra attention to place the cell body

in the center of the smallest circle (Fig. 4.1A) [4]. The number of dendrites that crossed each concentric circle was counted and the number of dendritic intersections per circle was plotted against the distance of the circle. Additionally, the primary, secondary and tertiary dendrites of each neuron were counted and traced using the Axiovision software (Zeiss, Verison 4.8) (Fig. 4.1B). Both analyses were performed by two independent investigators masked to the genotype of the animals. Statistical significance was determined by two-way ANOVA (Analysis of Variance) followed by Bonferroni's multiple comparison test using the GraphPad Prism 5.0b (GraphPad Software).

RESULTS

Defect in dendritic arborization in granule cells deficient in BLOC-1

I analyzed the dendritic arborization of hippocampal neurons in the Dentate Gyrus (Fig. 4.2 A,B) and CA1 (Fig. 4.2 C,D) of P60 WT and pallid mice. Sholl analysis revealed a 15-24% decrease in the number of processes crossing the 30-60 μm away from the cell body, in pallid granule neurons as compared to WT (Fig. 4.3A). On the other hand, no differences were found in the numbers, of apical and basal dendrites of CA1 between pallid and WT pyramidal neurons (Fig 4.3 B,C). Next, the length and number of primary, secondary and tertiary dendrites were examined to further characterize the dendritic arbors. Again, pallid granule cells displayed a significantly, decreased number of all orders of dendrites (Fig. 4.4A), and a significant decrease in the branch points of only the the tertiary dendrites (Fig. 4.4B) compared to those of the WT. No abnormalities were found in the length of the dendrites in the pallid granules or pyramidal cells (Fig. 4.4C, Fig. 4.5A-D).

DISCUSSION

Here I examined the dendritic arborization of BLOC-1-deficient hippocampal neurons was examined *in vivo.* The results showed that, in the Dentate Gyrus, the BLOC-1-deficient granule neurons had fewer dendrites, particularly tertiary dendrites, than the WT granule neurons. Additionally, the BLOC-1-deficient granule neurons had fewer branch points in the tertiary dendrites than the WT granule neurons. These results suggest that the BLOC-1-deficient granule neurons have a decrease in the complexity of the dendritic arborization, possibly leading to cognitive and behavioral deficiencies [5].

A few possible mechanisms by which BLOC-1 regulates neurite outgrowth can be proposed. For instance, our lab reported that BLOC-1 interacts with the SNARE proteins, SNAP-25, and syntaxin 13 [1], known to be involved in delivery of membranes from an intracellular compartment to the growth cones [7-10]. Another important player may be VAMP7, for which a role of neurite outgrowth in cultured cells was proposed by Galli and colleagues [11-13]. Marcs and colleagues [14,15] showed that VAMP7 is a BLOC-1-dependent cargo protein. Furthermore, VAMP7 interacts with SNAP-47, another component of the BLOC-1 interactome [1,16]. Thus, it is possible that through the interaction with or regulation of these proteins, BLOC-1 may affect neurite development. Altogether these findings, including mine, suggest that BLOC-1 plays a critical role(s) in brain development, one of them being regulation of process outgrowth in neural cells (not limited to neurons). Most importantly, its lack causes delays in central nervous system development and disturbs proper brain wiring leading to cognitive and behavioral deficits.

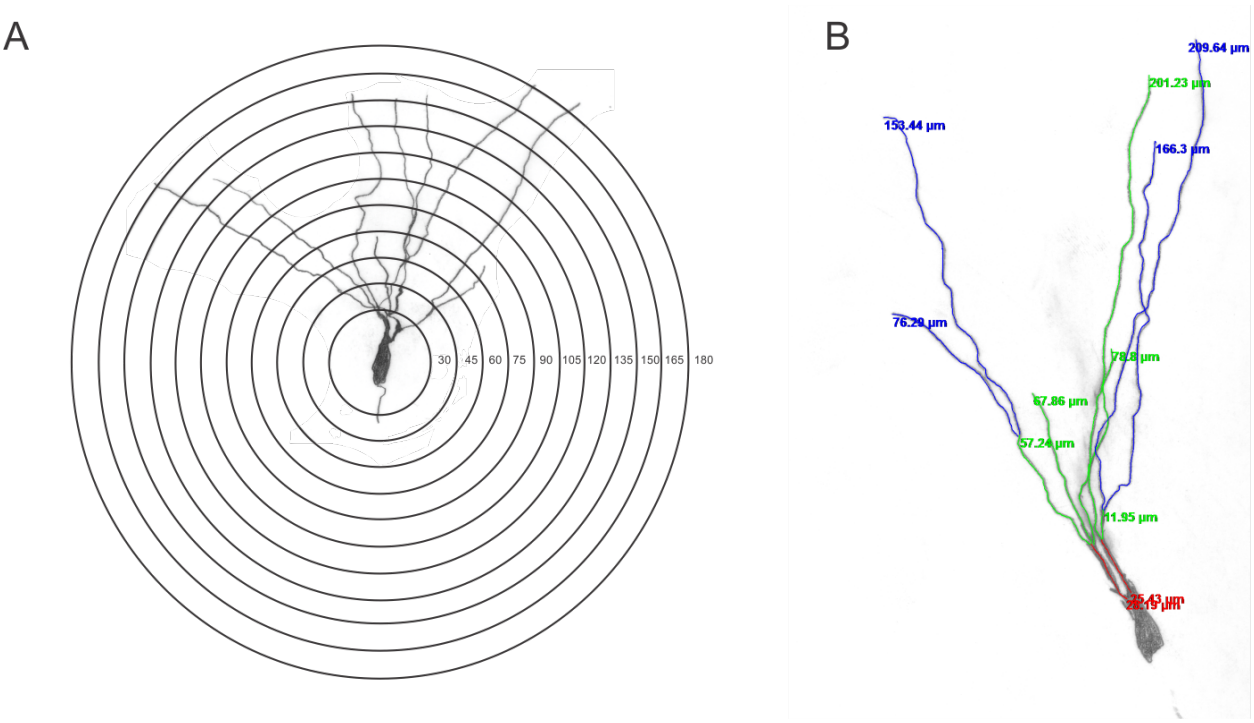

Figure 4.1 Image analyses of Golgi-stained hippocampal neurons. (A) For the Sholl analysis, a template of concentric circles was placed on the trace image of hippocampal neurons. The smallest circle was 30 µm from the center and the other concentric circles were spaced 15 µm apart from the preceding circle. The number of dendrites that cross each concentric circle was determined (B) The primary, secondary, and tertiary dendrites were traced. The red, green, and blue lines are representative traces of primary, secondary, and tertiary dendrites respectively. The number of dendrites and the length of each dendrite were measured.

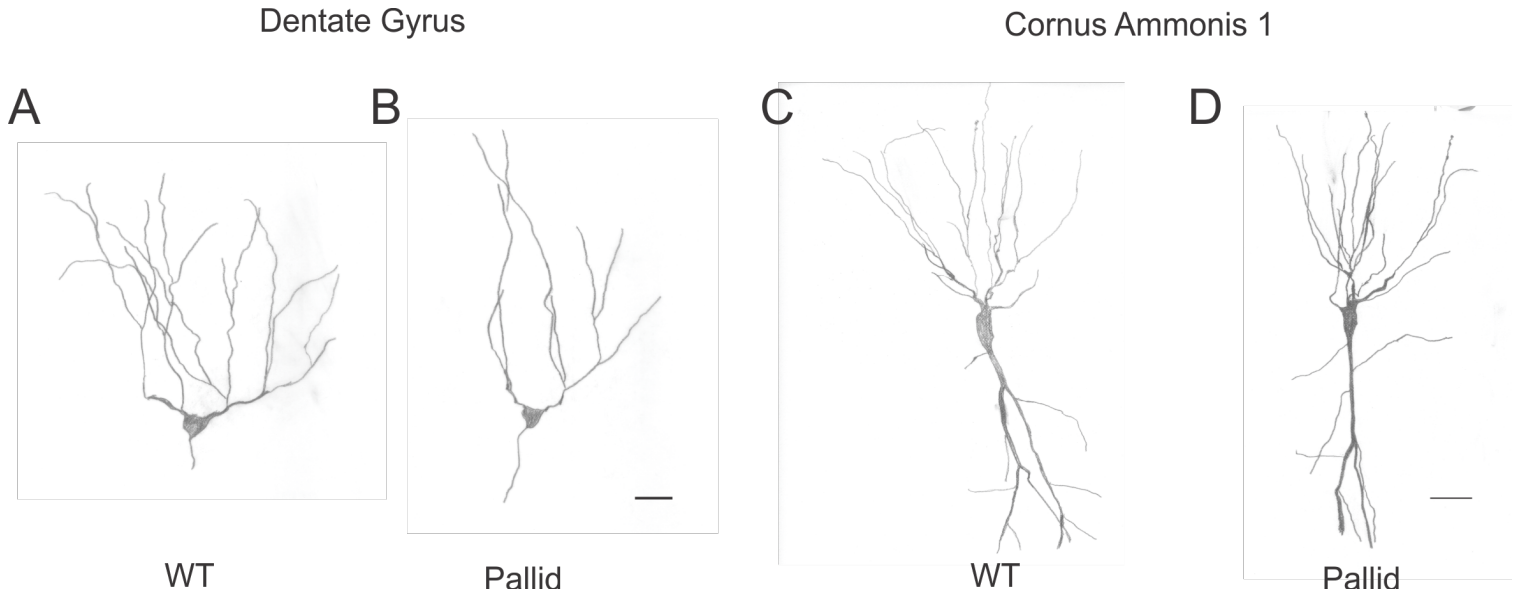

Figure 4.2 Representative traced images of Golgi-stained granule neurons from the dentate gyrus (A,B) and pyramidal neurons from cornus ammonis 1 (C,D) of wild-type (A,C) and pallid (B,D) mice. Whole brains from wild type and pallid mice at postnatal day 60 were stained with Golgi, sectioned, and neurons were projected and traced. Scale bars, 25 μm

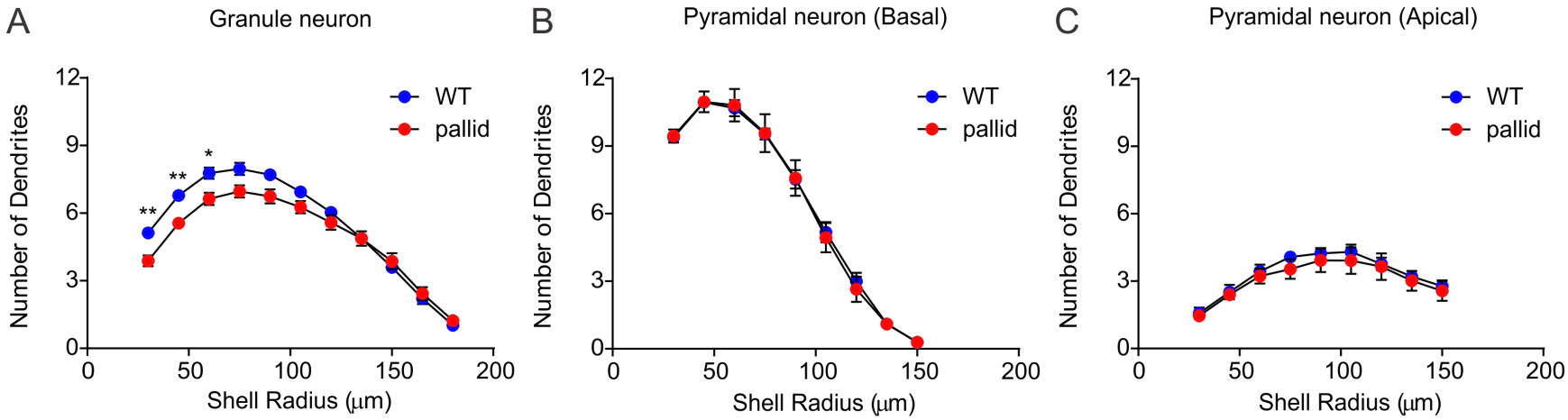

Figure 4.3 Defects in the arborization of granule neurons from the dentate gyrus (DG), but not in neurons of the cornus ammonis 1 (CA1), of pallid mice. (A-C) Sholl analysis of granule neurons from the DG (A), and of basal (B) and apical (C) dendrites of pyramidal neurons from the CA1, from wild-type (WT, blue circles) and pallid (red circles) male mice. Values represent means ± S.E.M. of 5 animals per genotype. The number of dendrites (Y Axis) that cross through each concentric circles distributed at equal distances from the neuronal cell body (X Axis) were plotted. A minimum of 15 neurons per animal per genotype in both DG and CA1 areas were selected. Statistical significance was determined using two-way ANOVA (analysis of variance) followed by Bonferroni's multiple comparison tests. **$p<0.01$, *$p<0.05$.

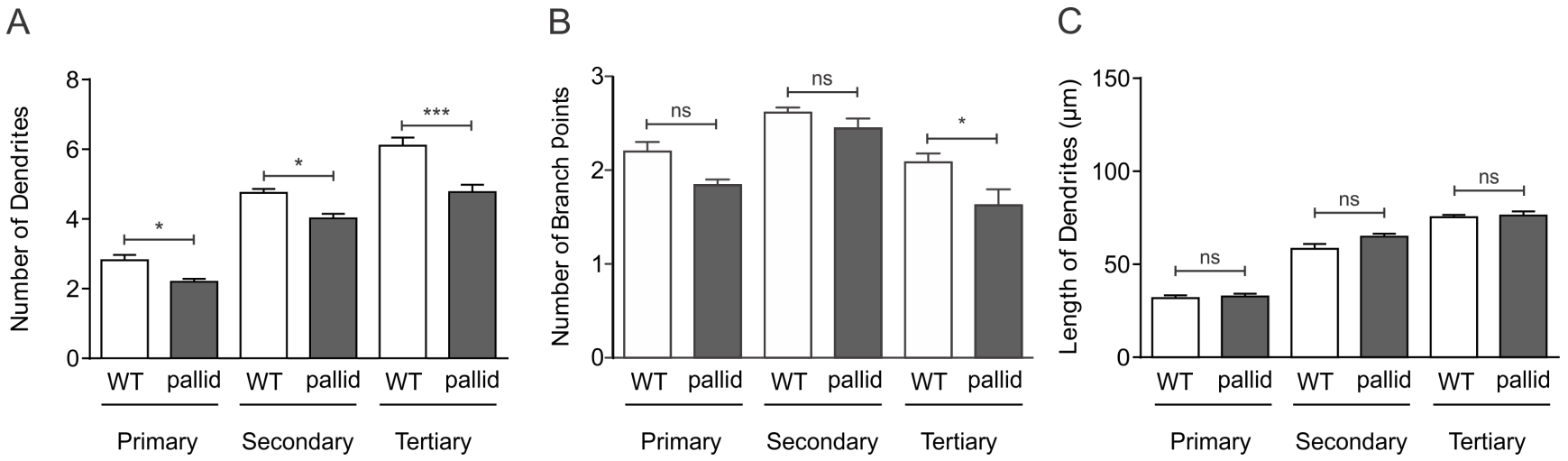

Figure 4.4 Analysis of the primary, secondary and tertiary dendrites show a decrease in the number of dendrites in the pallid dentate gyrus (DG) granule neurons. Primary, secondary and tertiary dendrites of each granule neuron were analyzed to measure the number of branches, the length of each branch, and the number of branch points. WT, wild type. (A-C) Values represent means ± S.E.M of the number of dendrites (A), the length of each dendrite (B), and the number of branch points (C). A minimum of 15 neurons per animal per genotype in the DG were selected and a total of 5 animals per genotype were examined. Statistical significance was determined using two-way ANOVA (analysis of variance) followed by Bonferroni's multiple comparison tests. ***$p<0.001$, *$p<0.05$ ns, not significant.

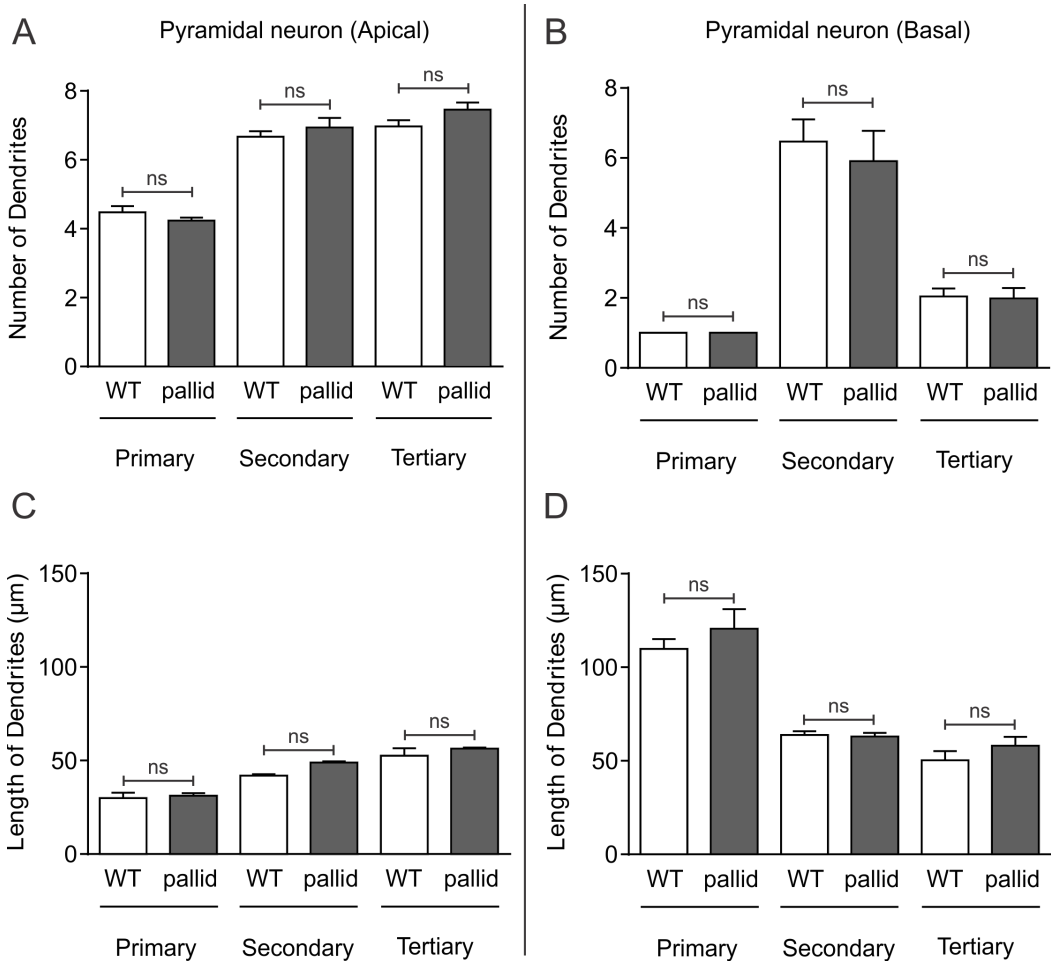

Figure 4.5 Analysis of the primary, secondary and tertiary dendrites show no differences in pyramidal neurons of the wild-type (WT) and pallid mice. Primary, secondary and tertiary dendrites of each pyramidal neuron were analyzed to measure the number of branches and the length of each branch. (A,B) Values represent means ± S.E.M of the number of dendrites from the apical (A) and basal (B) dendrites (C,D) Values represent means ± S.E.M of the length of each dendrite from the apical (C) and basal (D) dendrites. A minimum of 15 neurons per animal per genotype in CA1 areas were selected and a total of 5 animals per genotype were examined. Statistical significance was determined using a two-way ANOVA (analysis of variance) followed by Bonferroni's multiple comparison tests. ns, not significant.

REFERENCE

1. Ghiani CA, Starcevic M, Rodriguez-Fernandez IA, Nazarian R, Cheli VT, Chan LN, Malvar JS, de Vellis J, Sabatti C, Dell'Angelica EC. The dysbindin-containing complex (BLOC-1) in brain: developmental regulation, interaction with SNARE proteins and role in neurite outgrowth. Mol Psychiatry. 2010 Feb;15(2):115, 204-15. PMC2811213.

2. Ma X, Fei E, Fu C, Ren H, Wang G. Dysbindin-1, a schizophrenia-related protein, facilitates neurite outgrowth by promoting the transcriptional activity of p53. Mol Psychiatry. 2011 Nov;16(11):1105-16.

3. Ito H, Morishita R, Shinoda T, Iwamoto I, Sudo K, Okamoto K, Nagata K. Dysbindin-1, WAVE2 and Abi-1 form a complex that regulates dendritic spine formation. Mol Psychiatry. 2010 Oct;15(10):976-86.

4. Sholl DA. Dendritic organization in the neurons of the visual and motor cortices of the cat. J Anat. 1953 Oct;87(4):387-406.

5. Spiegel S, Chiu A, James AS, Jentsch JD, Karlsgodt KH. Recognition deficits in mice carrying mutations of genes encoding BLOC-1 subunits pallidin or dysbindin. Genes Brain Behav. 2015 Nov;14(8):618-24.

6. Kempermann G, Song H, Gage FH. Neurogenesis in the Adult Hippocampus. Cold Spring Harb Perspect Biol. 2015 Sep 1;7(9):a018812.

7. Osen-Sand A, Catsicas M, Staple JK, Jones KA, Ayala G, Knowles J, Grenningloh G, Catsicas S. Inhibition of axonal growth by SNAP-25 antisense oligonucleotides in vitro and in vivo. Nature. 1993 Jul 29;364(6436):445-8.

8. Delgado-Martínez I, Nehring RB, Sørensen JB. Differential abilities of SNAP-25 homologs to support neuronal function. J Neurosci. 2007 Aug 29;27(35):9380-91.

9. Aikawa Y, Lynch KL, Boswell KL, Martin TF. A second SNARE role for exocytic SNAP25 in endosome fusion. Mol Biol Cell. 2006 May;17(5):2113-24.

10. Hirling H, Steiner P, Chaperon C, Marsault R, Regazzi R, Catsicas S. Syntaxin 13 is a developmentally regulated SNARE involved in neurite outgrowth and endosomal trafficking. Eur J Neurosci. 2000 Jun;12(6):1913-23.

11. Martinez-Arca S, Alberts P, Zahraoui A, Louvard D, Galli T. Role of tetanus neurotoxin insensitive vesicle-associated membrane protein (TI-VAMP) in vesicular transport mediating neurite outgrowth. J Cell Biol. 2000 May 15;149(4):889-900.

12. Martinez-Arca S, Coco S, Mainguy G, Schenk U, Alberts P, Bouillé P, Mezzina M, Prochiantz A, Matteoli M, Louvard D, Galli T. A common exocytotic mechanism mediates axonal and dendritic outgrowth. J Neurosci. 2001 Jun 1;21(11):3830-8.

13. Racchetti G, Lorusso A, Schulte C, Gavello D, Carabelli V, D'Alessandro R, Meldolesi J. Rapid neurite outgrowth in neurosecretory cells and neurons is sustained by the exocytosis of a cytoplasmic organelle, the enlargeosome. J Cell Sci. 2010 Jan 15;123(Pt 2):165-70.

14. Salazar G, Craige B, Styers ML, Newell-Litwa KA, Doucette MM, Wainer BH, Falcon-Perez JM, Dell'Angelica EC, Peden AA, Werner E, Faundez V. BLOC-1 complex deficiency alters the targeting of adaptor protein complex-3 cargoes. Mol Biol Cell. 2006 Sep;17(9): 4014-26.

15. Dennis MK, Delevoye C, Acosta-Ruiz A, Hurbain I, Romao M, Hesketh GG, Goff PS, Sviderskaya EV, Bennett DC, Luzio JP, Galli T, Owen DJ, Raposo G, Marks MS. BLOC-1 and BLOC-3 regulate VAMP7 cycling to and from melanosomes via distinct tubular transport carriers. J Cell Biol. 2016 Aug 1;214(3):293-308.

16. Kuster A, Nola S, Dingli F, Vacca B, Gauchy C, Beaujouan JC, Nunez M, Moncion T, Loew D, Formstecher E, Galli T, Proux-Gillardeaux V. The Q-soluble N-Ethylmaleimide-sensitive Factor Attachment Protein Receptor (Q-SNARE) SNAP-47 Regulates Trafficking of Selected Vesicle-associated Membrane Proteins (VAMPs). J Biol Chem. 2015 Nov 20;290(47):28056-69.

CHAPTER 5

Examination of the assembly of BLOC-1 with alternative subunits

ABSTRCT

The BLOC-1 subunits were first identified in liver and in skin fibroblasts, but more recently there has been a growing interest in the role of BLOC-1 in brain. Two of the BLOC-1 subunits, dysbindin and pallidin, have alternatively spliced variants that are expressed in brain, and some of them seem to be human-specific. Some groups have suggested that one ore more of these alternatively spliced variants may not assemble into BLOC-1 and instead function independently of the complex. In addition to these subunit variants generated by alternative splicing, the genomes of humans and other mammals - but not those of other vertebrates - contain an uncharacterized gene encoding a paralog of the cappuccino subunit. To test whether or not these alternative forms of BLOC-1 subunits can assemble into a complex with the other subunits, I utilized a polycistronic plasmid that expresses all eight subunits of BLOC-1 in bacteria. Results show that dysbindin isoform B is able to assemble into a stable complex. In contrast, dysbindin isoform C, a second isoform of pallidin, and the cappuccino paralog are unable to.

INTRODUCTION

Some of the BLOC-1 subunits have alternative isoforms or paralogs. Dysbindin is described to have multiple isoforms, but only three of them, isoforms A, B, and C, have been reported to be expressed in human brains [1]. Dysbindin isoform A is the full-length form of dysbindin and is encoded by a transcript with 10 exons (Fig. 5.1). Dysbindin isoform B is encoded by a transcript that includes exons 1-9, followed by an alternative sequence (Fig. 5.1). Dysbindin isoform C is encoded by a transcript that has a different start codon, within exon 5, and so is truncated in the N-terminal (Fig. 5.1). Because of the initial study linking *DTNBP1* and schizophrenia, the protein expression of the dysbindin isoforms was examined in postmortem brains of normal and schizophrenic individuals. It was reported that protein levels of dysbindin isoforms were decreased in specific brain areas of individuals with schizophrenia in an isoform-dependent manner [1]. As a result, it was suggested that these alternative isoforms may have unique functions in the brain.

A few studies tried to further characterize dysbindin isoform B and C by examining whether these alternative isoforms were part of a complex like BLOC-1, but led to conflicting results. One study reported that isoforms A, B, and C were expressed in mice, and that isoforms B, and C did not assemble into a complex like BLOC-1 [2]. However, another group reported that only isoforms A, and C were expressed in mice, and that isoform C did not assemble into a complex like BLOC-1 [3]. To make matters more confusing, the first study identified by immunoblot analysis, a 35-kDa band as

isoform B and a 32-kDa band as isoform C, while the second study identified a 35-kDa band as isoform C [2,3].

Pallidin is another subunit of BLOC-1 that is reported to have an alternatively spliced isoform. Pallidin isoform 1 is the full-length form and has 172 residues, while pallidin isoform 2 has 101 residues (Fig. 5.2). The transcript encoding pallidin isoform 2 shares only exon 2 with the transcript encoding pallidin isoform 1. In a previous study, it was reported only pallidin isoform 2 was expressed in human brain, suggesting that in the human brain BLOC-1 would have to assemble with pallidin isoform 2 [4].

Lastly, it was reported that the *BCAS4* gene encodes a paralog of cappuccino [5]. In a study that investigated cytosolic protein interactions involving dysbindin, it was reported that the BCAS4 protein was one of several binding partner of dysbindin [6]. In a second unbiased proteomic study, a BCAS4 fusion protein was one of 2,594 baits used to identify protein interaction networks. It was found that the BCAS4 protein associated with all the BLOC-1 subunits except cappuccino, suggesting that BCAS4 might be able to replace cappuccino as a subunit of BLOC-1 [7].

Previously, a polycistronic plasmid was designed with the open reading frame (ORF) encoding all eight subunits of BLOC-1, and two of the subunits, dysbindin and pallidin, had affinity tags, GST and HIS_6 respectively (Fig. 5.3) [8]. In that study, it was shown that when recombinant BLOC-1 was disrupted by removing parts of some subunits, two subcomplexes formed: subcomplex-1, which includes pallidin, cappuccino, and BLOS1, and subcomplex-2, which includes dysbindin, BLOS2, and snapin [8].

To answer the question of whether these alternatively spliced isoforms or paralog could form a stable complex with the other BLOC-1 subunits, I have obtained the polycistronic plasmid that expresses recombinant BLOC-1, and engineered variations of this plasmid where the ORFs of full-length subunits were removed and replaced with those of the alternative subunits. Additionally, the yeast two-hybrid (Y2H) system was used to examine binary interactions of the alternative isoforms. Lastly size-exclusion chromatography analysis was done to determine the size of complexes containing alternative isoforms of dysbindin.

EXPERIMENTAL PROCEDURES

DNA constructs

A modified polycistronic pST39 vector that had the human cDNA sequences of all BLOC-1 subunits, pallidin, dysbindin, BLOS2, cappuccino, snapin, BLOS3, BLOS1 and muted was given as a gift from the laboratories of Drs. James Hurley and Juan Bonifacino [8]. In this polycistronic pST39 vector each, ORF contained the Shine-Dalgarno translational start signal. A histidine (HIS_6)-tag was attached to the N-terminus of pallidin and a glutathione S-transferase (GST)-tag was attached to the C-terminus of dysbindin. Two tobacco etch virus (TEV) protease cleavage sites were placed in the construct, one between pallidin and HIS_6-tag and the other located within dysbindin (between residues 259 and 260).

To replace the full-length ORF of dysbindin, pallidin, and cappuccino with their alternative isoforms or paralogs, the cDNA sequence was designed and ordered for synthesis in the pCR2.1 plasmid by Eurofins. The ORFs of the full-length subunits were removed with appropriate restriction enzymes and replaced with those of the alternative forms in-frame.

Y2H plasmids

The ORFs of dysbindin isoform B, dysbindin isoform C, and pallidin isoform 2, were designed and ordered for synthesis by Eurofin. The ORFs were cloned into the EcoRI/SalI sites of pGBT9 or pGAD424 vectors (Clonetech) to generate the expression constructs used in the Y2H analysis.

The Y2H construct expressing the BCAS4 protein was generated by Marta Starcevic [10]. All other Y2H constructs are described in [9].

Production of recombinant proteins

For production of the recombinant BLOC-1, *E.coli* strain BL21 Star (DE3) (Invitrogen by Thermo Fisher Scientific) was transformed with the appropriate plasmid and cultured in 1.2 liters of 2xYT media [18 g/l tryptone, 11 g/l yeast extract, 5.6 g/l NaCl] in two 2-liter Erlenmeyer flasks. At an optical density at 600 nm (OD 600) of 0.6, protein expression was induced with 0.2 mM isopropyl-beta-D-thiogalactopyranoside (IPTG) for 14-16 hours at 20°C. Pelleted cells, obtained by centrifugation at 6,000 x g for 15 mins, were homogenized in 30 ml of buffer A [20 mM Tris (pH 8.0) and 500 nM NaCl] supplemented with 30 µl of protease inhibitor mixture (Sigma, catalog number P8849), and sonicated using a Branson Sonifier 450 (output #5, 50% duty cycle, 30 seconds on, 15 seconds off, 6 times). Appropriate amounts of triton X-100 were added to bring its concentration of 1%, and the homogenate was incubated in 4°C for 30 min. Lysates were cleared by centrifugation at 6,000 x g for 15 mins.

For the GST-affinity purification, the cleared lysates were incubated for 1 h at 4°C with 300 µL of glutathione-Sepharose 4 Fast-Flow beads (GE Healthcare Life Sciences). The beads were washed once with 30 ml of buffer A with 1% (w/v) triton X-100 and three times with 30 ml of buffer A. The recombinant proteins were eluted 4 times with 700 µL of 20 mM glutathione in 0.1M Tris-HCl, pH 8.0.

For the HIS_6-affinity purification, the cleared lysates were incubated for 1 h at 4°C with 300 µL of Talon® Superflow resin (Clonetech). The beads were washed once with 30 ml of buffer A with 1% (w/v) triton X-100, once with 30 mL of buffer A alone, once with 30 mL of buffer A with 20 mM Imidazole, and three times with 30 ml of buffer A. The recombinant proteins were eluted 4 times with 700 µL of 1 M Imidazole in T1 buffer [300mM NaCl, and 50 mM Na_2PO_4, pH 7.0].

For the sequential affinity purification (tandem purification), *E.coli* strain with the appropriate plasmid was cultured in 3.6 liters of 2xYT media in six 2 liter erlenmeyer flasks and the GST-purification steps were followed as described above. The eluted proteins were pooled together, to a total volume of 8.4 mL. 10 mL of buffer A with 0.1% (w/v) BSA, 1% (w/v) triton X-100, supplemented with protease inhibitors, and 300 µL of Talon® Superflow resin, supplemented with protease inhibiter were added to the eluted GST-purified samples and incubated for 1 hr at 4°C. The beads were washed once with 30 ml of buffer A with 1% (w/v) triton X-100, once with 30 mL of buffer A, once with 30 mL of buffer A with 20 mM Imidazole, and three times with 30 ml of buffer A. The recombinant proteins were eluted 4 times with 700 µL of 1 M Imidazole in T1 buffer.

Antibodies

The monoclonal antibody to pallidin clone (2G5) and the antiserum to anti-muted were described previously in [11]. Polyclonal antibodies against dysbindin, snapin, BLOS3, BLOS2, and BLOS1 were described in [9]. The polyclonal antibody to GST is described in [12]. The

monoclonal antibody to cappuccino (clone 6C3) was purchased from Novus Biologicals. The monoclonal antibody to HIS_6 (catalog number 34660) was purchased from Qiagen. Primary antibodies were used at the following concentrations: rabbit anti-BLOS1 = 1:1,000; rabbit anti-BLOS2 = 1:1,000; rabbit anti-BLOS3 = 1,000; mouse anti-cappuccino = 1:500; rabbit anti-dysbindin = 1:10,000; rabbit anti-GST = 1:5,000; mouse anti-HIS_6 = 1:1,000; rabbit anti-muted = 1:1,000; mouse anti-pallidin = 1:1,000; rabbit anti-Snapin = 1:1,000. Rabbit and mouse HRP horseradish peroxidase-conjugated secondary antibodies (GE Healthcare Life) were used at a concentration of 1:3,000.

Gel electrophoresis and Coomassie-blue staining

Induced bacterial pellets and purified proteins were heated to 65°C for 5 mins and 95°C for 5 mins following the addition of an equal volume of 2X sodium dodecyl sulfate polyacrylamide gel electrophoresis (SDS-PAGE) sample buffer [50 mM Tris-HCl, pH 6.8, 15.6 g/l dithiothreitol, 0.1 g/l bromophenol blue, 4% (w/v) SDS, 12% (w/v) glycerol]. Proteins were resolved by SDS-PAGE on 4-20% Tris-Glycine gels (Invitrogen by Thermo Fisher Scientific). Analysis for the Coomassie-blue staining was carried out as described previously in [13]. Briefly, gels were incubated in Coomassie-blue staining solution [0.1% (w/v) Coomassie brilliant blue R-250, in 30% (v/v) methanol, 10% (v/v) acetic acid in distilled water] with gentle agitation for 1 hour. Coomassie-blue staining solution was removed and the gel was briefly rinsed with distilled water. Stained gels were then incubated in ~100 mL of destaining solution [30% (v/v) methanol, 10% (v/v) acetic acid in distilled water] until the solution became as dark as the gel matrix. The

destaining solution was then discarded, and gels were incubated in new destaining solution until the gel had a clear background. Gels were imaged on the ChemiDoc Imaging System (Biorad).

Immunoblotting analysis

Proteins were resolved by SDS-PAGE as described above and were transferred onto polyvinylidene difluoride membranes (BioRad) at 100 V for 60 mins at 4°C in transfer buffer [25 mM Tris-base, 192mM glycine, 20% (v/v) methanol]. The membranes were incubated in blocking buffer [5% (w/v) non-fat dry milk and 0.2% (w/v) Tween® 20 in phosphate-buffered saline (PBS)] overnight at 4°C. Membranes were then incubated with primary antibody diluted in blocking buffer for 1 hour, washed 3 times for 10 min in PBS, incubated for 30 mins at room temperature with appropriate secondary antibody diluted in blocking buffer, and again washed 3 times for 10 min in PBS. Detection was performed using the ECL Prime^{TM} Western Blotting Detection Reagent (GE Healthcare Life Sciences) according to the manufacturer's instructions. For quantitative analysis of protein expression levels, enhanced chemiluminescence signals were captured on the ChemiDoc Imaging System (Biorad) and digitally integrated using the National Institutes of Health Image Software (Image J, http://rsb.info.nih.gov/ij/). For the comparison of relative protein levels, the mean pixel intensity was measured for each band using the same area for bands on the same membrane. The pixel intensity of the background was subtracted from the pixel intensity of each band on the same membrane. Background-corrected values were then divided by the background-corrected values of the affinity tags (GST or HIS_6) used for purification. Statistical significance was determined by Student's T-test using the GraphPad Prism 5.0b (GraphPad Software). Because multiple tests were done, the threshold for

significance was made more stringent by dividing the $\alpha = 0.05$ by number of tests. This new α was used as the threshold for significance.

Silver staining

Analysis with silver staining was carried out as described previously in [13]. Proteins were resolved by SDS-PAGE as described above. In each step, gels were incubated with gentle agitation. Gels were incubated in 50% (v/v) ethanol in water for 20 mins. This step was repeated 2 more times for a total of three pretreatment steps. Gels were then incubated in deionized water for 5 mins. Deionized water was discarded and gels were incubated in 100 mL of thiosulfate solution [0.02% (w/v) $Na_2SO_5 \cdot 5H_2O$ in water] for exactly 1 min, washed with deionized water three times for 20 sec each and incubated in silver nitration solution [0.2%(w/v) $AgNO_3$ with 75 µL of 37% (w/v) formaldehyde per 100 mL of water] for 20 mins. The container was covered with aluminum foil to protect from light exposure. Gels were then washed with deionized water, three times for 20 sec each, and incubated in developer solution [6% (w/v) Na_2CO_3, 0.0004% (w/v) $Na_2SO_5 \cdot 5H_2O$, 50 µL of 37% formaldehyde per 100 mL of water] for $\leq$ 10 mins until the protein bands of interest became visible. Gels were then washed with deionized water three times for 30 sec each, incubated in a solution [50% (v/v) methanol, 12% (v/v) acetic acid in deionized water] for 10 mins, and then incubated in 50% (v/v) methanol in deionized water. Gels were then removed from the 50% (v/v) methanol solution, placed on the platform of the ChemiDoc Imaging System (Biorad) and imaged.

Size-exclusion chromatography analysis

After purification of the recombinant BLOC-1 with the glutathione-Sepharose 4 Fast-Flow beads, 4 μL of TEV protease (Invitrogen) were added to the purified samples and the purified samples were dialyzed against dialysis buffer [50 mM Tris (pH 7.4), 300 mM NaCl and 5 mM β-mercaptoethanol]. The GST tag was removed from the digested sample by incubating with 100 μL of glutathione-Sepharose 4 Fast-Flow beads. For size-exclusion chromatography, 500 μL of purified protein sample were loaded onto a Superose 6 column connected to a Fast Protein Liquid Chromatography system (Amersham Biosciences). Proteins were eluted at 4°C in FPLC buffer [0.4 M NaCl, 0.05 M Tris (pH 7.4), 1 mM EDTA, 1 mM tris(2-carboxyethyl) phosphine, and 5% (v/v) glycerol] at a flow rate of 0.4 ml/min, collected into 0.4 ml fractions, and analyzed by silver staining and immunoblotting. Calibration of the column was performed using blue dextran (Sigma), to determine the exclusion volume, and the following standard proteins (Stokes radii in parentheses): bovine thyroglobulin (85Å, Sigma), horse spleen apoferritin (61Å, Sigma), bovine serum albumin (36Å, Fisher Scientific), carbonic anhydrase (24Å, Sigma), and horse heart cytochrome c (17Å, Sigma).

Y2H analysis

Expression constructs were co-transformed into *Saccharomyces cerevisiae* strain AH109 using the lithium acetate method [14], and double transformants were selected in SD minimal medium [0.7% (w/v) yeast nitrogen base without amino acids (Sigma) and 2 % (w/v) glucose, pH 5.5] supplemented with the appropriate nutritional requirements (adenine and histidine) except leucine and tryptophan. Cell suspensions of each co-transformant (OD 600 = 0.4) were spotted onto control plates containing adenine and histidine as well as on and selective plates lacking

histidine and lacking or containing 5 mM 3-amino-1,2,4-triazole (3-AT). Plates were incubated for 3 days at 30°C before imaging on the ChemiDoc Imaging System (Biorad).

RESULTS

Expression and purification of recombinant BLOC-1

After receiving the polycistronic plasmid that expressed recombinant BLOC1, I wanted to verify that I was able to express and purify all eight subunits of BLOC-1. To this end, *E. Coli* was transformed with this polycistronic plasmid, and immunoblot analysis was done using antibodies to the eight subunits of BLOC-1 (Fig. 5.4). From here on, the recombinant BLOC-1 expressed from this plasmid will be referred to as BLOC-1(WT). To determine if a complex was forming, I performed tandem purification of the BLOC-1(WT) using both GST- and HIS_6- tags. The tandem purification was optimized and is described in further detail under Experimental Procedures. Coomassie-blue staining of the tandem purified BLOC-1(WT) showed eight bands, and immunoblot analysis was used to identify the eight bands as the BLOC-1 subunits (Fig. 5.5).

Dysbindin isoform B, but not isoform C, was able to replace dysbindin isoform A to form a stable complex.

Next, I designed new constructs that replaced the ORF encoding the full-length dysbindin with those encoding the alternative forms of dysbindin, isoform B or C, in-frame. Recombinant BLOC-1 with dysbindin isoform B will be referred to as BLOC-1(IsoB) and recombinant BLOC-1 with dysbindin isoform C will be referred to as BLOC-1(IsoC). Because the TEV site had been originally designed within the dysbindin subunit in BLOC-1(WT), I made a new construct where the TEV site was moved to the sequence between dysbindin and the GST tag. The recombinant BLOC-1 expressed from this new construct will be referred to as BLOC-1

(IsoA). All eight subunits of BLOC-1 were co-expressed from these three polycistronic plasmids in *E. Coli* (Fig. 5.6). GST-, HIS_6- and tandem purification of BLOC-1(IsoB) yielded comparable amounts of each BLOC-1 subunit (Fig. 5.6) and quantification of the signal intensity from the immunoblots to the BLOC-1 subunits showed equal amounts of almost every subunits after GST- (Fig 5.7) or HIS_6-purification (Fig. 5.8). Although not statistically significant, it appeared that there was an increase in the protein levels of the cappuccino subunits after GST purification of BLOC-1(IsoB) (Fig. 5.7). However, after the affinity tags were cleaved by TEV protease, the sample dialyzed, and the GST tag removed by incubating again with glutathione beads, the levels of cappuccino in BLOC-1(IsoB) were comparable to those in BLOC-1(IsoA), suggesting that there may have been a weak or transient interaction between BLOC-1(IsoB) and an additional molecule of cappuccino (Fig. 5.9). After GST- and HIS_6-purification of BLOC-1(IsoC), all subunits of BLOC-1 were detected, but after tandem purification of BLOC-1(IsoC), the cappuccino subunit was absent (Fig. 5.6). Quantification of the signal intensity from the immunoblots to the BLOC-1 subunits showed signficant decreases in some of the BLOC-1 subunits in both GST- (Fig. 5.10) and others in the HIS_6-purifications (Fig. 5.11) of BLOC-1(IsoC), indicating that BLOC-1(IsoC) does not form a stable complex.

To examine direct interactions of dysbindin isoforms B and C with subunits known to interact with dysbindin isoform A, the Y2H system was used. Dysbindin isoforms were fused to the Gal4 DNA-activation domain, and dysbindin isoforms B and C were found to interact with pallidin, snapin and muted, the same subunits that dysbindin isoform A interacted with (Fig. 5.12).

Because it seemed that BLOC-1(IsoB) was forming a stable complex and that BLOC-1(IsoC) might be forming a sub-complex, size-exclusion chromatography analysis was performed to determine the size of BLOC-1(IsoB) and BLOC-1(IsoC). In an initial experiment with the GST-purified BLOC-1(IsoA), a clear species could not be resolved, but instead BLOC-1 subunits, particularly dysbindin-GST, were detected in a number of fractions, suggesting that the GST tag was dimerizing. To resolve this issue, the GST tag was removed by digestion with TEV protease. Upon digestion, there was a shift in apparent molecular weight for all three dysbindin isoforms (Fig. 5.13, arrows and arrowheads). The digested BLOC-1(IsoA), BLOC-1(IsoB) and BLOC-1(IsoC) were analyzed by size-exclusion chromatography, and the species in the fractions were analyzed by SDS-PAGE followed by silver staining and immunoblot with antibodies to selected BLOC-1 subunits. For BLOC-1(IsoA), the bulk of BLOC-1 subunits eluted from the column in fractions corresponding to a Stokes radius of ~98 Å (Fig. 5.12), similar to the reported Stokes radius (~94 Å) of BLOC-1 in liver [9]. Several of the BLOC-1 subunits eluted in later fractions (Fig. 5.14), indicating that not every molecule of BLOC-1(IsoA) subunits assembled into a complex. For BLOC-1(IsoB), the bulk of BLOC-1 subunits eluted from the column in fractions corresponding to a Stokes radius of ~89 Å (Fig. 5.15). Like BLOC-1(IsoA), several of the BLOC-1 subunits of BLOC-1(IsoB) also eluted in later fractions (Fig. 5.15). Lastly for BLOC-1(IsoC), there was no clear fraction that included all the BLOC-1 subunits (Fig. 5.16). Instead, the different subunits were eluting in different fractions.

Pallidin isoform 2 could not replace pallidin isoform 1 to form a stable complex with the other BLOC-1 subunits.

To determine if the alternative isoform of pallidin could replace the full-length pallidin and form a complex with the other BLOC-1 subunits, I designed a new construct where the ORF encoding pallidin isoform 1 was replaced with that of pallidin isoform 2. Recombinant BLOC-1 with pallidin isoform 2 will be referred to as BLOC-1(Iso2). All subunits of BLOC-1 were co-expressed from the polycistronic plasmid with the ORF encoding pallidin isoform 2, but the protein levels of cappuccino appeared to be less than the cappuccino levels expressed from the WT polycistronic plasmid, already indicating that the steady-state protein levels were disrupted in BLOC-1(Iso2) (Fig. 5.17). After GST-purification of BLOC-1(Iso2), subunits of subcomplex-2 were present, but the protein levels of the other subunits appeared to be decreased or absent (Fig. 5.17). After HIS_6-purification of BLOC-1(Iso2), subunits of subcomplex-2 were detected along with pallidin isoform 2, muted and BLOS3 (Fig. 5.17). After tandem purification, none of the BLOC-1 subunits were detected, except for a small amount of dysbindin (Fig. 5.17). These results suggested that pallidin isoform 2 may have a weak interaction with subcomplex-2 but not be able to form a stable complex. Quantification of the signal intensity from the immunoblots to the BLOC-1 subunits after GST purification (Fig. 5.18) and HIS_6-purifications (Fig. 5.19) confirmed these observations. Analysis of the binary interactions between pallidin isoform 2 with subunits known to interact with pallidin isoform 1 showed that the former does not interact with any of the BLOC-1 subunits that the latter interacted with (Fig. 5.20), which further supported that BLOC-1(Iso2) does not form a stable complex.

The BCAS4 protein could not replace cappuccino to form a stable complex with the other BLOC-1 subunits.

To determine if the paralog of cappuccino, the BCAS4 protein, could replace the cappuccino subunit, the ORF encoding cappuccino was replaced with that encoding the BCAS4 protein. As a negative control, the ORF encoding cappuccino was removed and not replaced with anything. Recombinant BLOC-1 with the BCAS4 protein will be referred to as BLOC-1(BCAS4) and the recombinant BLOC-1 without cappuccino will be referred to as BLOC-1(-CNO). All seven subunits of BLOC-1 and the BCAS4 protein were co-expressed from the polycistronic plasmid in *E. Coli* (Fig. 5.21). However after GST-purification of BLOC-1(BCAS4), little to no amounts of BLOC-1 subunits were detected and in the tandem purification of BLOC-1(BCAS4), none of the BLOC-1 subunits were purified (Fig 5.21). Analysis of the binary interaction between BCAS4 and subunits known to interact with cappuccino showed that BCAS protein interacts with pallidin, but not with snapin and BLOS1 (Fig. 5.22)

DISCUSSION

I have used a heterologous expression system to determine if alternative isoforms of BLOC-1 can form a stable complex with the other BLOC-1 subunits. Of the alternative isoforms examined, only dysbindin isoform B appeared to form a complex with the other BLOC-1 subunits. After GST-, HIS_6-, and tandem-purification of BLOC-1(IsoB), all BLOC-1 subunits were detected. By size-exclusion chromatography analysis, BLOC-1(IsoB) was estimated to have a Stokes radius of ~89.Å, which is less than the Stokes radius of BLOC-1(IsoA). Dysbindin isoform B has a difference of 48 residues from dysbindin isoform A. It is unlikely that the 48 residue difference between isoform A and B could be causing this difference of 9 Å. Instead, it is possible that residues in dysbindin isoform B that differ from dysbindin isoform A are causing the complex to form a more spherical shape, hence causing BLOC-1(IsoB) to elute in later fractions. This difference in conformation could mean that BLOC-1(IsoB) might have functional differences from BLOC-1(IsoA). Little is known about the function of dysbindin isoform B. More recently, the laboratory of Qi Xu in China has published three studies focused on characterization of dysbindin isoform B. When GFP-tagged dysbindin isoforms were transfected into COS1 cells, the dysbindin isoform B was shown to form aggresomes at perinuclear regions whereas dysbindin isoforms A and C were diffused in the cytoplasm [15]. A mouse model was engineered to expressed the endogenous human dysbindin isoform B, and it was reported that dysbindin isoform B also aggregated in the neurons of these mice [16]. Lastly, in these mice that over-expressed human dysbindin isoform B, the expression of the other BLOC-1 subunits were decreased, and the subunits were found to be aggregated into deposits colocalized to dysbindin

isoform B [17]. As a result, they have suggested that dysbindin isoform B forms toxic aggregation that co-aggregates with BLOC-1 subunits, and in turn impairs the cognitive function of schizophrenia patients. The interpretation of these results should be approached with caution for two reasons. The first is the issue with the association between the gene encoding dysbindin, *DTNBP1*, and schizophrenia. As discussed in Chapter 1, *DTNBP1* is no longer considered a top candidate gene for schizophrenia by many leading researchers in the field [18]. However, many groups still hold to the view that it is, even though the genetic studies no longer support their view. The second is that all these experiments were over-expressions of dysbindin isoform B. It can be argued that dysbindin isoform A and C did not aggregate when over-expressed, but as some of my results indicate, the complex that dysbindin isoform B forms may have a different shape than BLOC-1, which might make dysbindin isoform B more susceptible to aggregation. It should be noted that the study did find that over-expression of dysbindin isoform B affected expression of the other BLOC-1 subunits, further supporting the fact that dysbindin isoform B and the BLOC-1 subunits have an interaction.

Dysbindin isoform C, on the other hand, was not able to form a stable complex. Although dysbindin isoform C was able to directly interact with the same subunits as dysbindin isoform A, purification of the BLOC-1(IsoC) did not yield equal amounts of all the BLOC-1 subunits suggesting that a stable complex was not formed. It was previously shown that the coiled-coil region of dysbindin was enough to interact with pallidin, snapin, and muted [19], so it was not surprising that dysbindin isoform C, which has the coiled-coil region, was able to interact with pallidin, snapin and muted. The size-exclusion chromatography analysis made it clear that a BLOC-1(IsoC) was not forming a stable complex. In a recent study from Wei Li's group, the

function of dysbindin isoform C was examined. In this study, they used the sandy mouse, which has a mutation in the gene encoding dysbindin, and the muted mouse, which has a mutation in the gene encoding muted. They showed by sedimentation velocity analysis, that the dysbindin isoform C was not co-sedimenting with known subunits of BLOC-1 [3]. Hence they concluded that dysbindin isoform C was not part of BLOC-1 and showed by immunoblot analysis that the band they identified as dysbindin isoform C was still expressed in the muted mouse. Because of these results, they argued that the muted was null for dysbindin isoform A, but not for dysbindin isoform C, and so could be used as a model to study the function of dysbindin isoform C specifically. They reported that analysis of the muted and sandy mouse suggests that dysbindin isoform C, but not A, regulates adult hippocampal neurogenesis in the dentate gyrus [3]. It is true that it is difficult to examine the functions of these different isoforms and that there is not a simple experimental setup to do so. However, in the experimental setup of this study there is a clear assumption that is not addressed. It is assumed that the different background strain of the sandy, in the DBA/2J background, and muted, in the CHMU/Le background, mouse strains were not causing the differences that they see.

Purification of BLOC-1 subunits with pallidin isoform 2 indicated that pallidin isoform 2 is unable to form a stable complex. HIS-purification of these subunits was able to purify parts of subcomplex-2 (dysbindin, BLOS2, and snapin), but GST purification only purified subcomplex-2 and not pallidin isoform 2, suggesting that pallidin isoform 2 may have a weaker or transient interaction with subcomplex-2. The Y2H analysis showed that pallidin isoform 2 was not even able to interact with the subunits that pallidin isoform 1 interacted with. From these findings, combined with the previous report that only pallidin isoform 2 is expressed in human

brains, one might think that BLOC-1 may not form in the human brain. However, it has recently come to light that many of the reported results from the first author (Andrew R. Cullinane) of this study had been falsified [4, 20]. In light of this recent revelation, the findings from this report need to be taken with a extreme caution. It is likely that BLOC-1 does exist in the human brain as a stable complex with pallidin isoform 1. In fact, it is reported in a new database (The Human Protein Atlas) that the transcript and protein of pallidin isoform 1 is expressed in the human brain [21].

Lastly, the BCAS4 protein was not able to replace the cappuccino subunit to form a stable complex. One possibility is that the BCAS4 protein is an interacting partner of the whole complex. However, in the previous study that used the BCAS4 protein as a bait, it was shown that the BCAS4 protein interacts with all the BLOC-1 subunits except cappuccino [7]. If the BCAS4 protein was just an interacting parter of the whole BLOC-1, cappuccino should also have been present. The other possibility is that the BCAS4 protein does form a complex with BLOC-1 subunits, but requires additional subunits. In the proteomic study, there were four other protein encoded by the genes *ATG4A*, *SRCIN1*, *PKD2*, and *LOH12CR1* that were also identified as interacting with the BCAS4 protein [7]. It is possible that the BCAS4 protein forms a complex with some of the BLOC-1 subunits in addition to one or more of these 4 proteins. Further analysis is required to address this question.

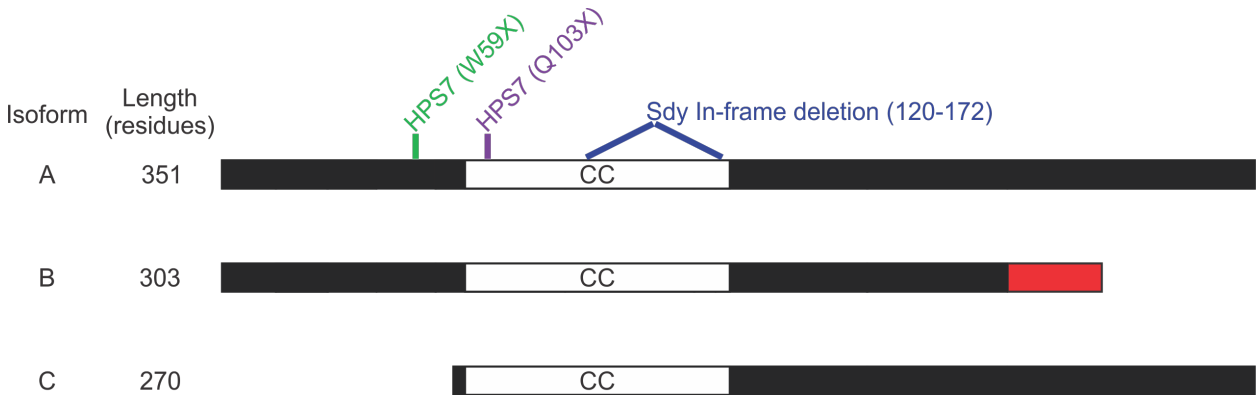

Figure 5.1 Schematic of previously characterized human dysbindin isoforms A-C. Dysbindin is encoded by the gene *DTNBP1* and has multiple splice variants. Dysbindin isoform A is the full-length form with 351 amino acids, and its transcript includes 10 exons. The transcript that encodes dysbindin isoform B has exons 1-9, but has an alternative sequence encoding alternative residues in the C-terminal (shown in red). The transcript encoding dysbindin isoform C is predicted to have a downstream start codon within exon 5 and as a result it includes parts of exon 5 and exons 6-10. There are two patients with Hermansky-Pudlak Syndrome type 7 (HPS7) with nonsense mutations in the gene encoding dysbindin (location of the mutations are indicated green and purple). The sandy mouse has an in-frame deletion in the gene encoding dysbindin (location equivalent to the mouse gene indicated in blue). CC, predicted coiled coil region.

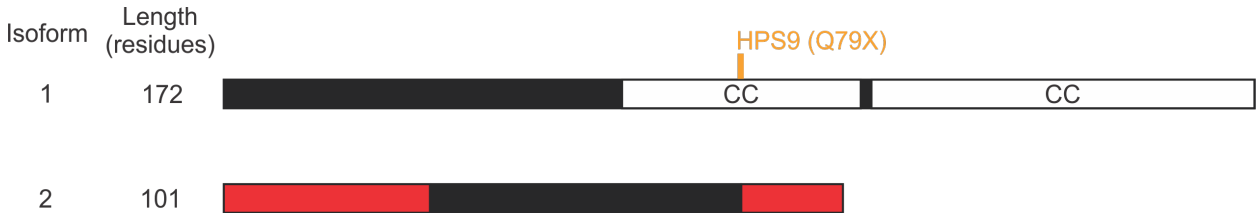

Figure 5.2 Schematic of previously characterized human pallidin isoforms 1 and 2. Pallidin isoform 1 is encoded by the gene *BLOC1S6,* and is the full-length form with 172 residues. The transcript that encodes pallidin isoform 1 has 5 exons. A splice variant that only shares exon 2 with the full-length form, encodes pallidin isoform 2, which has 101 residues. The residues in pallidin isoform 2 that differ from pallidin isoform 1 are represented by the red bars. There is one patient with Hermansky-Pudlak Syndrome type 9 (HPS9) reported to have a nonsense mutation in *BLOC1S6* (location indicated in orange). CC, predicted coiled coil regions.

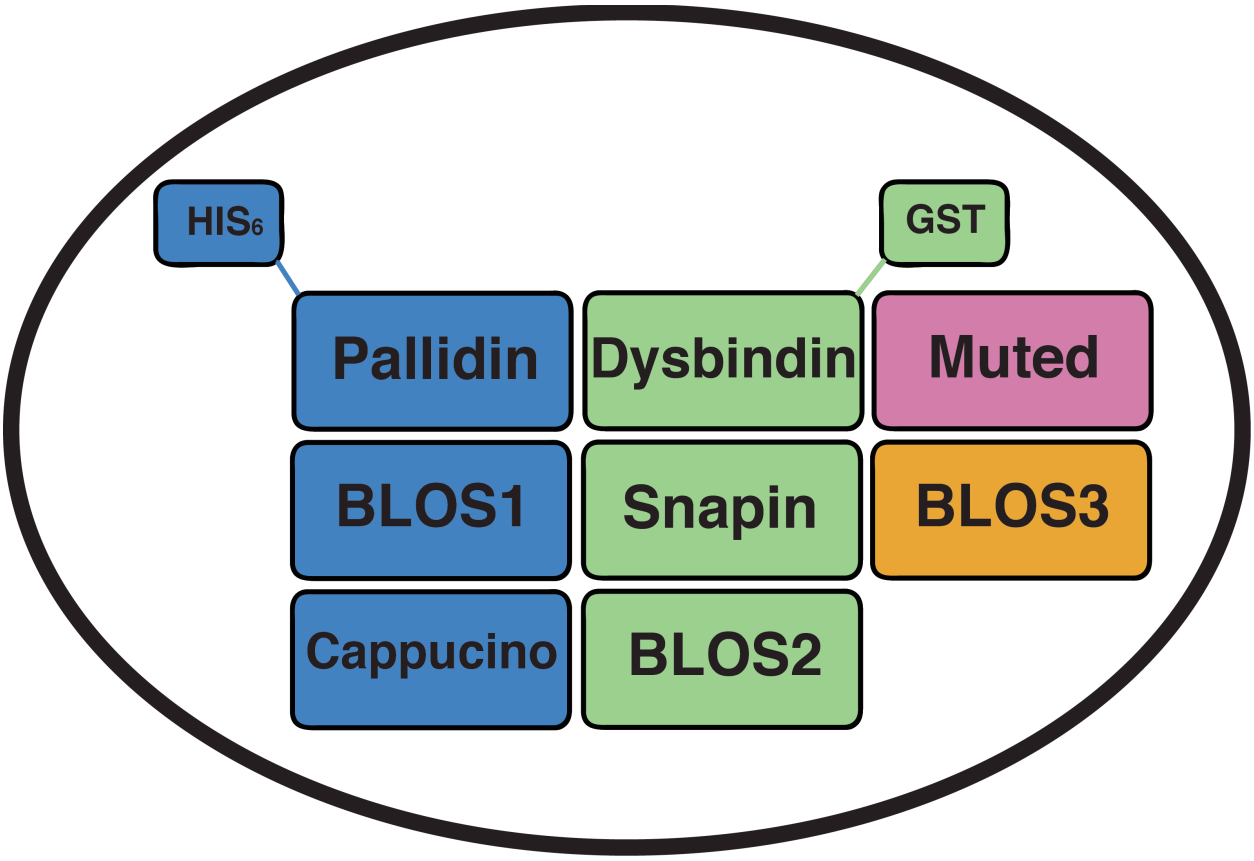

Figure 5.3 Schematic of BLOC-1(WT) expressed from a polycistronic plasmid. All eight subunits of BLOC-1 were expressed from a polycistronic plasmid. The pallidin subunit was fused with a HIS_6- affinity tag on the N-terminal and the dysbindin subunit was fused with a GST-affinity tag on the C-terminal. Two subcomplexes have been described [13]: subcomplex-1, which includes pallidin, BLOS1, and cappuccino (shown in blue) and subcomplex-2, which includes dysbindin, snapin, and BLOS2 (shown in green). The other two subunits, muted (pink) and BLOS3 (orange) are thought not to be part of any subcomplex.

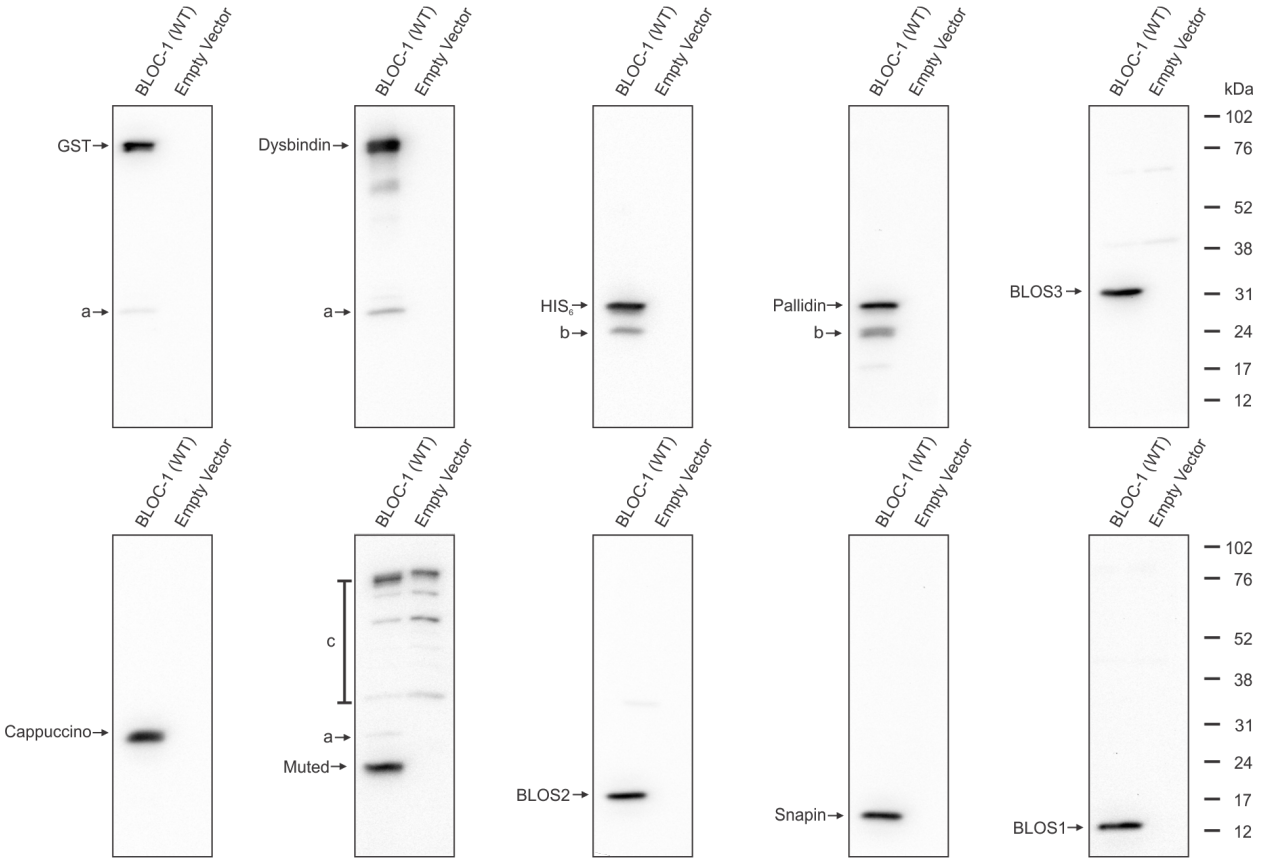

Figure 5.4 Expression of recombinant BLOC-1 subunits in *E. coli*. *E. coli,* transformed with a polycistronic plasmid that expresses all eight subunits of BLOC-1, was cultured in 2xYT media, and protein expression was induced with IPTG. Pelleted cells were obtained by centrifugation and boiled in the presence of SDS-PAGE sample buffer. Immunoblot analysis was done to demonstrate that the bacteria expressed all eight subunits. *E.coli* with an empty vector was used as a negative control. The band labeled as "a" is a degradation product of Dysbindin-GST and likely is GST itself. The band labeled as "b" is likely a degradation product of HIS_6-pallidin and is detected in the immunoblots for HIS_6 and pallidin. The multiple bands labeled as "c" likely correspond to bacterial proteins cross-reacting with the anti-muted antiserum, which was used without purification.

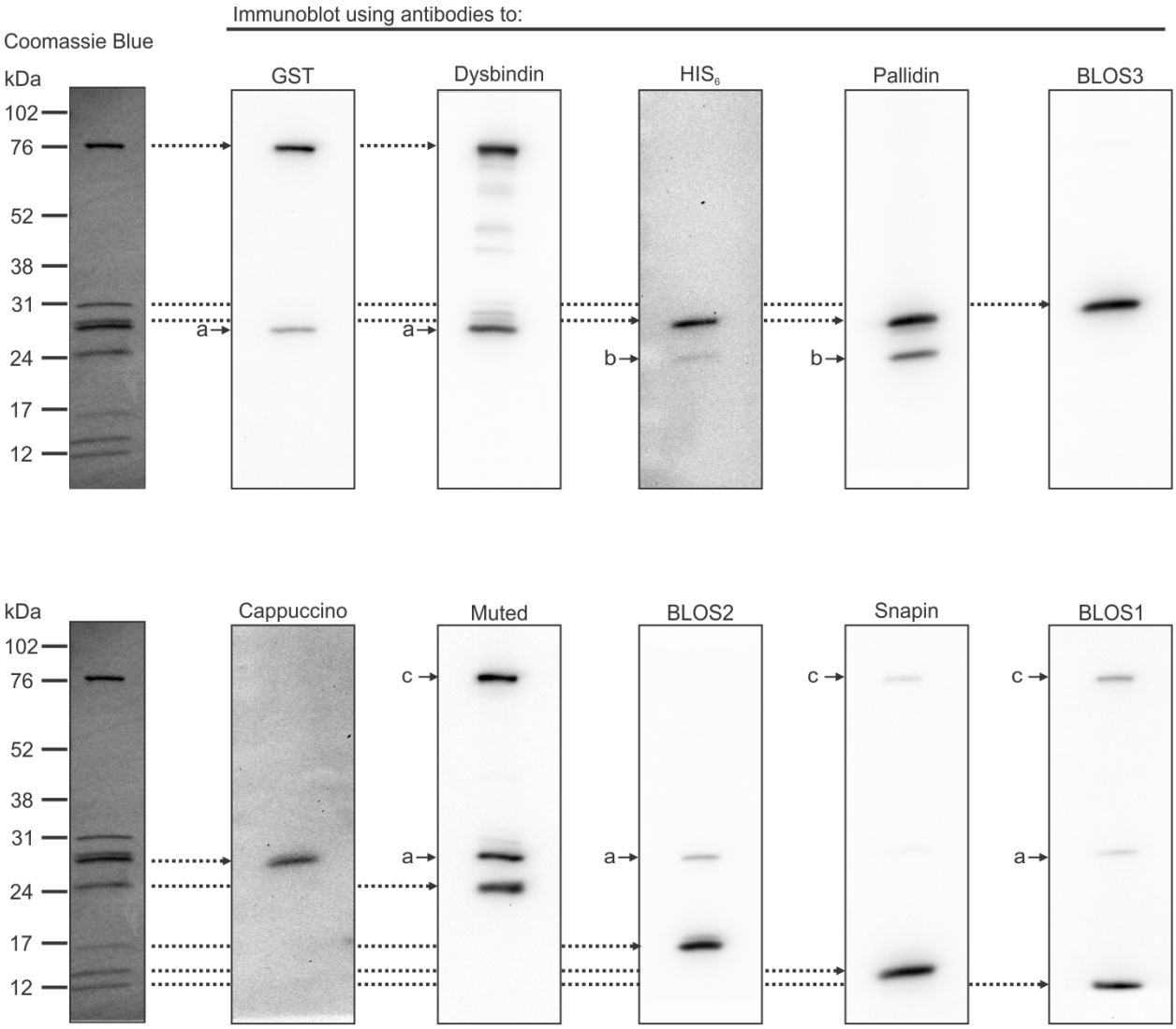

Figure 5.5 Coomassie Blue and immunoblot analysis of the BLOC-1 subunits after tandem purification (GST>HIS$_6$). The purification of recombinant BLOC-1 was optimized using a tandem purification method (GST-purification followed by HIS-purification). *E. coli,* transformed with a polycistronic plasmid that expresses all eight subunits of BLOC-1, was cultured in 2xYT media and protein expression was induced with IPTG. Pelleted cells were lysed and the cleared lysates were incubated with glutathione-sepharose beads. Proteins were eluted and rebound to Talon resins. Proteins were eluted again and boiled in the presence of SDS-PAGE sample buffer. Coomassie Blue staining of the purified recombinant BLOC-1 shows 8 distinct bands. Each of the bands visible in the Coomassie was identified as one of the eight subunits of BLOC-1 by immunoblot analysis. a: GST degradation product of Dysbindin-GST (containing the GST moiety), which cross-reacted with several of the antibodies raised against GST-fusion proteins. b: degradation product of HIS$_6$-pallidin. c: Dysbindin-GST.

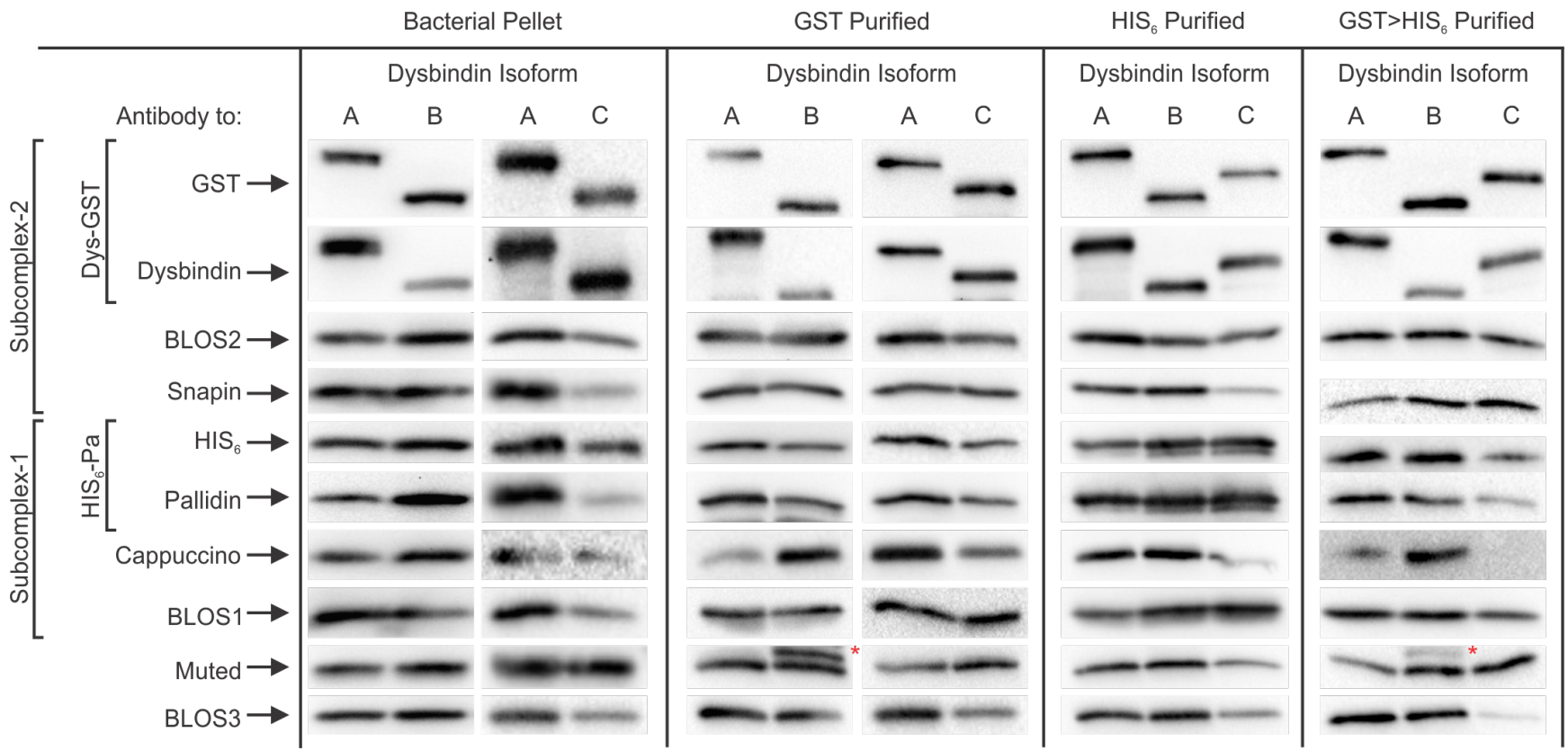

Figure 5.6 Representative immunoblot analyses of BLOC-1(IsoA), BLOC-1(IsoB), and BLOC-1(IsoC). The open reading frame (ORF) encoding dysbindin isoform A was replaced with those encoding dysbindins isoform B or C, each of them fused in frame with that encoding GST. Bacterial pellets from *E. Coli* transformed with these constructs were examined by immunoblot analysis for the expression of BLOC-1 subunits. BLOC-1(IsoA), BLOC-1(IsoB) and BLOC-1(IsoC) were purified by the GST tag alone, the HIS_6 tag alone, and by both (GST>HIS_6 tandem purification), and the representative immunoblots of those purified samples are shown above. *: A degradation product of Dysbindin(IsoformB)-GST detected by the anti-muted antiserum. Dys-GST: Dysbindin-GST, HIS_6-Pa: HIS_6-pallidin

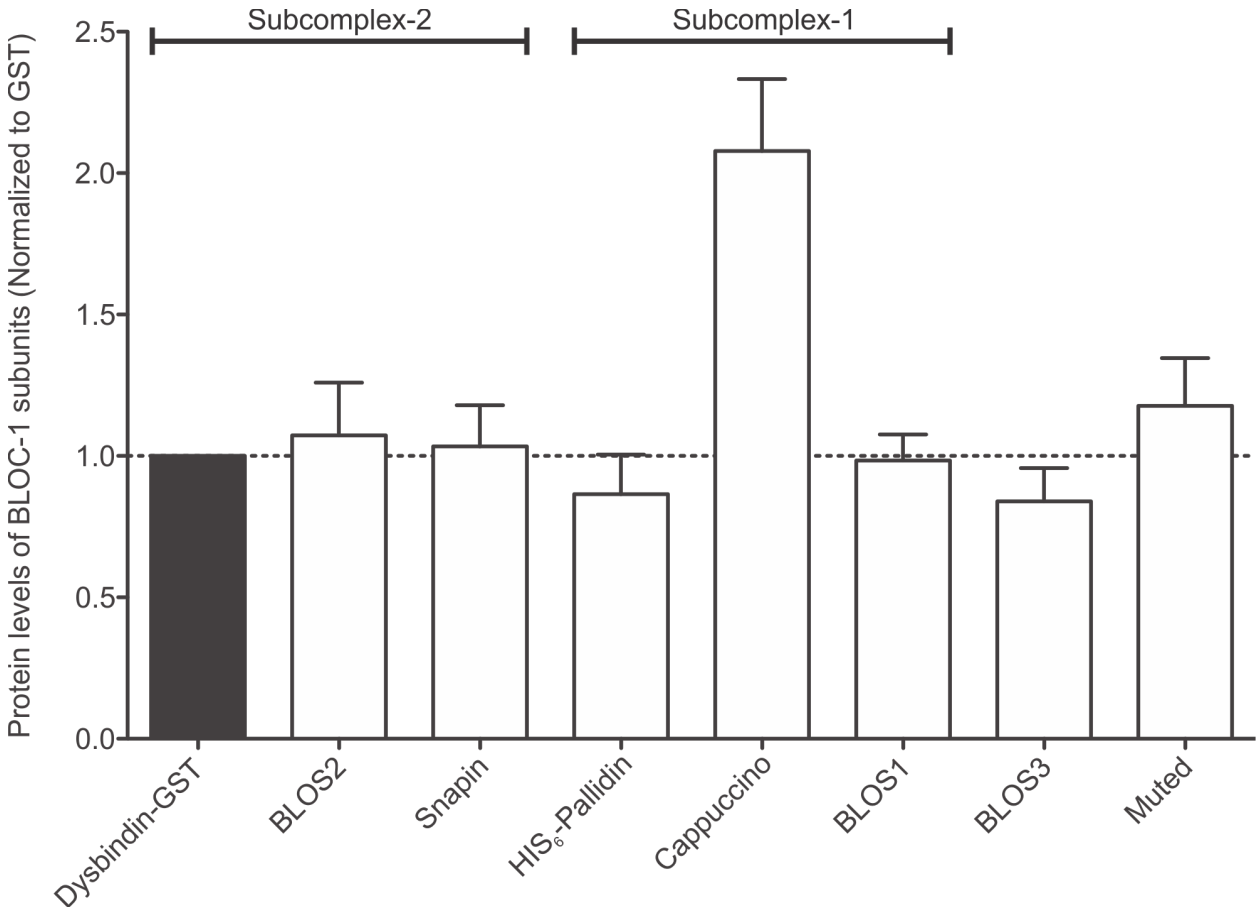

Figure 5.7 Quantification of signal intensity of BLOC-1(IsoB) after GST-purification. BLOC-1(IsoA) and BLOC-1(IsoB) were purified on glutathione-sepharose beads. Protein levels of each subunit in the purified samples were analyzed by immunoblotting. The signal intensity of the bands from the immunoblots was quantified and background corrected. To quantify relative yields, the signal intensity of each subunit was divided by the signal intensity of the Dysbindin-GST subunit. Then, these normalized ratios of each BLOC-1(IsoB) subunit were divided by the normalized ratios of the corresponding subunit of BLOC-1(IsoA). Bars and error bars represent means ± S.E.M. of 5 separate sets of GST-purifications. A one sample t-test was performed for each subunit. None of the tests reached statistical significance upon correction for multiple testing.

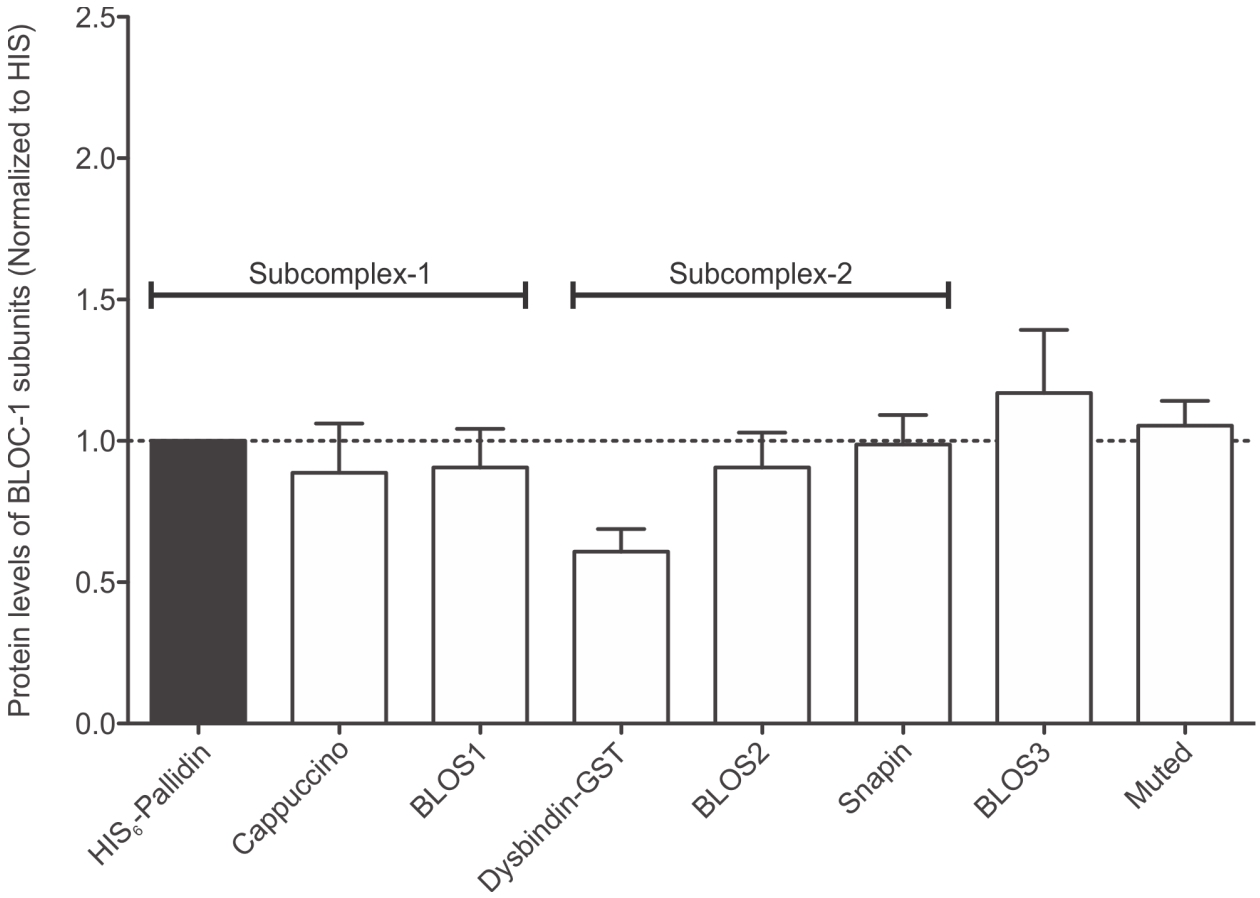

Figure 5.8 Quantification of signal intensity of BLOC-1(IsoB) after HIS_6-purification. BLOC-1(IsoA) and BLOC-1(IsoB) were purified on the Talon resins. Protein levels of each subunit in the purified samples were analyzed by immunoblotting. The signal intensity of the bands from the immunoblots was quantified and background corrected. To quantify relative yields, the signal intensity of each subunit was divided by the signal intensity of the HIS_6-Pallidin subunit. Then, these normalized ratios of each BLOC-1(IsoB) subunit were divided by the normalized ratios of the corresponding subunit of BLOC-1(IsoA). Bars and error bars represent means ± S.E.M. of 5 separate sets of HIS_6-purifications. A one sample t-test was performed for each subunit. None of the tests reached statistical significance upon correction for multiple testing.

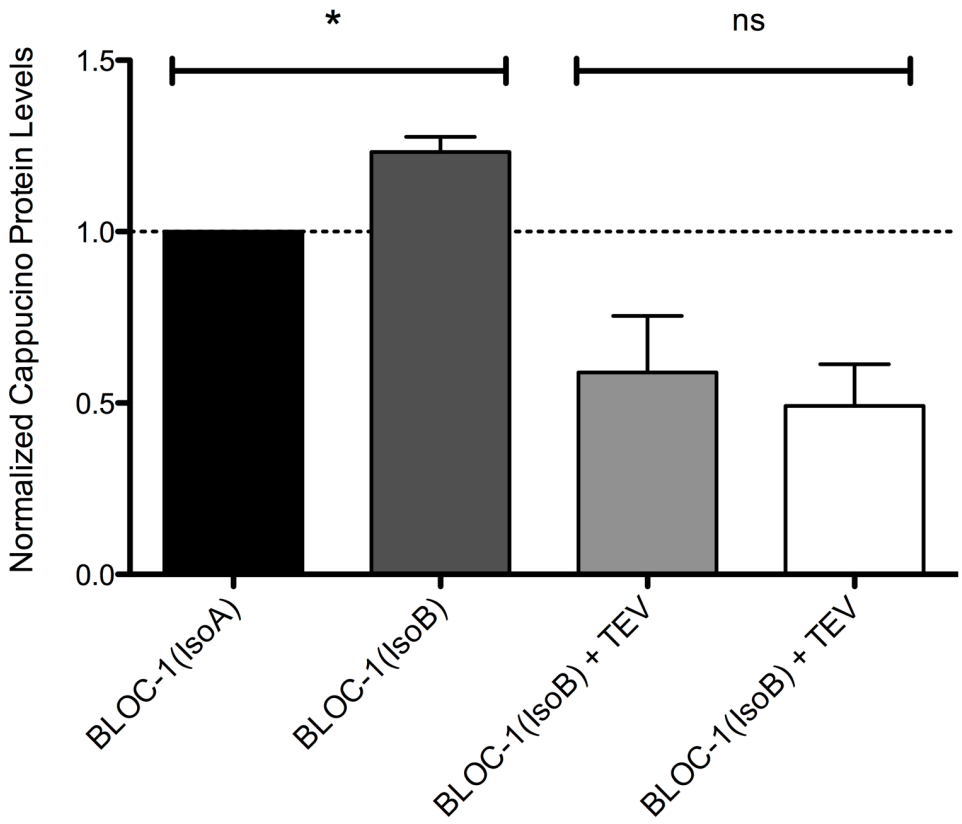

Figure 5.9 Quantification of signal intensity of cappuccino from GST-purified BLOC-1(IsoA) and BLOC-1(IsoB). BLOC-1(IsoA) and BLOC-1(IsoB) were purified on glutathione-sepharose beads. Samples were incubated with Tobacco Etch Virus (TEV) protease and dialyzed to cleave the GST tag from dysbindin. After dialysis, the samples were incubated again with glutathione-sepharose beads to remove the GST tag. The resulting TEV-treated samples, together with control samples not treated with protease, were analyzed by immunoblotting using antibodies to cappuccino, BLOS1, and BLOS3. The signal intensities of the bands from the immunblots to cappuccino, BLOS3 and BLOS1 were quantified and each value background corrected. Because the GST tag was removed, the signal intensities of BLOS3 and BLOS1 were used to normalize for relative yield. The signal intensity of cappuccino was divided by the averaged signal intensity of BLOS3 and BLOS1. The normalized cappuccino signal ratios were then divided by those of the undigested BLOC-1(IsoA). Bars and error bars represent means ± S.E.M. of 3 separate sets of GST-purifications. A one sample t-test was performed for cappuccino levels of BLOC-1(IsoB). *$p<0.05$. A Student's t-test was performed for comparison of normalized cappuccino levels of BLOC-1(IsoA) + TEV versus BLOC-1(IsoB) + TEV. ns, not significant.

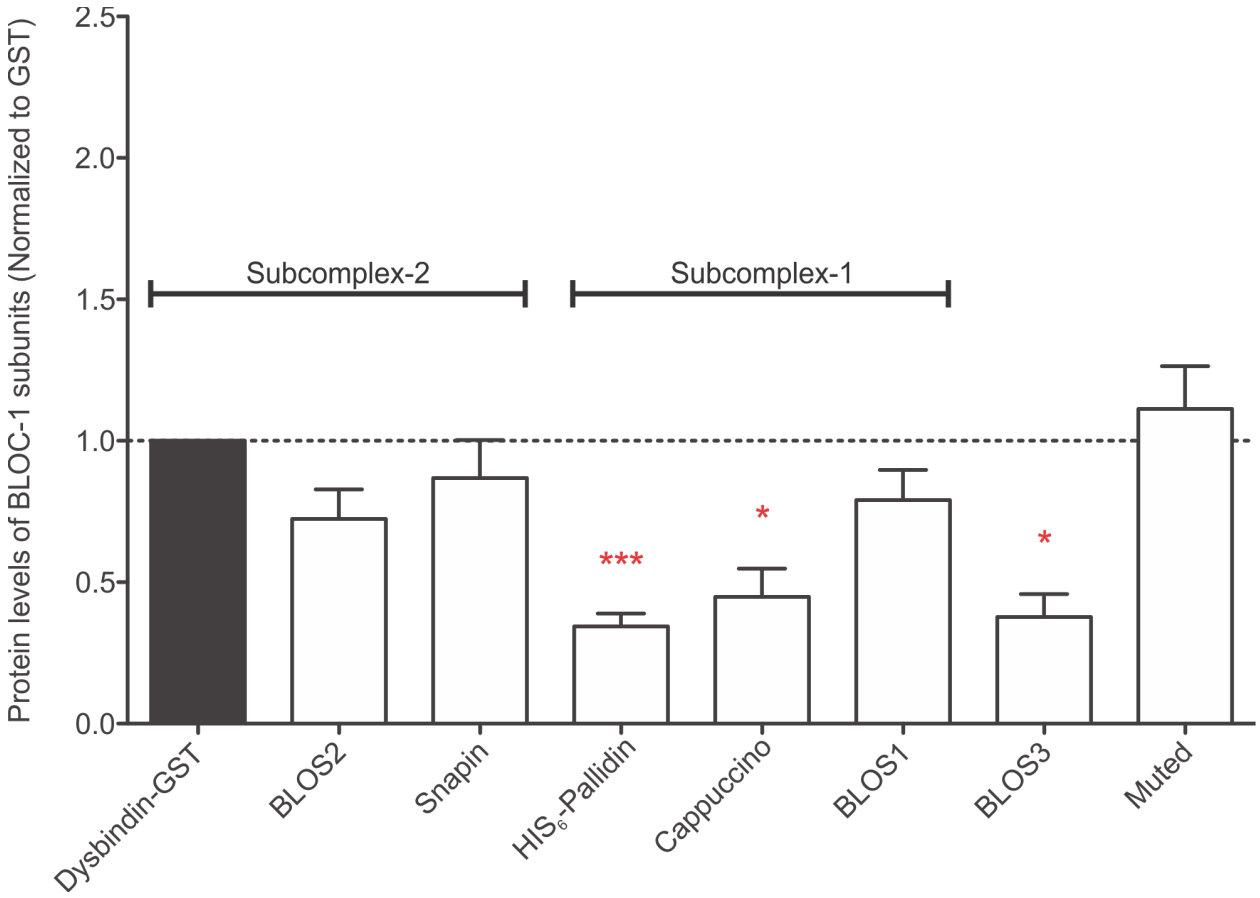

Figure 5.10 Quantification of signal intensity of BLOC-1(IsoC) after GST-purification. BLOC-1(IsoA) and BLOC-1(IsoC) were purified on glutathione-sepharose beads. Protein levels of each subunit in the purified samples were analyzed by immunoblotting. The signal intensity of the bands from the immunoblots was quantified and background corrected. To quantify relative yields, the signal intensity of each subunit was divided by the signal intensity of the Dysbindin-GST subunit. Then, these normalized ratios of each BLOC-1(IsoC) subunit were divided by the normalized ratios of the corresponding subunit of BLOC-1(IsoA). Bars and error bars represent means ± S.E.M. of 5 separate sets of GST-purifications. A one sample t-test was performed for each subunit and p-values were corrected for multiple testing. Corrected p-values: *$p<0.05$, ***$p<0.001$

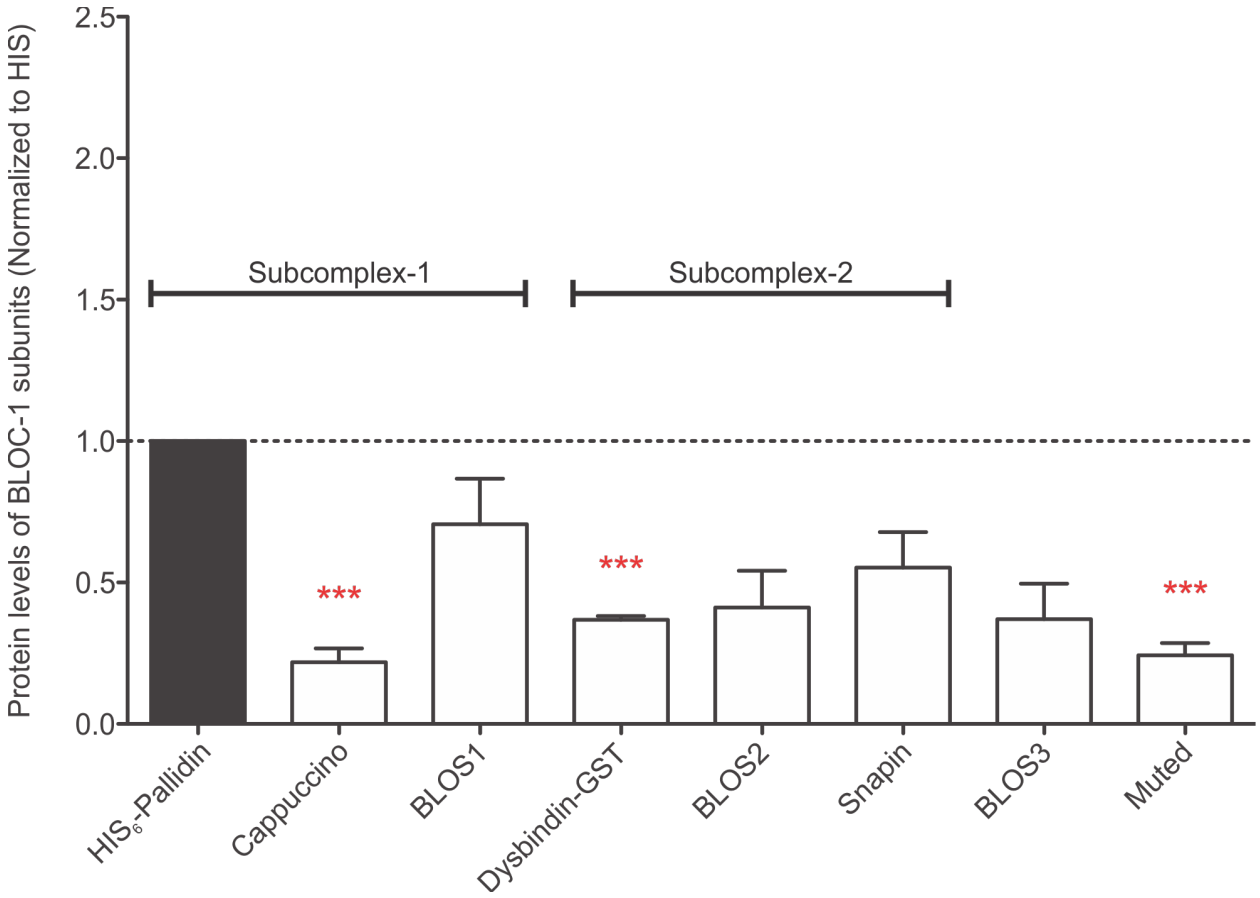

Figure 5.11 Quantification of signal intensity of BLOC-1(IsoC) after HIS_6-purification. BLOC-1(IsoA) and BLOC-1(IsoC) were purified on the Talon resins. Protein levels of each subunit in the purified samples were analyzed by immunoblotting. The signal intensity of the bands from the immunoblots was quantified and background corrected. To quantify relative yields, the signal intensity of each subunit was divided by the signal intensity of the HIS_6-Pallidin subunit. Then, these normalized ratios of each BLOC-1(IsoC) subunit were divided by the normalized ratios of the corresponding subunit of BLOC-1(IsoA). Bars and error bars represent means ± S.E.M. of 5 separate sets of HIS_6-purifications. A one sample t-test was performed for each subunit and p-values were corrected for multiple testing. Corrected p-values: ***$p<0.001$

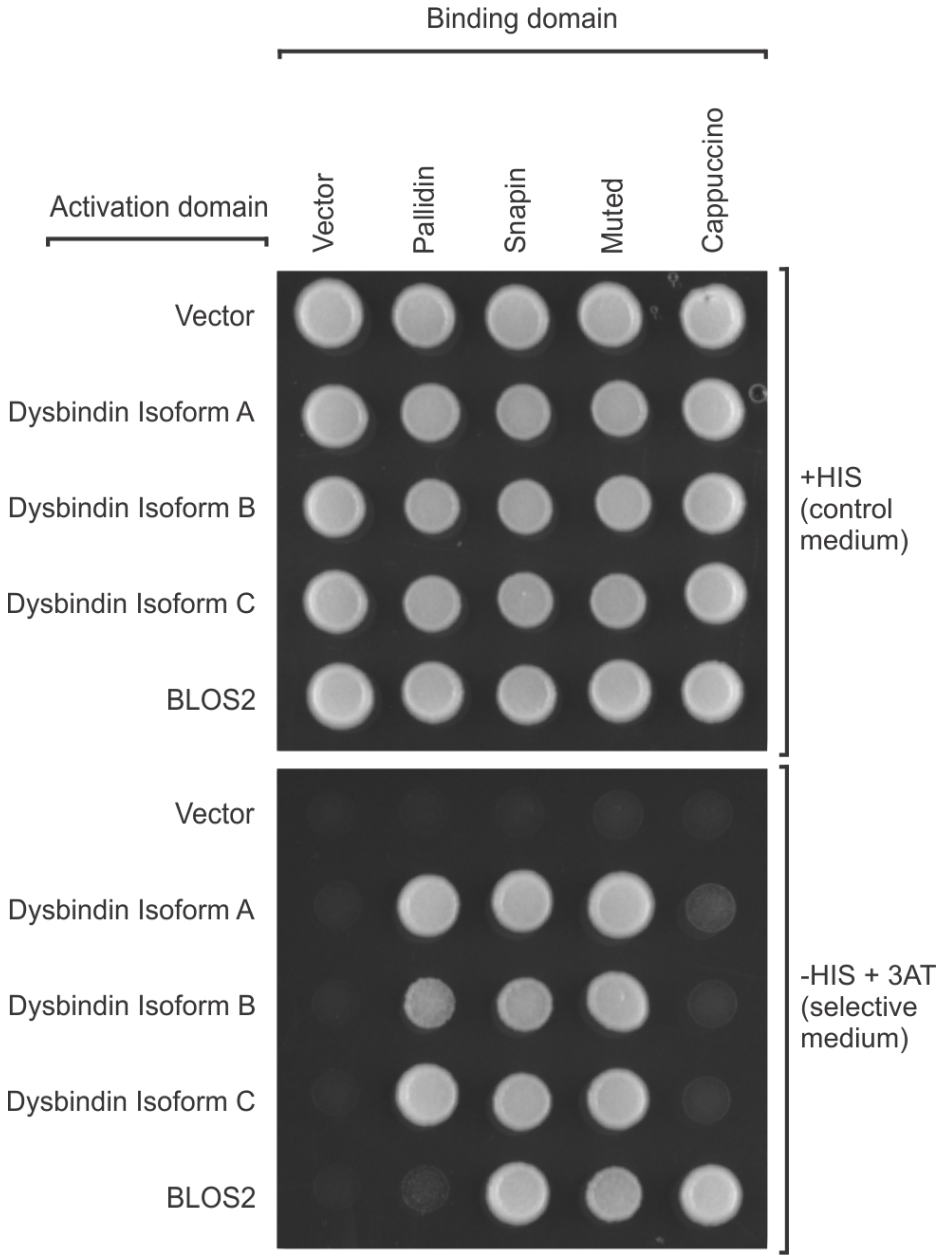

Figure 5.12 Yeast two-hybrid analysis of binary interactions between selected BLOC-1 subunits and dysbindin isoforms B and C. Yeast cells were co-transformed with Gal4 DNA-binding and activation domains alone (vector) or fused in-frame to the indicated human ORFs. Double transformants were first selected on minimal medium lacking leucine and tryptophan and then spotted onto planes containing the same medium (as a control) or selective medium also lacking histidine (HIS) and containing 5 mM 3AT.

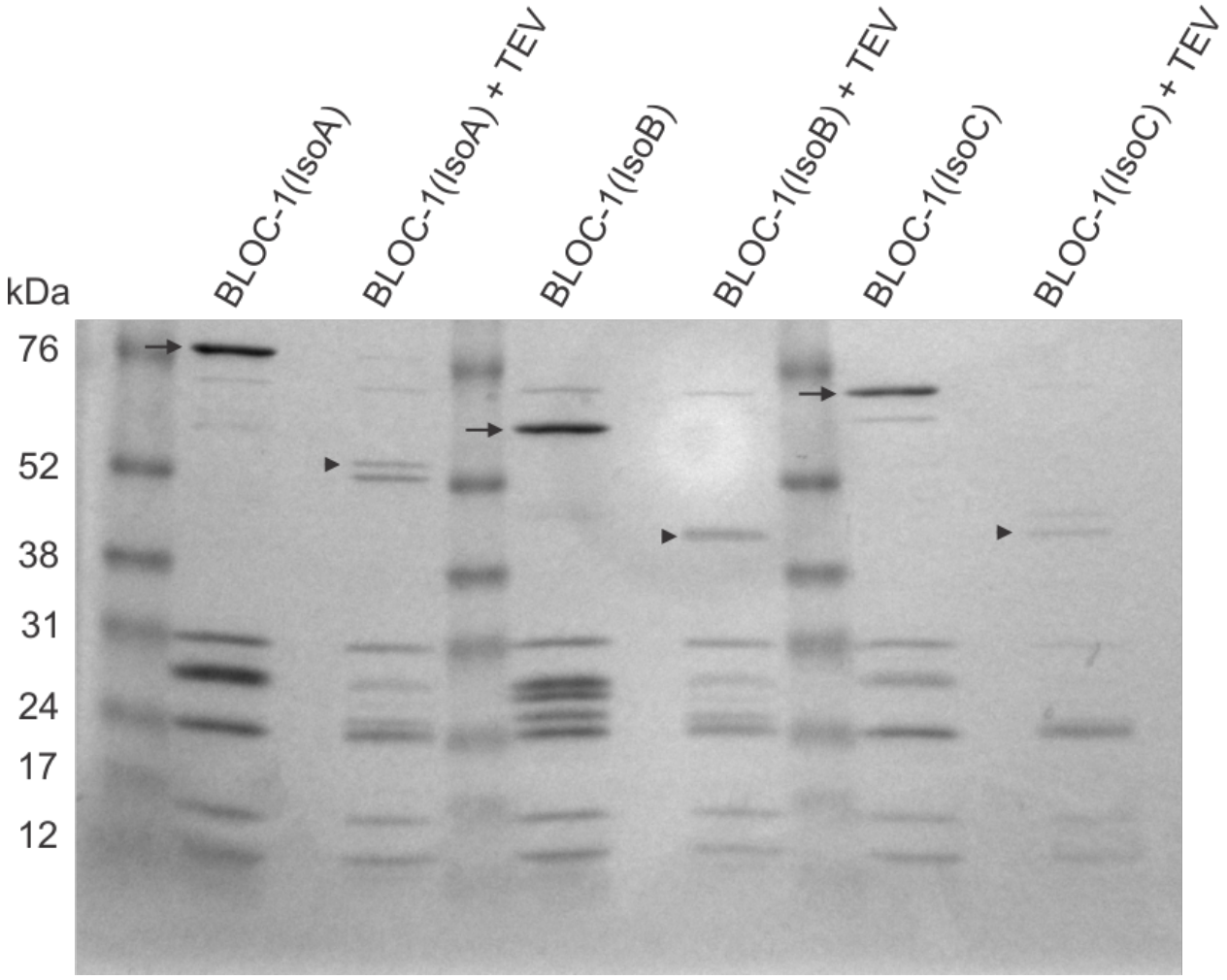

Figure 5.13 Tobacco Etch Virus protease digestion of BLOC-1(IsoA), BLOC-1(IsoB) and BLOC-1(IsoC) after GST-purification. BLOC-1(IsoA), BLOC-1(IsoB) and BLOC-1(IsoC) were purified on glutathione-sepharose beads. An aliquot of each sample was boiled in the presence of SDS-PAGE sample buffer and the rest was incubated with Tobacco Etch Virus protease and dialyzed. The purified samples were re-incubated with the glutathione-sepharose beads to removed the GST tag. An aliquot of the digested samples was then boiled in the presence of SDS-PAGE sample buffer. Notice that the bands corresponding to dysbindin-GST from BLOC-1(IsoA), BLOC-1(IsoB), and BLOC-(IsoC) (arrows) had a shift in apparent molecular weight after digestion (arrowheads).

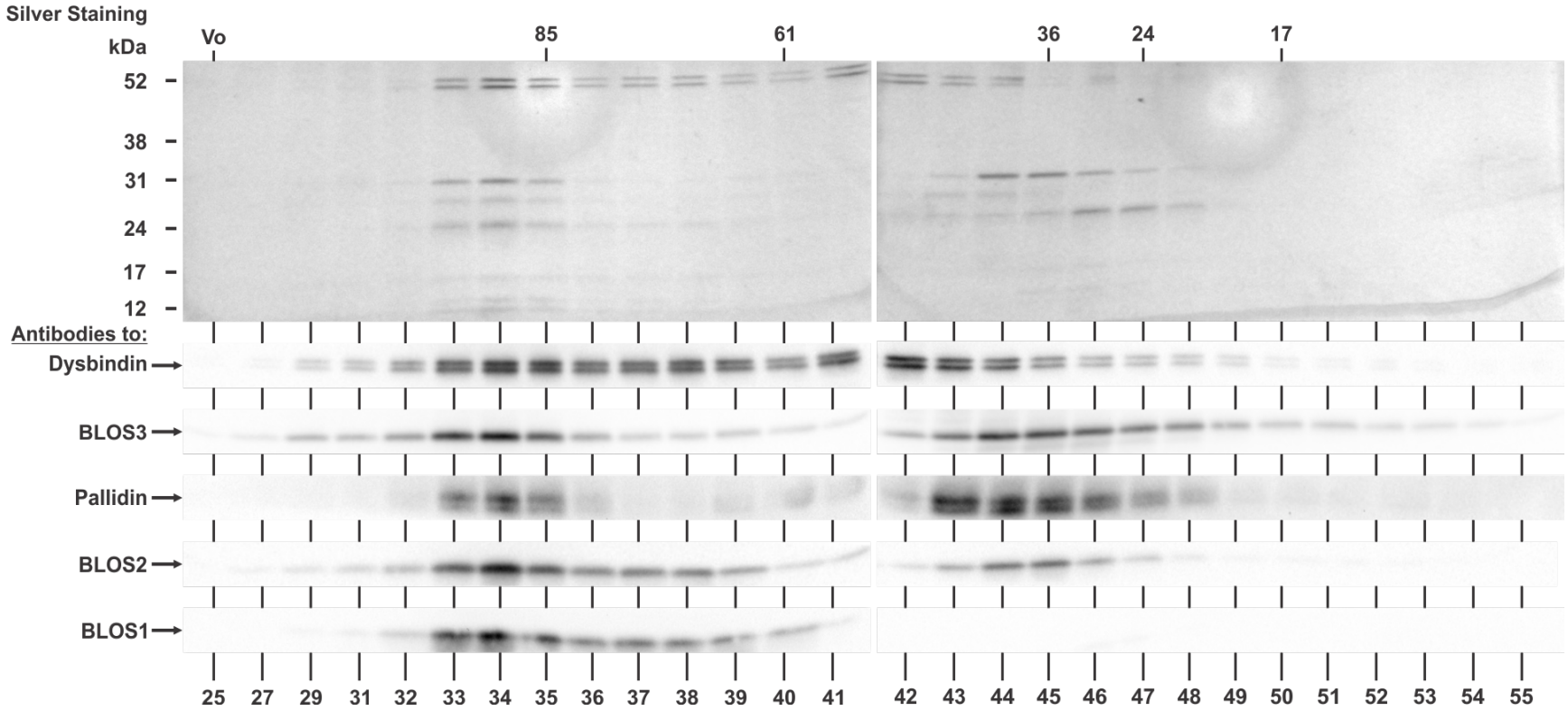

Figure 5.14 Size-exclusion chromatography analysis of recombinant BLOC-1(IsoA). BLOC-1(IsoA) was purified on glutathione-sepharose beads and digested with Tobacco Etch Virus protease. The digested purified proteins were fractioned on a Superose 6 column. Resulting fractions were analyzed by silver staining and immunoblotting using antibodies to selected BLOC-1 subunits. The exclusion volume (V_o) as well as the elution positions of standard proteins are indicated on the top, with the numbers representing Stoke's radii in Å.

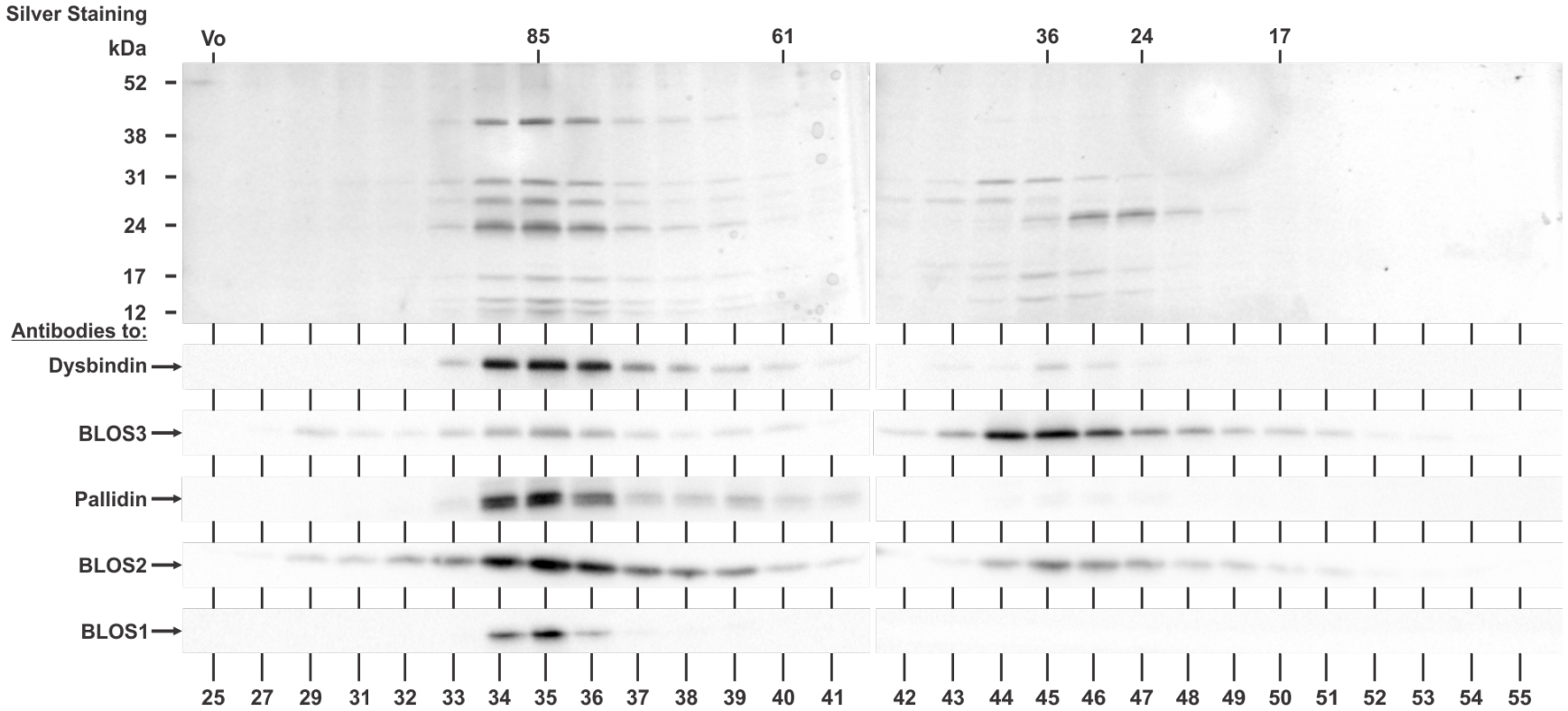

Figure 5.15 Size-exclusion chromatography analysis of recombinant BLOC-1(IsoB). BLOC-1(IsoB) was purified on glutathione-sepharose beads and digested with Tobacco Etch Virus protease. The digested purified proteins were fractioned on a Superose 6 column. Resulting fractions were analyzed by silver staining and immunoblotting using antibodies to selected BLOC-1 subunits. The exclusion volume (V_o) as well as the elution positions of standard proteins are indicated on the top, with the numbers representing Stoke's radii in Å.

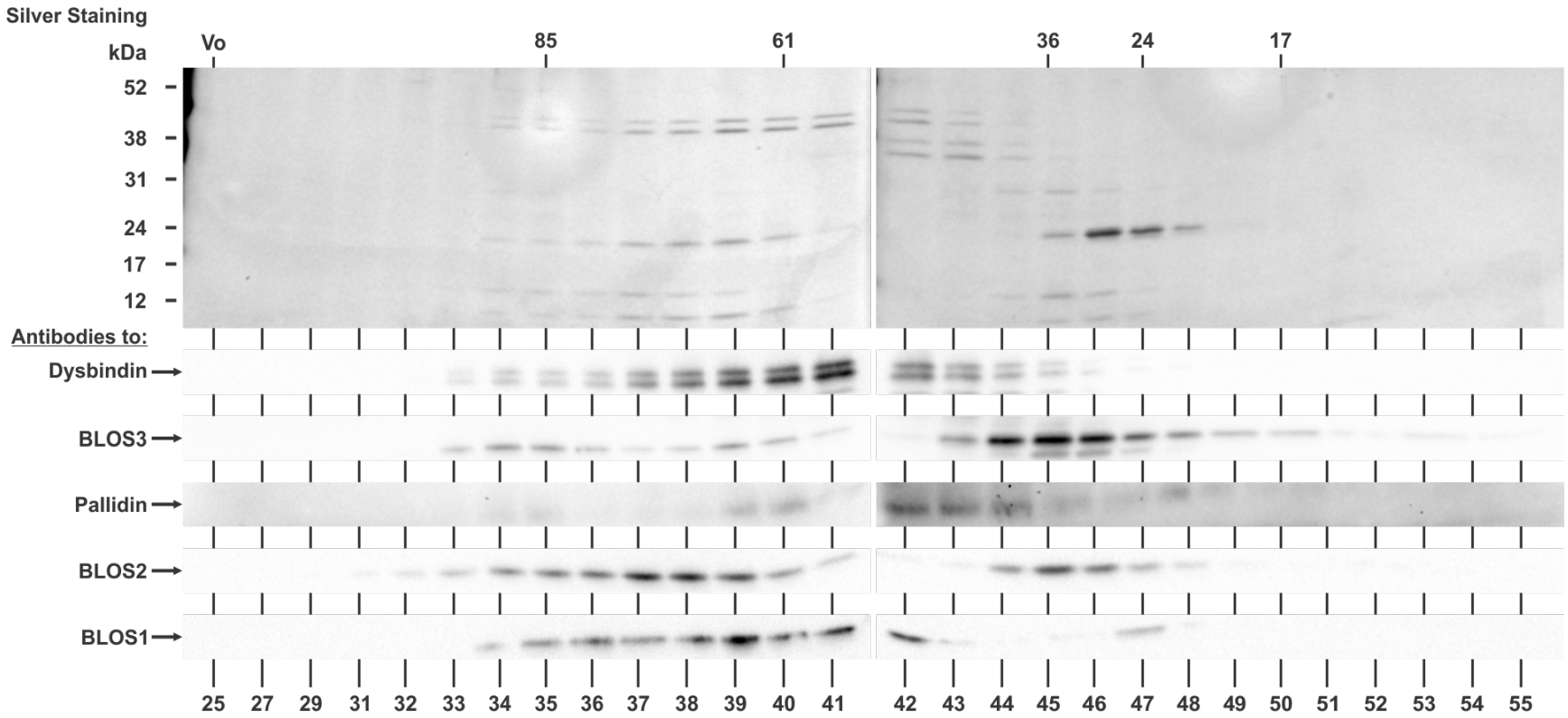

Figure 5.16 Size-exclusion chromatography analysis of recombinant BLOC-1(IsoC). BLOC-1(IsoC) was purified on glutathione-sepharose beads and digested with Tobacco Etch Virus protease. The digested purified proteins were fractioned on a Superose 6 column. Resulting fractions were analyzed by silver staining and immunoblotting using antibodies to selected BLOC-1 subunits. The exclusion volume (V_o) as well as the elution positions of standard proteins are indicated on the top, with the numbers representing Stoke's radii in Å.

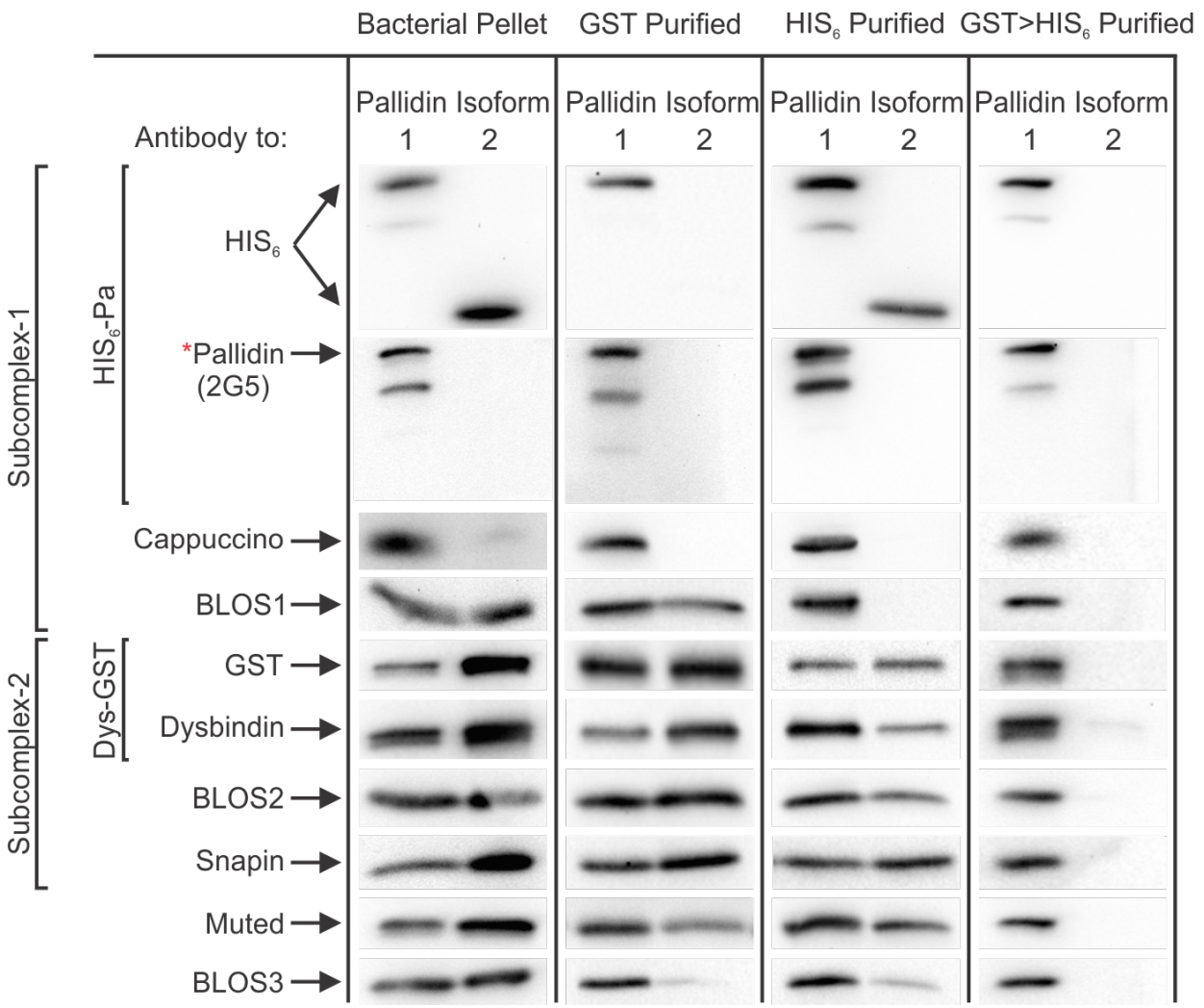

Figure 5.17 Representative immunoblot analyses of BLOC-1(WT) and BLOC-1(Iso2). The open reading frame (ORF) encoding pallidin isoform 1 was replaced with that encoding pallidin isoform 2, fused in frame with that encoding HIS_6. Bacterial pellets from *E. Coli* transformed with this construct were examined by immunoblot analysis for the expression of BLOC-1 subunits. BLOC-1(WT) and BLOC-1(Iso2) were purified by the GST tag alone, the HIS_6 tag alone, and by both (GST>HIS_6 tandem purification) and the representative immunoblots of those purified samples are shown above. *: The pallidin antibody (Monoclonal 2G5) recognizes an epitope that is missing from pallidin isoform 2. Dys-GST: Dysbindin-GST, HIS_6-Pa: HIS_6-pallidin.

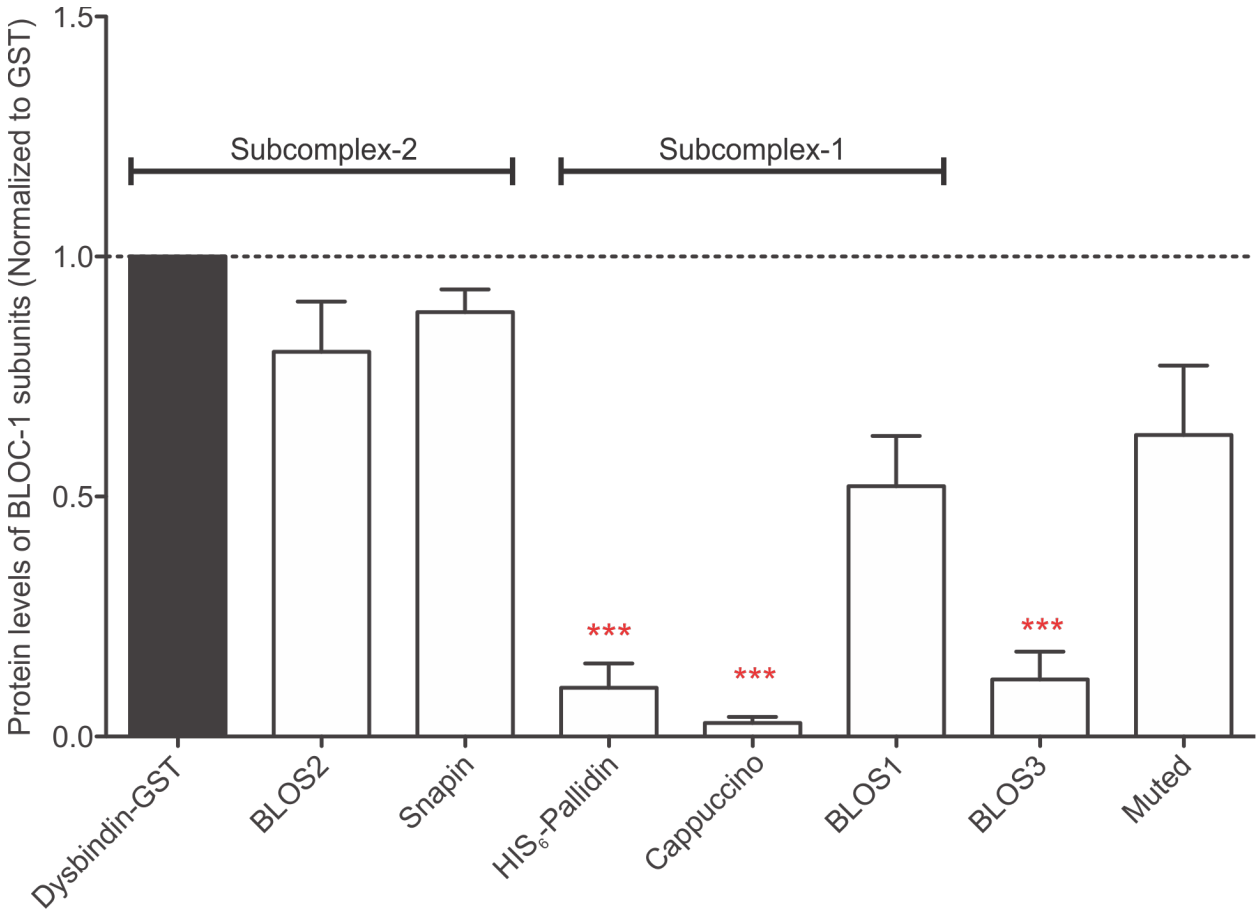

Figure 5.18 Quantification of signal intensity of BLOC-1(Iso2) after GST-purification. BLOC-1(WT) and BLOC-1(Iso2) were purified on glutathione-sepharose beads. Protein levels of each subunit in the purified samples were analyzed by immunoblotting. The signal intensity of the bands from the immunoblots was quantified and background corrected. To quantify relative yields, the signal intensity of each subunit was divided by the signal intensity of the Dysbindin-GST subunit. Then, these normalized ratios of each BLOC-1(Iso2) subunit were divided by the normalized ratios of the corresponding subunit of BLOC-1(WT). Bars and error bars represent means ± S.E.M. of 5 separate sets of GST-purifications. A one sample t-test was performed for each subunit and p-values were corrected for multiple testing. Corrected p-values: ***$p<0.001$

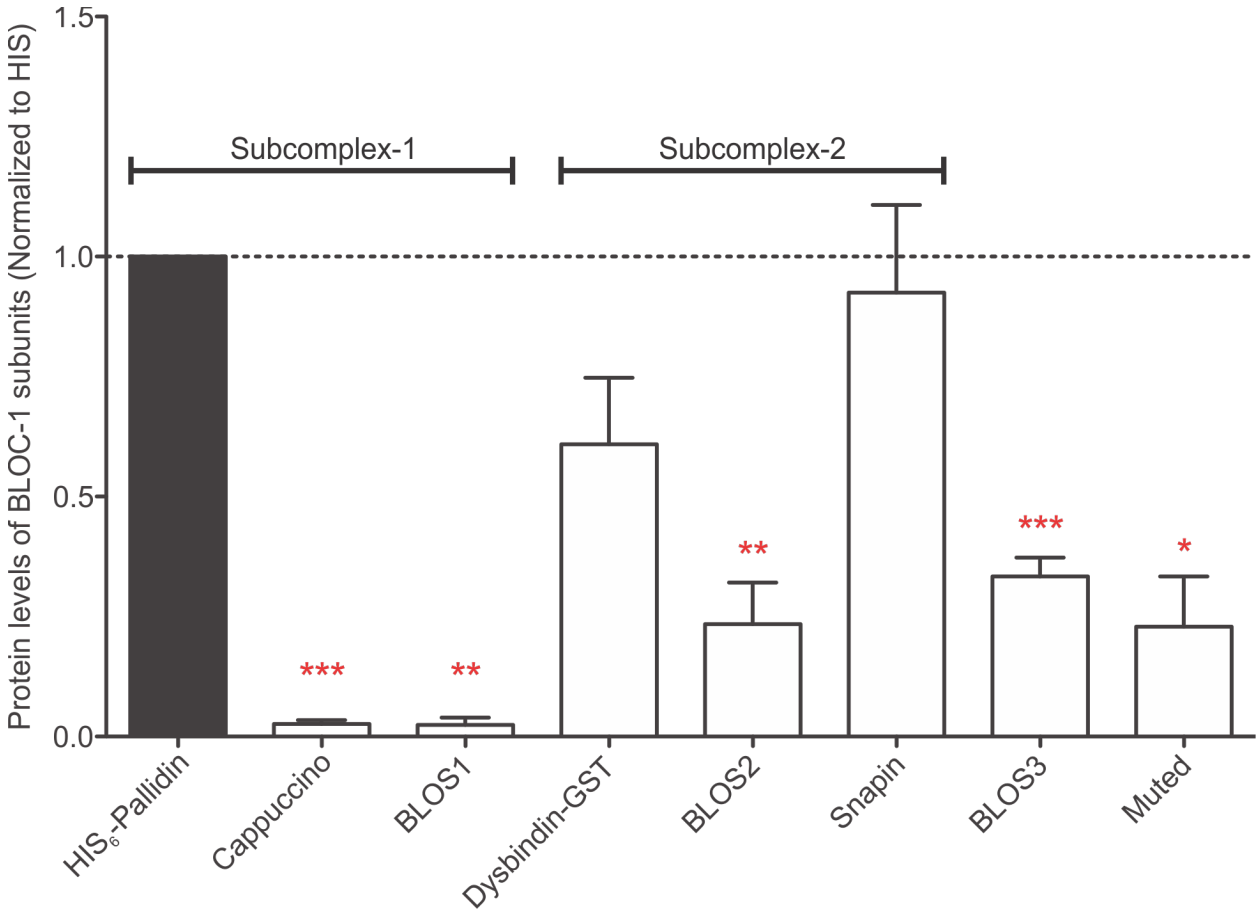

Figure 5.19 Quantification of signal intensity of BLOC-1(Iso2) after HIS_6-purification. BLOC-1(WT) and BLOC-1(Iso2) were purified on Talon resins. Protein levels of each subunit in the purified samples were analyzed by immunoblotting. The signal intensity of the bands from the immunoblots was quantified and background corrected. To quantify relative yields, the signal intensity of each subunit was divided by the signal intensity of the HIS_6-Pallidin subunit. Then, these normalized ratios of each BLOC-1(Iso2) subunit were divided by the normalized ratios of the corresponding subunit of BLOC-1(WT). Bars and error bars represent means ± S.E.M. of 5 separate sets of HIS_6-purifications. A one sample t-test was performed for each subunit and p-values were corrected for multiple testing. Corrected p-values: *$p<0.05$, **$p<0.01$, ***$p<0.001$

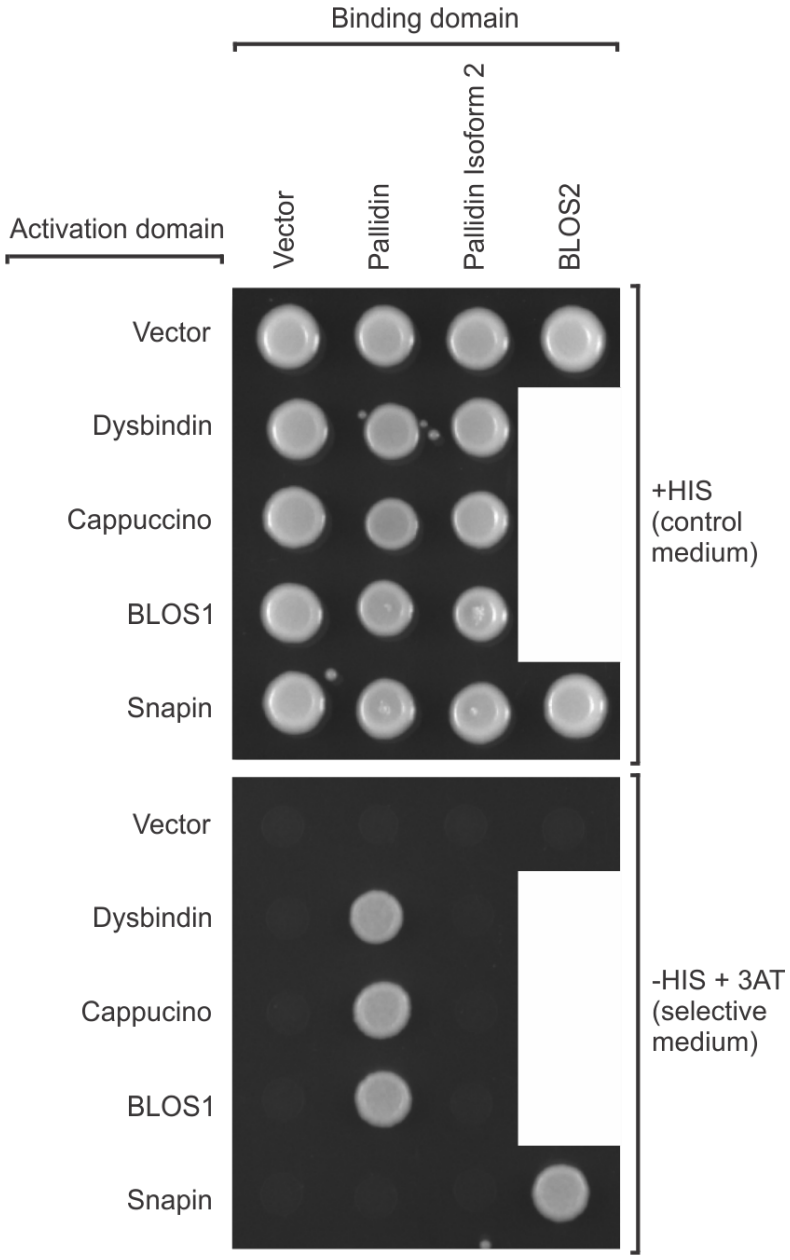

Figure 5.20 Yeast two-hybrid analysis of binary interactions between BLOC-1 subunits and pallidin isoform 2. Yeast cells were co-transformed with Gal4 DNA-binding and activation domains alone (vector) or fused in-frame to the indicated human ORFs. Double transformants were first selected on minimal medium lacking leucine and tryptophan and then spotted onto planes containing the same medium (as a control) or selective medium also lacking histidine (HIS) and containing 5 mM 3AT.

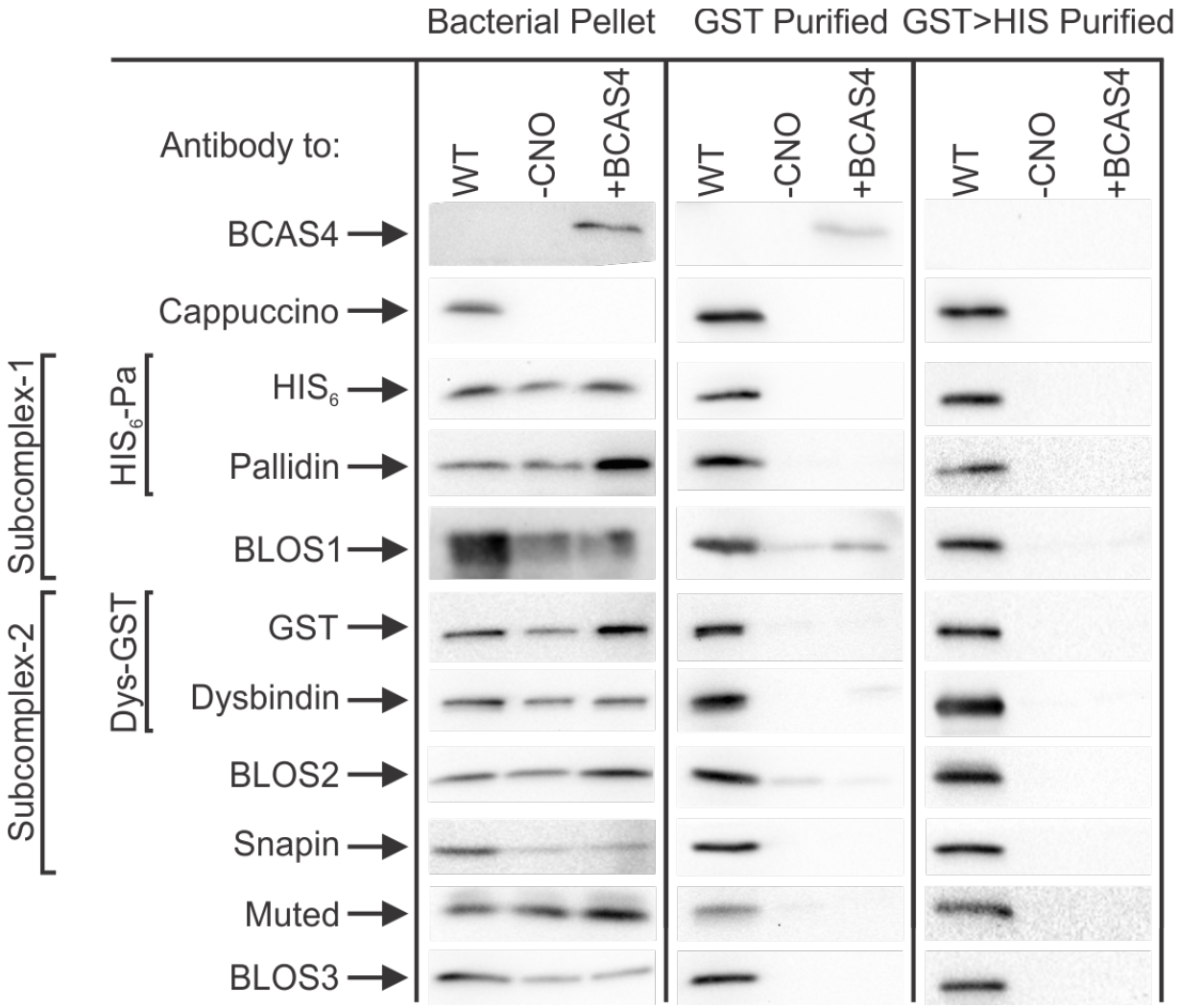

Figure 5.21 Representative immunoblot analyses of BLOC1(-CNO) and BLOC-1(BCAS4). The open reading frame (ORF) encoding cappuccino was replaced with that encoding BCAS4. As a negative control, the ORF encoding cappuccino was removed. Bacterial pellets from *E. Coli* transformed with these constructs were examined by immunoblot analysis for the expression of BLOC-1 subunits. BLOC-1(WT), BLOC-1(-CNO), and BLOC-1(BCAS4) were purified by the GST tag alone and by tandem purification (GST>HIS_6), and the representative immunoblots of those purified samples are shown above.

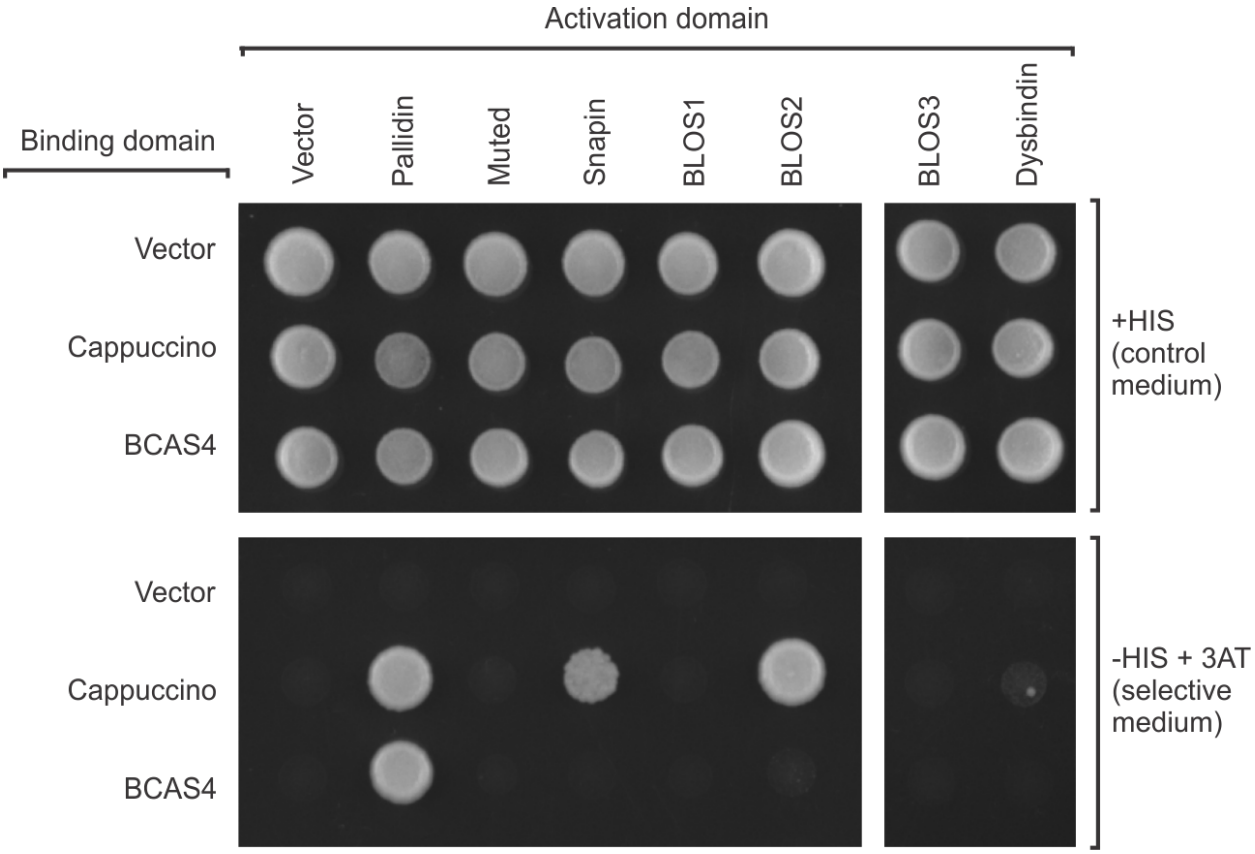

Figure 5.22 Yeast two-hybrid analysis of binary interactions between BLOC-1 subunits and theBCAS4 protein. Yeast cells were co-transformed with Gal4 DNA binding and activation domains alone (vector) or fused in-frame to the indicated full-length human ORFs. Double transformants were first selected on minimal medium lacking leucine and tryptophan and then spotted onto planes containing the same medium (as a control) or selective medium also lacking histidine (HIS) and containing 5 mM 3AT.

REFERENCES

1. Talbot K, Louneva N, Cohen JW, Kazi H, Blake DJ, Arnold SE. Synaptic dysbindin-1 reductions in schizophrenia occur in an isoform-specific manner indicating their subsynaptic location. PLoS One. 2011 Mar 1;6(3):e16886.
2. Han MH, Hu Z, Chen CY, Chen Y, Gucek M, Li Z, Markey SP. Dysbindin-associated proteome in the p2 synaptosome fraction of mouse brain. J Proteome Res. 2014 Nov 7;13(11):4567-80.
3. Wang H, Yuan Y, Zhang Z, Yan H, Feng Y, Li W. Dysbindin-1C is required for the survival of hilar mossy cells and the maturation of adult newborn neurons in dentate gyrus. J Biol Chem. 2014 Oct 17;289(42):29060-72.
4. Cullinane AR, Curry JA, Carmona-Rivera C, Summers CG, Ciccone C, Cardillo ND, Dorward H, Hess RA, White JG, Adams D, Huizing M, Gahl WA. A BLOC-1 mutation screen reveals that PLDN is mutated in Hermansky-Pudlak Syndrome type 9. Am J Hum Genet. 2011 Jun 10;88(6):778-87.
5. Ciciotte SL, Gwynn B, Moriyama K, Huizing M, Gahl WA, Bonifacino JS, Peters LL. Cappuccino, a mouse model of Hermansky-Pudlak syndrome, encodes a novel protein that is part of the pallidin-muted complex (BLOC-1). Blood. 2003 Jun1;101(11):4402-7.
6. Mead CL, Kuzyk MA, Moradian A, Wilson GM, Holt RA, Morin GB. Cytosolic protein interactions of the schizophrenia susceptibility gene dysbindin. J Neurochem. 2010 Jun; 113(6):1491-503.
7. Huttlin EL, Ting L, Bruckner RJ, Gebreab F, Gygi MP, Szpyt J, Tam S, Zarraga G, Colby G, Baltier K, Dong R, Guarani V, Vaites LP, Ordureau A, Rad R, Erickson BK, Wühr M, Chick

J, Zhai B, Kolippakkam D, Mintseris J, Obar RA, Harris T, Artavanis-Tsakonas S, Sowa ME, De Camilli P, Paulo JA, Harper JW, Gygi SP. The BioPlex Network: A Systematic Exploration of the Human Interactome. Cell. 2015 Jul 16;162(2):425-40.

8. Lee HH, Nemecek D, Schindler C, Smith WJ, Ghirlando R, Steven AC, Bonifacino JS, Hurley JH. Assembly and architecture of biogenesis of lysosome-related organelles complex-1 (BLOC-1). J Biol Chem. 2012 Feb 17;287(8):5882-90.
9. Starcevic M, Dell'Angelica EC. Identification of snapin and three novel proteins (BLOS1, BLOS2, and BLOS3/reduced pigmentation) as subunits of biogenesis of lysosome-related organelles complex-1 (BLOC-1). J Biol Chem. 2004 Jul 2;279(27):28393-401.
10. Starcevic M. Molecular characterization of biogenesis of lysosome -related organelles complex-1 (BLOC -1). PhD Dissertation. University of California, Los Angeles. 2005 141 p.
11. Falcón-Pérez JM, Starcevic M, Gautam R, Dell'Angelica EC. BLOC-1, a novel complex containing the pallidin and muted proteins involved in the biogenesis of melanosomes and platelet-dense granules. J Biol Chem. 2002 Aug 2;277(31):28191-9.
12. Dell'Angelica EC, Klumperman J, Stoorvogel W, Bonifacino JS. Association of the AP-3 adaptor complex with clathrin. Science. 1998 Apr 17;280(5362):431-4.
13. Dell'Angelica EC, Bonifacino JS. Staining proteins in gels. Curr Protoc Cell Biol. 2001 May;Chapter 6:Unit 6.6.
14. Ito H, Fukuda Y, Murata K, Kimura A. Transformation of intact yeast cells treated with alkali cations. J Bacteriol. 1983 Jan;153(1):163-8.

15. Xu Y, Sun Y, Ye H, Zhu L, Liu J, Wu X, Wang L, He T, Shen Y, Wu JY, Xu Q. Increased dysbindin-1B isoform expression in schizophrenia and its propensity in aggresome formation. Cell Discov. 2015 Nov 10;1:15032.
16. Zhu CY, Shen Y, Xu Q. Propagation of dysbindin-1B aggregates: exosome-mediated transmission of neurotoxic deposits. Neuroscience. 2015 Apr 16;291:301-16.
17. Yang W, Zhu C, Shen Y, Xu Q. The pathogenic mechanism of dysbindin-1B toxic aggregation: BLOC-1 and intercellular vesicle trafficking. Neuroscience. 2016 Oct 1;333:78-91.
18. Farrell MS, Werge T, Sklar P, Owen MJ, Ophoff RA, O'Donovan MC, Corvin A, Cichon S, Sullivan PF. Evaluating historical candidate genes for schizophrenia. Mol Psychiatry. 2015 May;20(5):555-62.
19. Nazarian R, Starcevic M, Spencer MJ, Dell'Angelica EC. Reinvestigation of the dysbindin subunit of BLOC-1 (biogenesis of lysosome-related organelles complex-1) as a dystrobrevin-binding protein. Biochem J. 2006 May 1;395(3):587-98.
20. Bennett J. Findings of Research Misconduct. Federal Register. 2016 Aug;81(168): 59642-59643.
21. Uhlén M, Fagerberg L, Hallström BM, Lindskog C, Oksvold P, Mardinoglu A, Sivertsson Å, Kampf C, Sjöstedt E, Asplund A, Olsson I, Edlund K, Lundberg E, Navani S, Szigyarto CA, Odeberg J, Djureinovic D, Takanen JO, Hober S, Alm T, Edqvist PH, Berling H, Tegel H, Mulder J, Rockberg J, Nilsson P, Schwenk JM, Hamsten M, von Feilitzen K, Forsberg M, Persson L, Johansson F, Zwahlen M, von Heijne G, Nielsen J, Pontén F. Proteomics. Tissue-based map of the human proteome. Science. 2015 Jan 23;347(6220):1260419.

CHAPTER 6

Analysis of critical residues of dysbindin for binding AP-3

ABSTRACT

BLOC-1 is well described to have a physical interaction with another multimeric protein complex, Adaptor Protein (AP)-3. A previous study reported that the dysbindin subunit of BLOC-1 is able to interact with AP-3. In this chapter I report the minimal region within dysbindin to bind AP-3. I used site-directed mutagenesis to identify the critical residues. Mutation of the critical residue in the context of the whole recombinant BLOC-1 disrupted binding to AP-3.

INTRODUCTION

Adaptor protein (AP)-3 is a heterotetrameic complex, which functions as a molecular sorting device that mediates the intracellular trafficking of proteins to lysosomes and related organelles (reviewed in [1]). AP-3 is composed of four subunits, δ, β3, μ3, and σ3 and has been described to interact with various proteins via different subunits (reviewed in [2]). One of these interactions is with BLOC-1 [3-7].

A physical interaction between BLOC-1 and AP-3 was initially observed by co-immunoprecipitation of the endogenous complexes from HeLa cells and mouse liver [3], and the interaction has been reproduced in different tissues and cell lines [4-7]. Mutations of subunits in both complexes are associated with a rare autosomal recessive disorder called Hermansky - Pudlak Syndrome (HPS) [8-13], and patients with HPS display oculocutaneous albinism and prolonged bleeding due to defective lysosome-related organelles. Mouse models with mutations in either complex also display HPS-like phenotypes (reviewed in [14]). Because BLOC-1 and AP-3 mutants share similar characteristics, it has been suggested that BLOC-1 and AP-3 work in the same machinery that controls protein sorting. However, the biological function of this interaction is still not clear.

Binding motifs for AP-1 [15-19], AP-2 [19-22], and AP-4 [23, 24] were previously described, but no such motif has been characterized in AP-3. A group in Japan reported that dysbindin specifically bound to AP-3, and that AP-3 recognized a minimal consensus sequence YXXØ in dysbindin, where Y is a tyrosine, Ø is a bulky hydrophobic residue and X represents any amino acid [7]. However, the YXXØ motif had been previously described as the binding

motif through which the other AP complexes interact with their cargoes and the interaction between AP complexes and cargoes via this motif has been characterized to be an weak interaction (reviewed in [25]). The interaction between BLOC-1 and AP-3, on the other hand, is not a weak or transient interaction as demonstrated by the previously mentioned studies [3-7], so it is unlikely that BLOC-1 is interacting with AP-3 via this motif only. Furthermore, the tyrosine of the YXXØ motif was mutated in a GST-dysbindin fusion protein and the mutated fusion protein was shown to still bind AP-3 [7]. Because of the concerns with analysis and interpretation of the data, I have sought to reanalyze the interaction between dysbindin and AP-3.

To identify the critical residues of dysbindin required to bind AP-3, I first used GST (glutathione S-transferase)-fusion proteins with different segments of dysbindin to delineate the minimum region of dysbindin for binding to AP-3. I then performed an alanine-scanning mutagenesis analysis of the delineated region to identify critical residue(s) of dysbindin required for binding to AP-3. These residue(s) in dysbindin were then mutated in the context of the whole BLOC-1 complex and the mutated BLOC-1 was examined for its ability to bind AP-3.

EXPERIMENTAL PROCEDURES

DNA constructs

All of the plasmids used in the present study consisted of human cDNA sequences that were cloned in-frame into the EcoRI-SalI sites of pGEX-5X-1 (Amersham Biosciences) to generate GST-fusion proteins. The constructs that express GST-dysbindin fragments 181-351, 181-351;Y215A, 181-258, and 181-246, and the GST-DBNDD2 protein were kindly provided by Verónica Cheli. The construct that expresses GST-dysbindin fragment 224-351, was kindly provided by Marta Starvcevic.

Antibodies

Monoclonal rabbit antibody to the μ3 subunit of AP-3 (clone: EPR16385) was purchased from Abcam and used at a concentration of 1:3,000.

Site-directed mutagenesis

To alter targeted residues within the C-terminal dysbindin fragment (181-351), mutagenic oligonucleotide primers were designed, ordered for synthesis (Eurofin) and used to change the codons of the targeted residues to those of alanine by site-directed mutagenesis using the QuikChange XL Site-Directed Mutagenesis Kit (Agilent Technologies). Mutagenesis was verified by DNA sequencing. The mutated sequence was digested and cloned in-frame into the EcoRI-SalI site of a new pGEX-5x-1 expression vector, to ensure that no unwanted mutations were introduced into the expression vector during the PCR amplification of the whole plasmid.

Production of GST-fusion proteins

E.coli strain BL21 Star (DE3) (Invitrogen by Thermo Fisher Scientific) was transformed with the appropriate plasmid and cultured in 2xYT media (18g/l tryptone, 11g/l yeast extract, 5.6 g/l NaCl). At an optical density at 600 nm (OD600) of 0.6, protein expression was induced with 0.1 mM isopropyl-beta-D-thiogalactopyranoside (IPTG) for 4 hours at 20°C. Pelleted cells, obtained by centrifugation at 6,000 x *g* for 15 mins, were homogenized in phosphate buffered saline (PBS) supplemented with 30 µl of protease inhibitor mixture (Sigma), and sonicated using a Branson Sonifier 450 (output #5, 50% duty cycle, 30 seconds on, 15 seconds off, 6 times). Appropriate amounts of triton X-100 were added to bring its concentration to 1% (w/v), and the homogenate was incubated in 4°C for 30 min. Following centrifugation at 6,000 x g for 15 mins, the cleared lysates were incubated with glutathione-Sepharose 4 Fast-Flow beads (GE Healthcare Life Sciences) for 1 h at 4°C. The beads were washed once with PBS with 1% (w/v) triton X-100, three times with 30 ml of PBS, and once with 0.1M Tris-HCl, pH 8.0. The proteins were eluted with 20 mM glutathione in 0.1M Tris-HCl, pH 8.0.

Tandem purification of the recombinant BLOC-1 is described in Chapter 5.

GST-pulldown assay

Frozen bovine brain was purchased from PelFreez. All purification steps were performed at 4°C. The bovine brain was cut into smaller pieces and as much white matter as possible was removed. The cut brain pieces (~260 g) were homogenized in Lysis Buffer [10mM Hepes, pH 7.4, 0.25 M

sucrose, 1 mM EGTA, 0.5 mM $MgCl_2$, 1 mM DTT] supplemented with a protease inhibitor mixture (Sigma) using a tissue blender (3 x 15 s). The homogenate was centrifuged at 13,000 x *g* for 15 min, filtered through gauze, centrifuged at 13,000 x g for another 15 mins, and filtered through gauze again. The resulting supernatant was further centrifuged at 120,000 x *g* for 90 mins to obtain cytosolic extract, which was stored at -80°C. Frozen bovine brain cytosol was thawed and diluted 1:1 (v/v) with diluting buffer [10 mM Hepes, pH 7.4, 150 mM KCl, 0.5mM $MgCl_2$, 1mM EGTA, 1mM dithiothreitol] supplemented with a protease inhibitor mixture (Sigma) and centrifuged at 120,000 x *g* for 30 mins. GST-fusion proteins were immobilized onto 15 µl of glutathione-Sepharose 4 Fast-Flow beads (GE Healthcare Life Sciences) washed, and then incubated with pre-cleared bovine brain cytosol for 1 hour at 4°C. The beads were washed three times with washing buffer [20mM Hepes, pH 7.4, 50 mM KCl, 1 mM EGTA, 0.5 mM $MgCl_2$] containing 0.1% (w/v) Triton X-100 and once in washing buffer alone, and bound proteins were analyzed by SDS-PAGE, and immunoblotting as described in Chapter 5. To determine how much of the GST-fusion protein bound to the beads, the bound proteins were loaded onto a separate gel and stained with Coomassie-blue as described in Chapter 5.

For quantitative analysis of protein expression levels, enhanced chemiluminescence signals were captured on the ChemiDoc Imaging System (Biorad) and digitally integrated using the National Institutes of Health Image Software (Image J, http://rsb.info.nih.gov/ij/). For the comparison of relative protein levels of AP-3 that bound to the GST-dysbindin fragments with a mutation in tyrosine 215, the mean pixel intensity was measured for each band using the same area for bands on the same membrane. The pixel intensity of the background was subtracted from the pixel

intensity of each band on the same membrane. To correct for loading, the background-corrected values of the blots were then divided by the background-corrected values of the Coomassie staining. The background- and loading-corrected values of AP-3 that bound to the GST-dysbindin fragments with a mutation in tyrosine 215 were divided by the background- and loading-corrected values of AP-3 that bound to the GST-dysbindin fragment with no mutation in tyrosine 215. A one-sample t-test was performed using GraphPad Prism 5.0b (GraphPad Software) to determine statistical significance from the theoretical value of 1.

Conservation analysis

The level of conservation in the 181-258 residues of dysbindin across all available mammalian species in BLAST (Basic Local Alignment Search Tool) was assessed using the Scorecons server at http://www.ebi.ac.uk/thornton-srv/databases/valdarprograms/scorecons_server_help.html based on the equations described in [26].

Secondary structure prediction

The secondary structure predictions were done using the Network Protein Sequence @nalysis server at https://npsa-prabi.ibcp.fr/NPSA/npsa_seccons.html, and the methods, DSC, HNNC, MLRC, PHD, Predator, and SOPM.

RESULTS

Mapping the minimal region required for dysbindin to bind AP-3

GST-fusion proteins of dysbindin fragments were purified and used to analyze binding to AP-3. The initial experiments done by a former postdoc (Verónica Cheli) revealed that the C-terminal region (residues 181-351) of dysbindin was sufficient to bind AP-3 and that dysbindin paralogs (DBNDD1 and DBNDD2), which have conserved regions in the C-terminal of dysbindin, were unable to bind AP-3 (Fig. 6.1, lanes 4, 6, and 7). To further narrow down the region within dysbindin required for AP-3 bind, I analyzed GST-dysbindin fragments with small increments of the C- and N-terminal removed. GST-dysbindin fragments with residues 181-246 and 224-351 were no longer able to bind AP-3, whereas GST-dysbindin fragment with residues 181-258 was still able to bind AP-3 (Fig. 6.1 lanes 10, 11, and 12). This suggested that there was a critical region in the N-terminus between amino acid 181-224 and another critical region in the C-terminus between amino acid 246-258.

Because of the previous study that reported that tyrosine 215 was critical for binding to AP-3, this tyrosine was analyzed. Mutation of the tyrosine decreased AP-3 binding, but did not prevent binding completely (Fig. 6.1, lane 5, Fig. 6.2), indicating that the tyrosine 215 is an important residue, but not critical for binding to AP-3. Additionally, the tyrosine motif, YLQI, was added to the dysbindin paralog DBNDD2, but it was still unable to bind AP-3 (Fig. 6.1, lane 8), again suggesting that the YXXØ motif is not the minimal consensus sequence in dysbindin to bind AP-3. The summary of these results is in Figure 6.3.

Site-directed mutagenesis of dysbindin residues 181-258

To select which residues to target first, the amino acid sequence of the human dysbindin was aligned with those of dysbindin orthologs from mouse, cattle, and frog as well as those of the dysbindin paralogs, DBNDD1 and DBNDD2. Residues conserved in all species, but not in the paralogs, were selected for mutagenesis. Selected residues that were in close proximity with each other were mutated together, and if no other selected residue was close, the residue was mutated alone. Some of GST-dysbindin fragments with these mutations had a decrease in binding to AP-3, but none of them had complete disruption of binding (Fig. 6.4, 6.5). Because the critical residues were not identified by this first method, the amino acid sequences of dysbindin orthologs from all mammals were aligned, and the degree of conservation of the residues was estimated (Fig. 6.15A). The residues with 100% conservation were then selected for mutagenesis (Fig. 6.6-Fig. 6.12). Two regions were found to be critical for binding AP-3. The first region included 6 residues from 206-212, excluding residue 208. Only when the six residues (DM-QYLS) were mutated, binding to AP-3 was completely disrupted (Fig. 6.6, lane 9, Fig. 6.10, lane 6, Fig. 6.11, lane 6, and Fig. 6.13, lane 11). The six residues were individually mutated in different GST-dysbindin fragments, but these GST-dysbindin fragments were still able to bind AP-3 (Fig. 6.10). Even when four or five of these residues were mutated together, the mutated GST-dysbindin fragment still bound AP-3 (Fig. 6.11, Fig. 6.13). The second region was closer to the C-terminus of the delineated region. GST-dysbindin fragments with mutations in residues 250-255 had a decrease in binding to AP-3 (Fig. 14, lanes 6 and 7), but when the leucine 256 was mutated, there was a complete loss of binding to AP-3 (Fig. 6.12, lane 7, Fig. 6.14, lane 9). Analysis of the critical residues is summarized in Figure 6.15C, and D. Lastly, the critical leucine

256 residue was mutated in the context of the recombinant BLOC-1. The wild-type BLOC-1 was able to bind AP-3 (Fig. 6.16 lane 6) whereas the mutant BLOC-1 was no longer able to bind (Fig. 6.16, lane 7). This suggests that dysbindin is the only subunit of BLOC-1 that binds AP-3 and that the mutation of the leucine 256 residue of dysbindin is able to disrupt binding between BLOC-1 and AP-3, at least *in vitro*.

DISCUSSION

Initial mapping of the minimal region of dysbindin required for binding to AP-3 delineated a large fragment spanning from residues 181-258. It was initially puzzling as to why such a large fragment was required. After analysis with smaller GST-dysbindin fragments, it seemed that two regions were required for binding. A small fragment of dysbindin with residues 181-246 was no longer able to bind AP-3, suggesting that there were residues between 246-258 critical for binding AP-3. Additionally, a dysbindin fragment with residues 224-351 no longer bound. This fragment contained the residues 246-258, but was still unable to bind AP-3, suggesting that there was a second region critical for binding between residues 181-224. Site-directed mutagenesis analysis made it clear that there were in fact two areas with critical residues to bind AP-3. The first was a group of 6 residues (DM-QYLS) between residues 206-212 and the second was a single leucine 256 residue. Analysis of the predicted secondary structure of residues 181-258 of dysbindin showed that these two critical areas lie in predicted helices separated by a region of coils (Fig. 6.14B), suggesting that these two critical areas could be brought closer by a bend in the coiled region, and thereby both interacting with AP-3. Because only one critical residue was identified, there was no motif that could be described.

A single mutation of the critical leucine 256 residue in the recombinant BLOC-1 was shown to disrupt binding to AP-3 completely. Assuming that mutation of this residue disrupts the interaction of BLOC-1 and AP-3 also *in vivo*, a model organism with a mutation in this leucine can be used to study the exact biological function that interaction between BLOC-1 and AP-3 has. Further analysis is required to address this point.

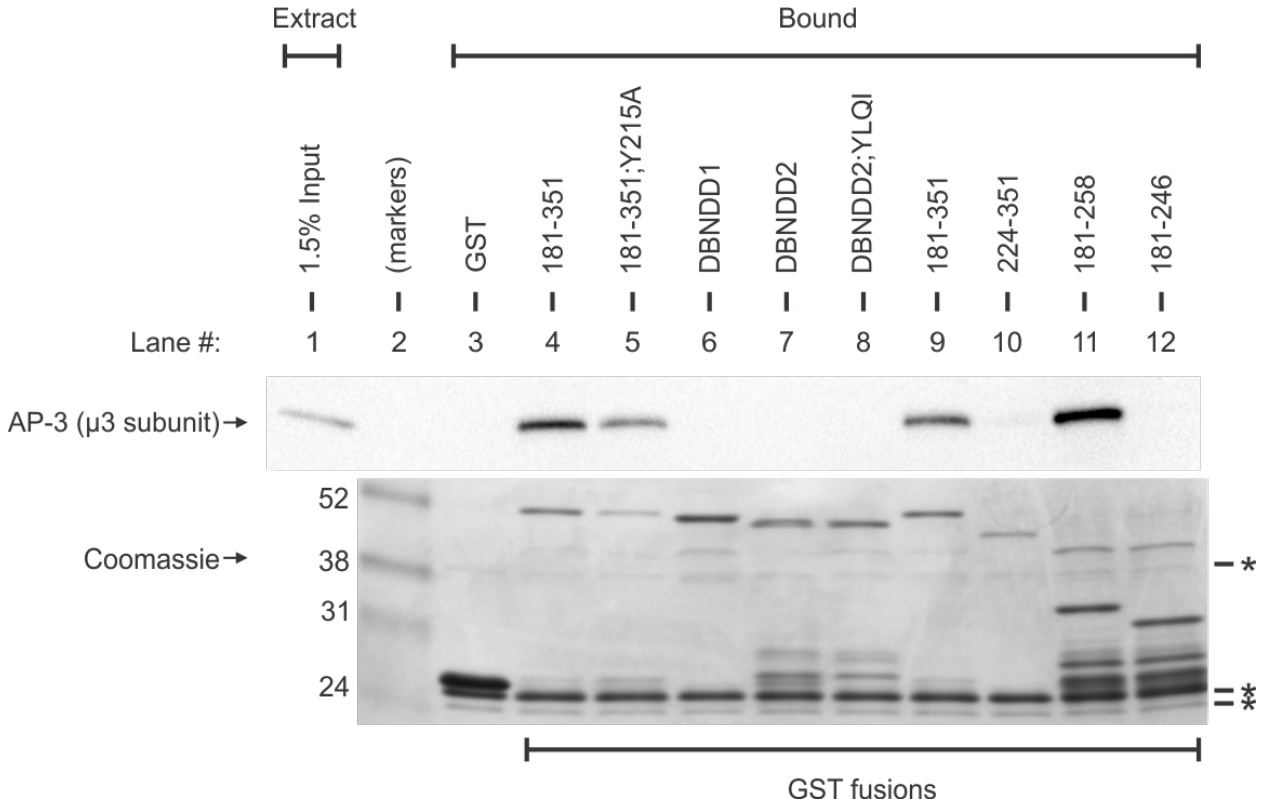

Figure 6.1 GST-pulldown assay of AP-3 with GST-dysbindin fragments and paralogs. GST-fusion proteins were purified, rebound to glutathione-Sepharose 4 Fast-Flow beads, and incubated with bovine brain cytosol. Beads were washed, and bound proteins were denatured by heating in the presence of SDS and analyzed by SDS-PAGE. AP-3 bound to the GST-fusion proteins was detected by immunoblot analysis using an antibody to its μ3 subunit. GST-fusion proteins bound to the beads were detected by Coomassie staining. Notice that the GST-dysbindin fragments 224-351 and 181-246 (lanes 10, and 12) and dysbindin paralogs (lanes 6, and 7) were unable to bind AP-3, but the fragment 181-258 (lane 11) was. *proteins from the bovine brain cytosol with affinity to the beads.

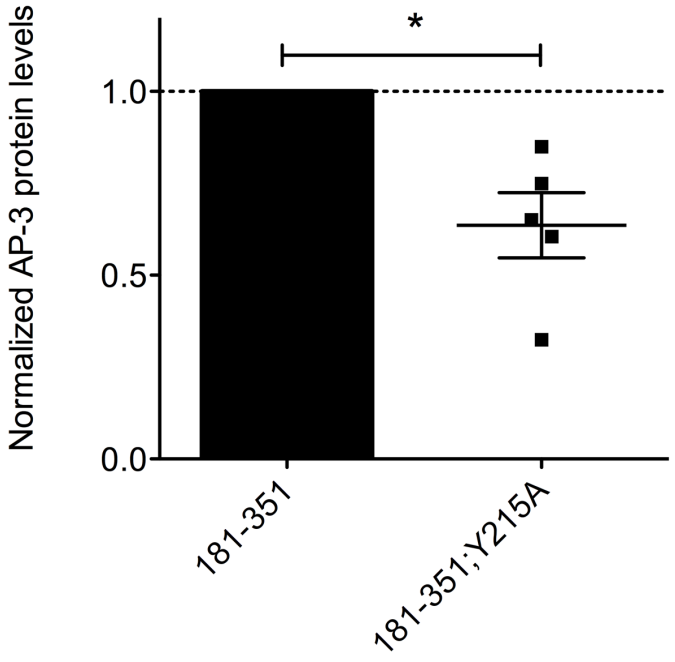

Figure 6.2 Mutation of tyrosine 215 to alanine decreased binding of dysbindin to AP-3. GST-pulldown analysis was performed using a GST-dysbindin fragment with a mutation in the tyrosine residue 215. AP-3 bound to the GST-fusion proteins was detected by immunoblot analysis using an antibody to its μ3 subunit, and band intensities were analyzed by densitometry. Square dots represent relative levels of AP-3 bound to the GST-dysbindin fragment (181-351;Y215A). Normalization of the data is explained in greater detail under Experimental Procedures. A one-sample t-test was done to determine statistical significance. *$p<0.05$.

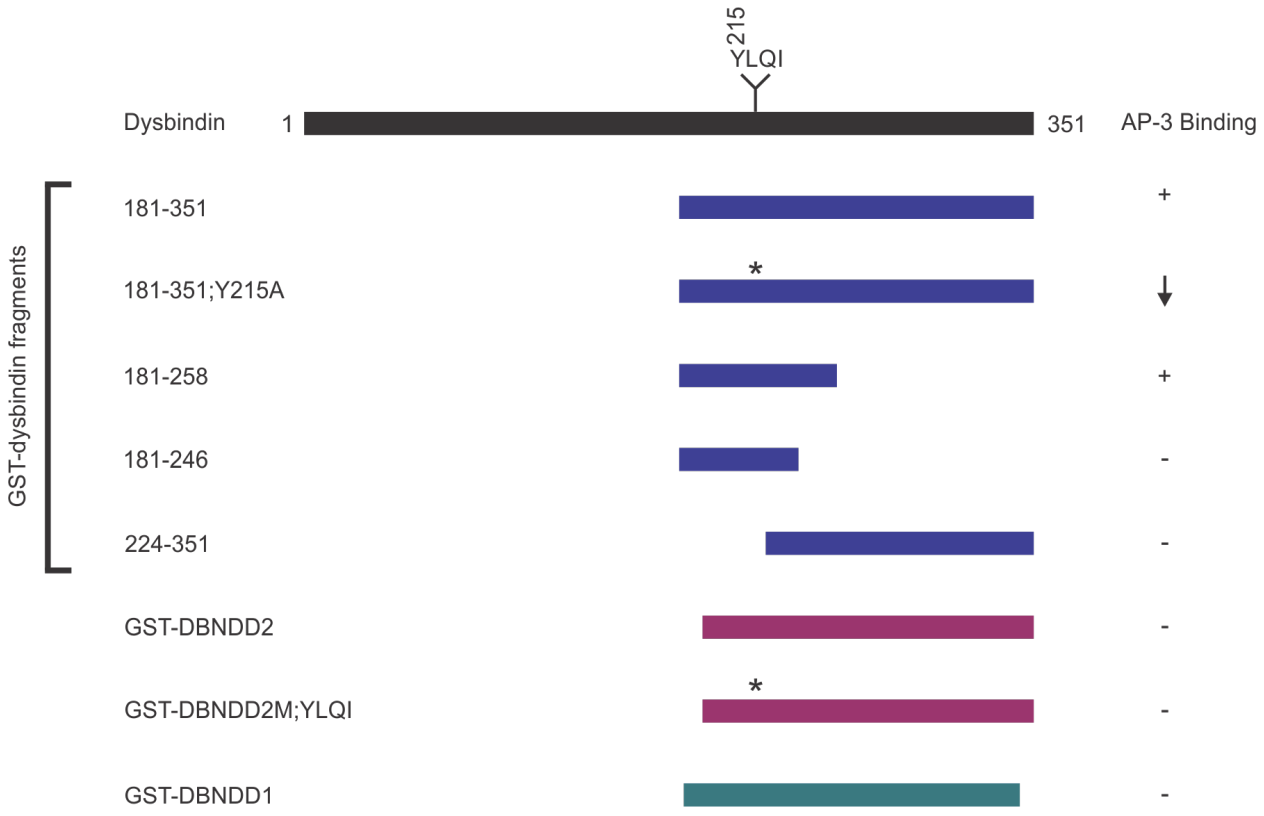

Figure 6.3 Schematic of GST-fusion proteins used to map the minimum residues of dysbindin required to bind to AP-3. The black bar represents the full-length dysbindin, which has 351 residues. Above the bar, the location of the previously described tyrosine-containing motif is marked (YLQI). The blue bars represent GST-dysbindin fragments that have been tested to bind AP-3. The residues included in each dysbindin fragment are on the left of the bars. The magenta bars represent GST-fusion proteins of the dysbindin paralog DBNDD2 and the teal bar represents the GST-fusion proteins of the dysbindin paralog DBNDD1. The asterisk identifies the location of mutations within the fragments. Ability of the fragment to bind AP-3 is on the right. +, AP-3 bound to GST-fusion protein. ↓, decreased amounts of AP-3 bound to GST-fusion protein. -, no AP-3 bound to GST-fusion protein.

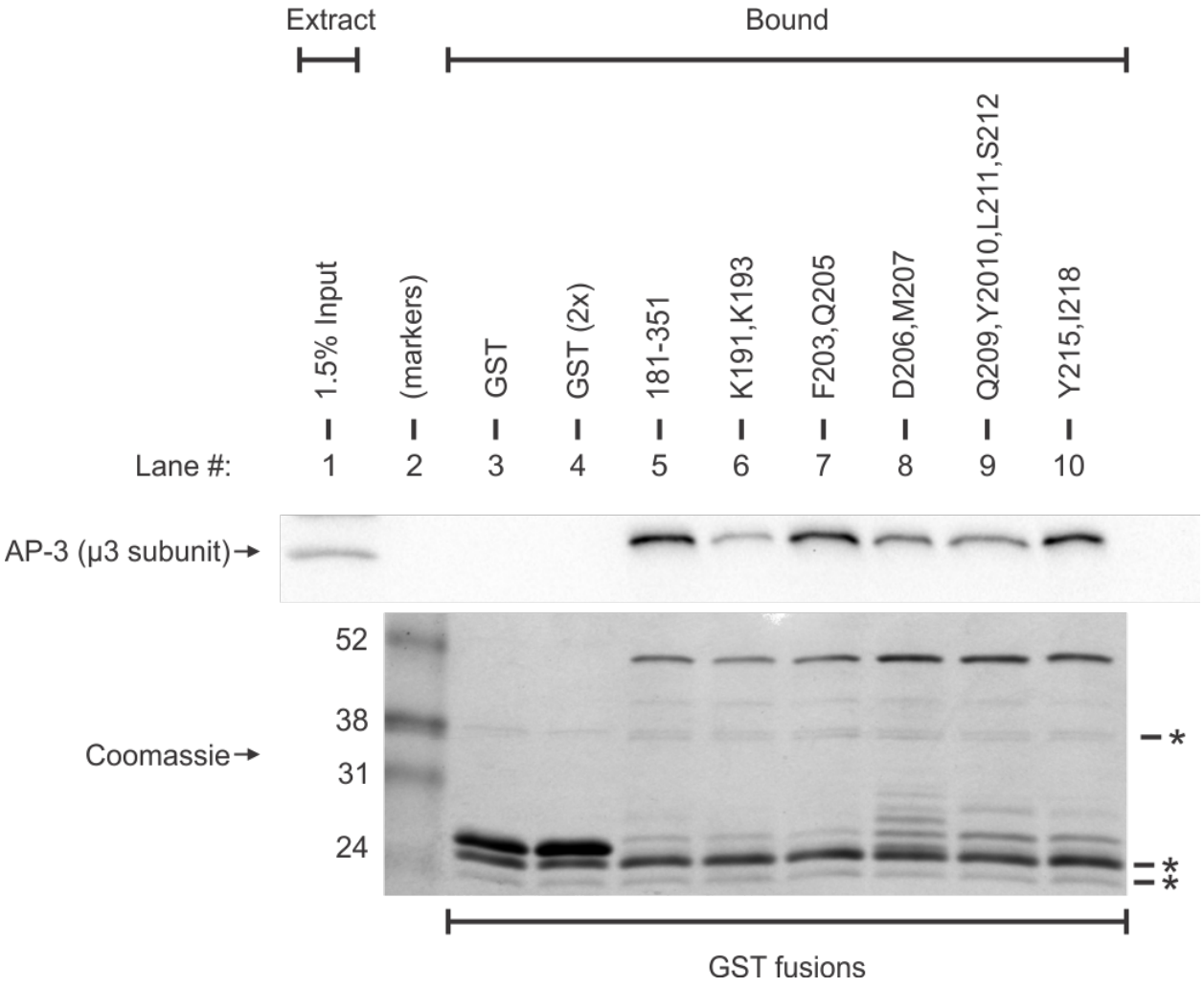

Figure 6.4 Site-directed mutagenesis of conserved dysbindin residues between 181-258 in human, mouse, cattle, and frog, but not in dysbindin paralogs. Conserved residues were mutated into alanine in GST-dysbindin fragments (181-351). GST-fusion proteins with mutations were purified, rebound to glutathione-Sepharose 4 Fast-Flow beads, and incubated with bovine brain cytosol. Beads were washed, and bound proteins were denatured by heating in the presence of SDS and analyzed by SDS-PAGE. AP-3 bound to the GST-fusion proteins was detected by immunoblot analysis using an antibody to its μ3 subunit. GST-fusion proteins bound to the beads were detected by Coomassie staining. Notice that all the GST-dysbindin fragments with mutations were able to bind AP-3 (lanes 6-10), but some had decreased binding to AP-3 (lanes 6, 8, and 9). *proteins from the bovine brain cytosol with affinity to the beads.

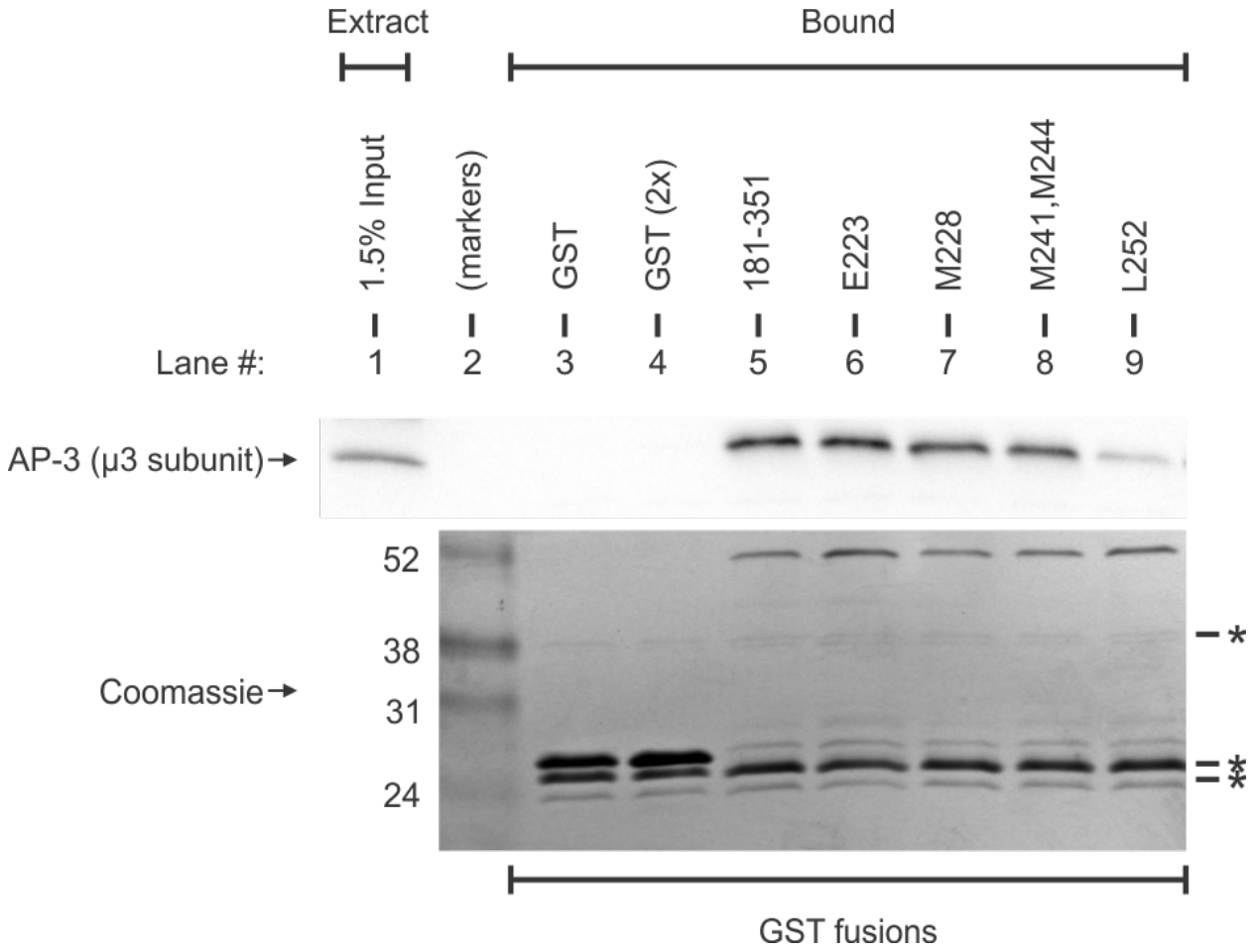

Figure 6.5 Site-directed mutagenesis of conserved dysbindin residues between 181-258 in human, mouse, cattle, and frog, but not in dysbindin paralogs. Conserved residues were mutated into alanine in GST-dysbindin fragments (181-351). GST-fusion proteins with mutations were purified, rebound to glutathione-Sepharose 4 Fast-Flow beads, and incubated with bovine brain cytosol. Beads were washed, and bound proteins were denatured by heating in the presence of SDS and analyzed by SDS-PAGE. AP-3 bound to the GST-fusion proteins was detected by immunoblot analysis using an antibody to its μ3 subunit. GST-fusion proteins bound to the beads were detected by Coomassie staining. Notice that all the GST-dysbindin fragments with mutations were able to bind AP-3 (lanes 6-9), but one had decreased binding to AP-3 (lane 9). *proteins from the bovine brain cytosol with affinity to the beads.

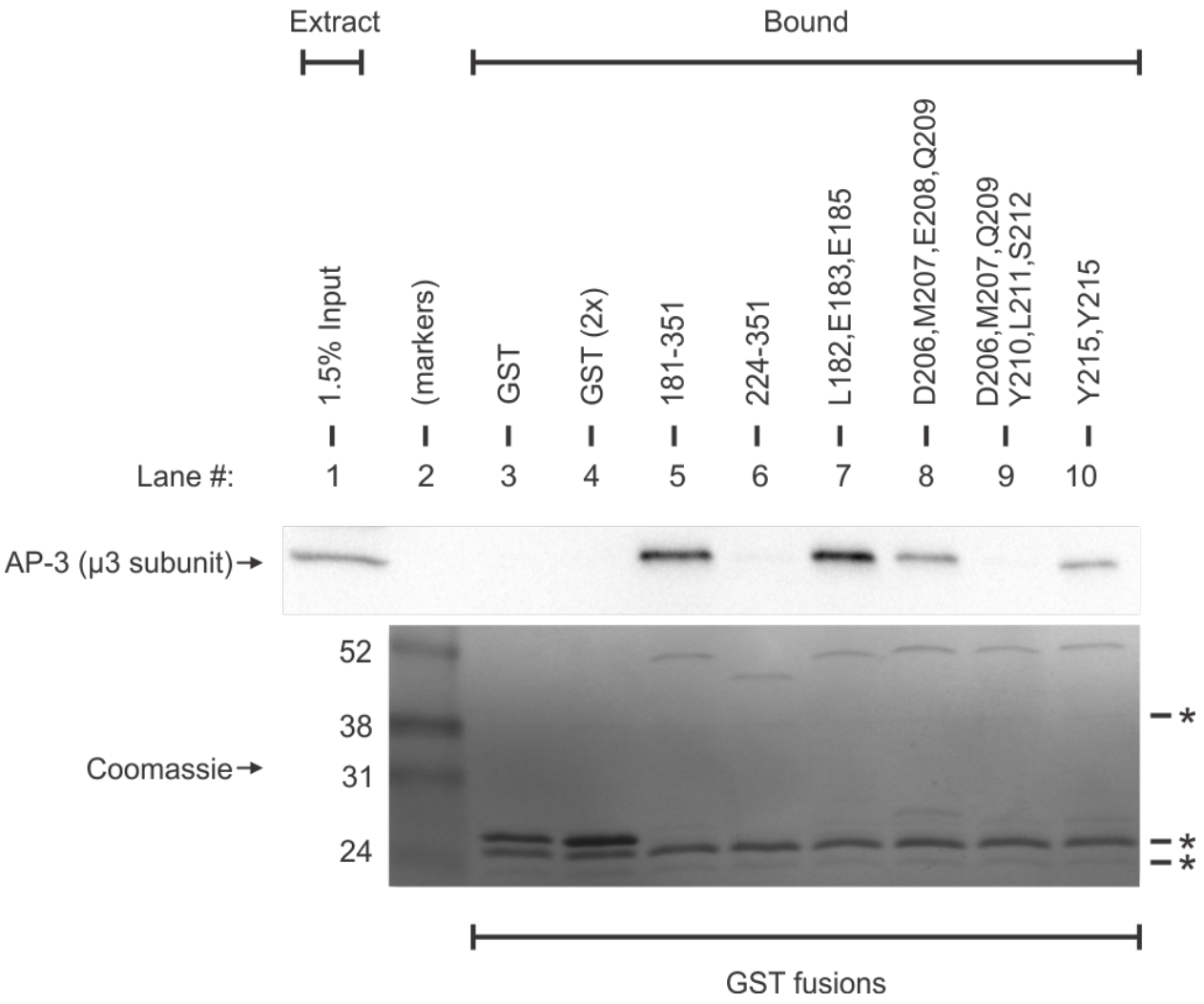

Figure 6.6 Site-directed mutagenesis of dysbindin residues 181-258 conserved in mammals. Conserved residues were mutated into alanine in GST-dysbindin fragments (181-351). GST-fusion proteins were purified, rebound to glutathione-Sepharose 4 Fast-Flow beads, and incubated with bovine brain cytosol. Beads were washed, and bound proteins were denatured by heating in the presence of SDS and analyzed by SDS-PAGE. AP-3 bound to the GST-fusion proteins was detected by immunoblot analysis using an antibody to its μ3 subunit. GST-fusion proteins bound to the beads were detected by Coomassie staining. Notice that the GST-dysbindin fragment in lane 9 did not bind AP-3 and the GST-dysbindin fragments in lanes 8 and 10 had decreased binding to AP-3.*proteins from the bovine brain cytosol with affinity to the beads.

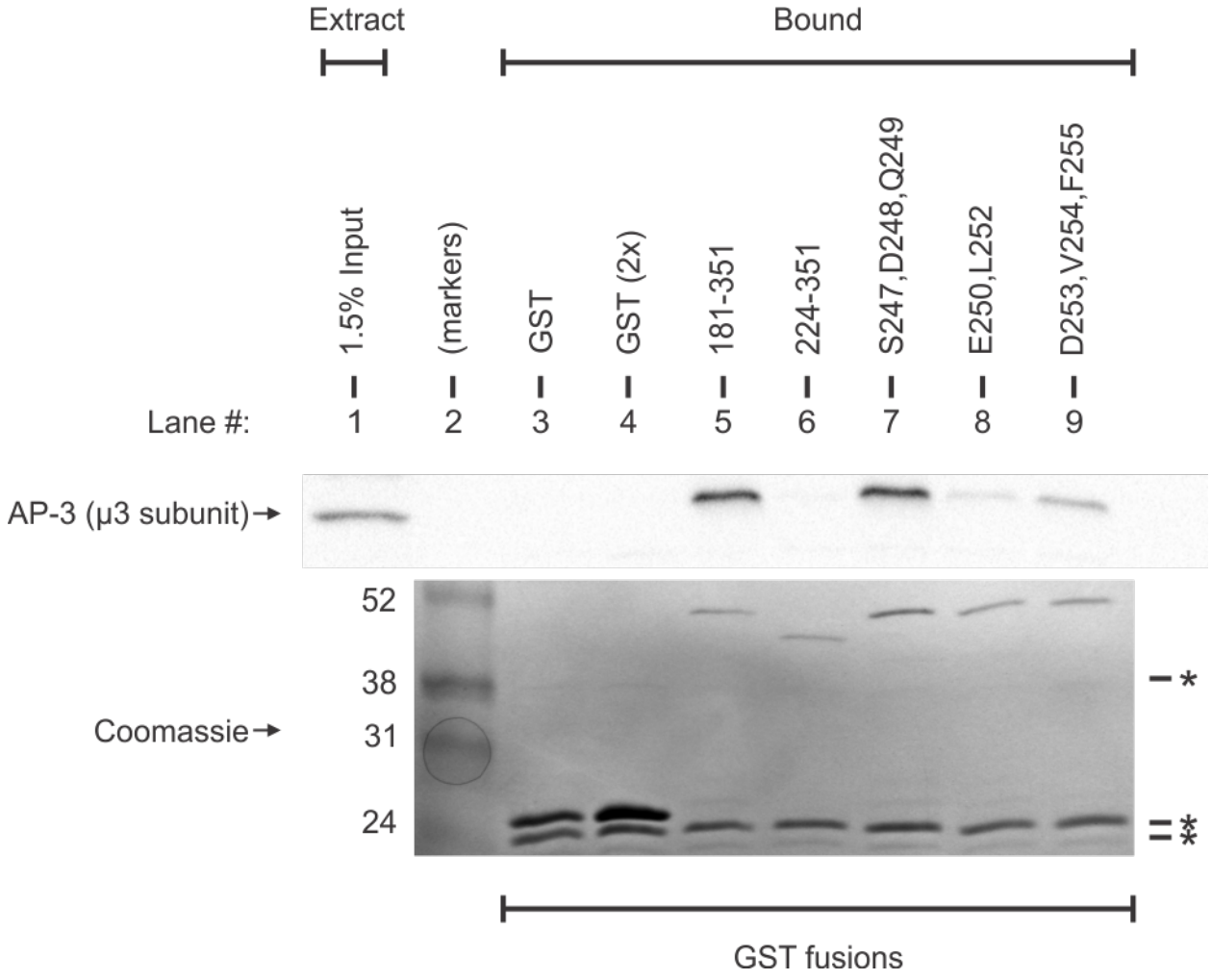

Figure 6.7 Site-directed mutagenesis of dysbindin residues 181-258 conserved in mammals. Conserved residues were mutated into alanine in GST-dysbindin fragments (181-351). GST-fusion proteins were purified, rebound to glutathione-Sepharose 4 Fast-Flow beads, and incubated with bovine brain cytosol. Beads were washed, and bound proteins were denatured by heating in the presence of SDS and analyzed by SDS-PAGE. AP-3 bound to the GST-fusion proteins was detected by immunoblot analysis using an antibody to its μ3 subunit. GST-fusion proteins bound to the beads were detected by Coomassie staining. Notice that the GST-dysbindin fragments in lanes 8 and 9 had decreased binding to AP-3. *proteins from the bovine brain cytosol with affinity to the beads.

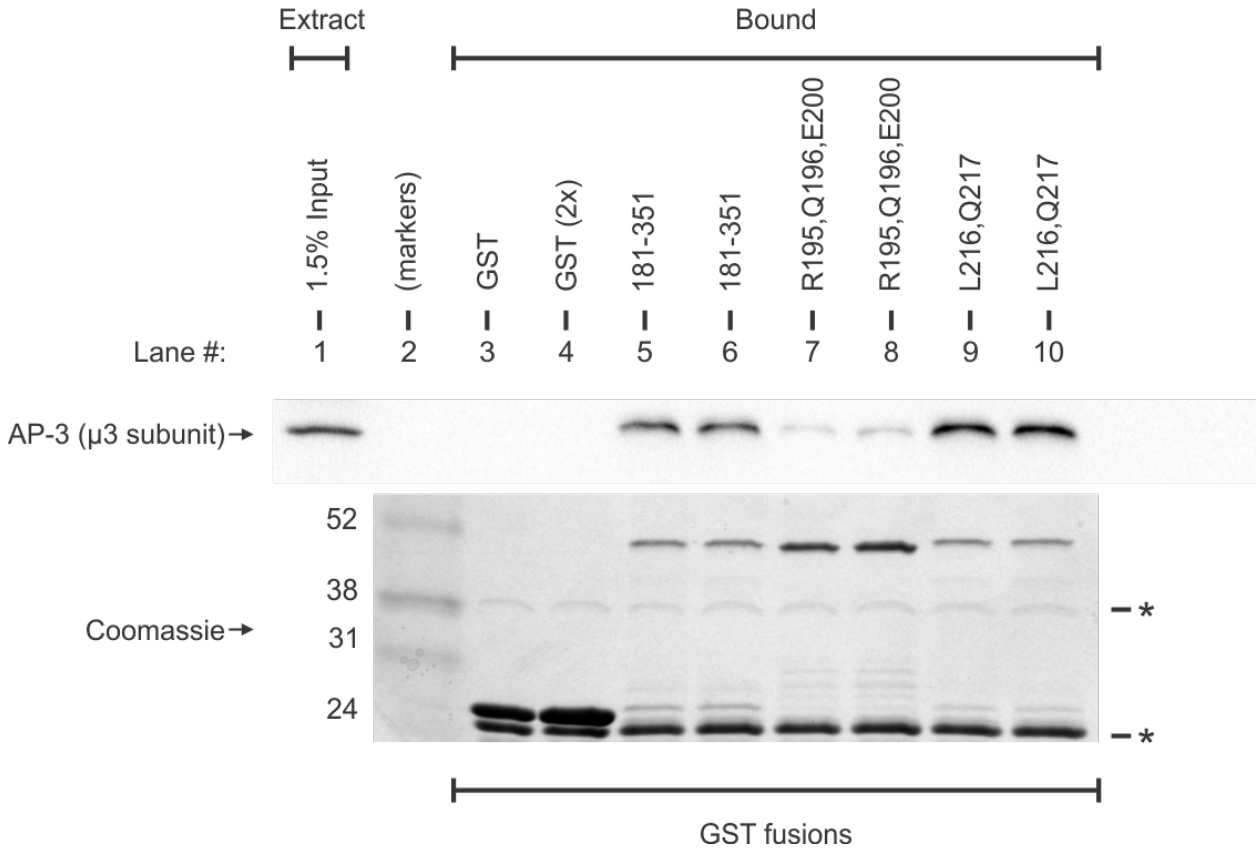

Figure 6.8 Site-directed mutagenesis of dysbindin residues 181-258 conserved in mammals. Conserved residues were mutated into alanine in GST-dysbindin fragments (181-351). GST-fusion proteins were purified, rebound to glutathione-Sepharose 4 Fast-Flow beads, and incubated with bovine brain cytosol. Beads were washed, and bound proteins were denatured by heating in the presence of SDS and analyzed by SDS-PAGE. AP-3 bound to the GST-fusion proteins was detected by immunoblot analysis using an antibody to its μ3 subunit. GST-fusion proteins bound to the beads were detected by Coomassie staining. Notice that in lanes 7 and 8 are replicates of the same GST-dysbindin fragments, which had decreased binding to AP-3. *proteins from the bovine brain cytosol with affinity to the beads.

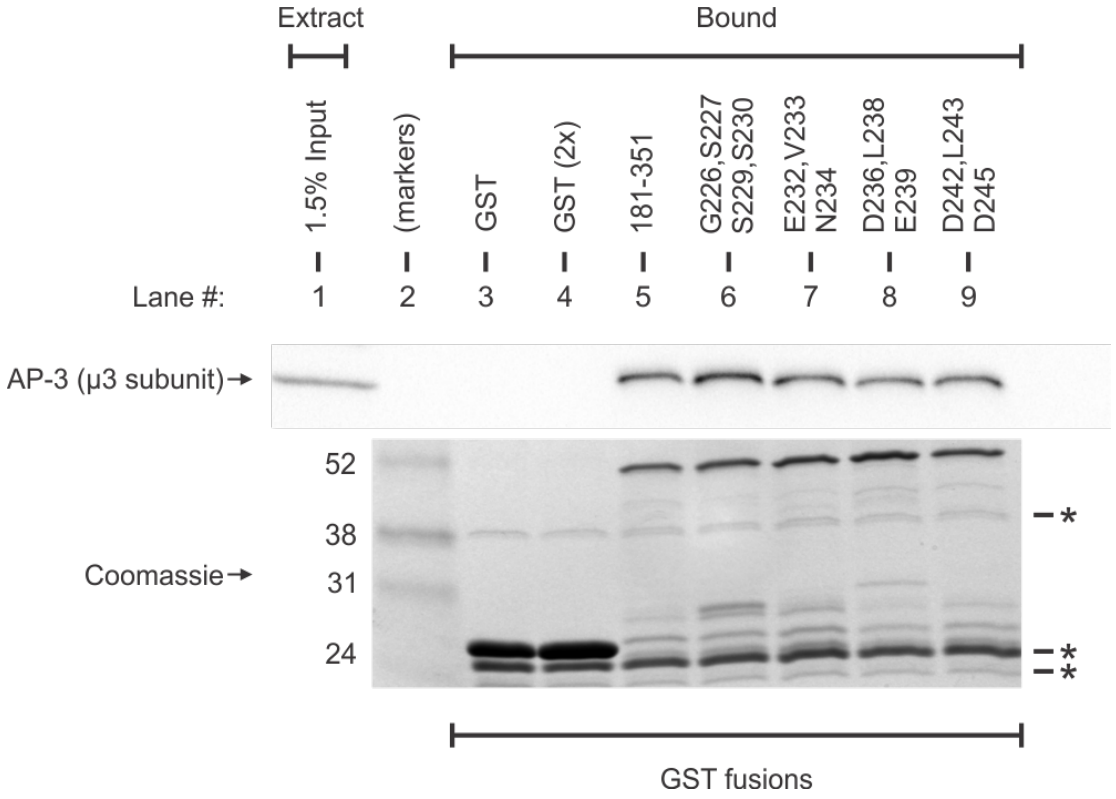

Figure 6.9 Site-directed mutagenesis of dysbindin residues 181-258 conserved in mammals. Conserved residues were mutated into alanine in GST-dysbindin fragments (181-351). GST-fusion proteins were purified, rebound to glutathione-Sepharose 4 Fast-Flow beads, and incubated with bovine brain cytosol. Beads were washed, and bound proteins were denatured by heating in the presence of SDS and analyzed by SDS-PAGE. AP-3 bound to the GST-fusion proteins was detected by immunoblot analysis using an antibody to its μ3 subunit. GST-fusion proteins bound to the beads were detected by Coomassie staining. Notice that the GST-dysbindin fragment in lanes 6-9 all bound AP-3. *proteins from the bovine brain cytosol with affinity to the beads.

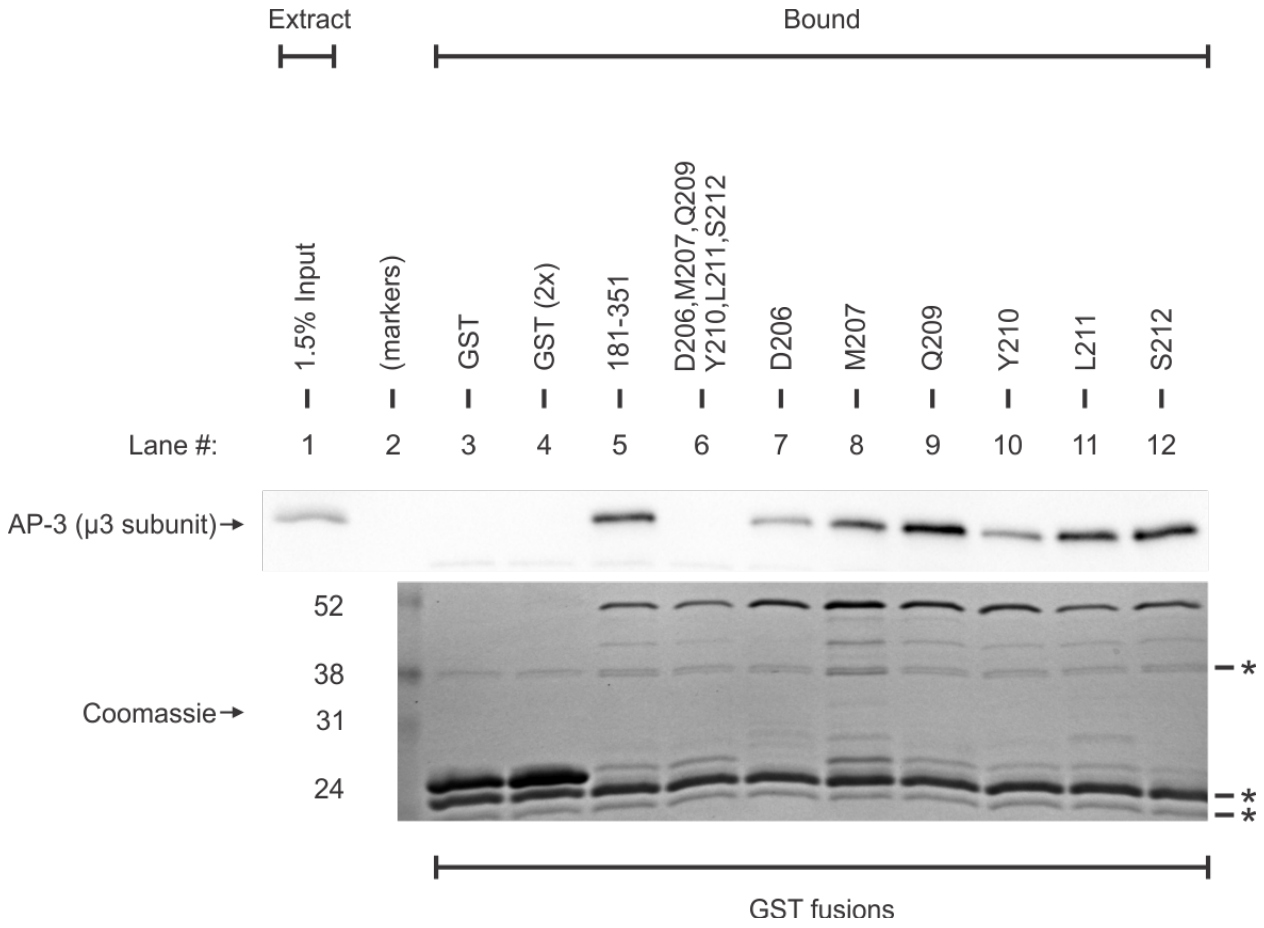

Figure 6.10 Site-directed mutagenesis of individual residues mutated in the GST-fragment that did not bind AP-3. Residues were mutated into alanine in GST-dysbindin fragments (181-351). GST-fusion proteins were purified, rebound to glutathione-Sepharose 4 Fast-Flow beads, and incubated with bovine brain cytosol. Beads were washed, and bound proteins were denatured by heating in the presence of SDS and analyzed by SDS-PAGE. AP-3 bound to the GST-fusion proteins was detected by immunoblot analysis using an antibody to its μ3 subunit. GST-fusion proteins bound to the beads were detected by Coomassie staining. The GST-dysbindin fragment in lane 6 is the same fragment that did not bind in Figure 6.6, lane 9. Notice that the GST-dysbindin fragments in lanes 7-12 did not have disrupted binding to AP-3. *proteins from the bovine brain cytosol with affinity to the beads.

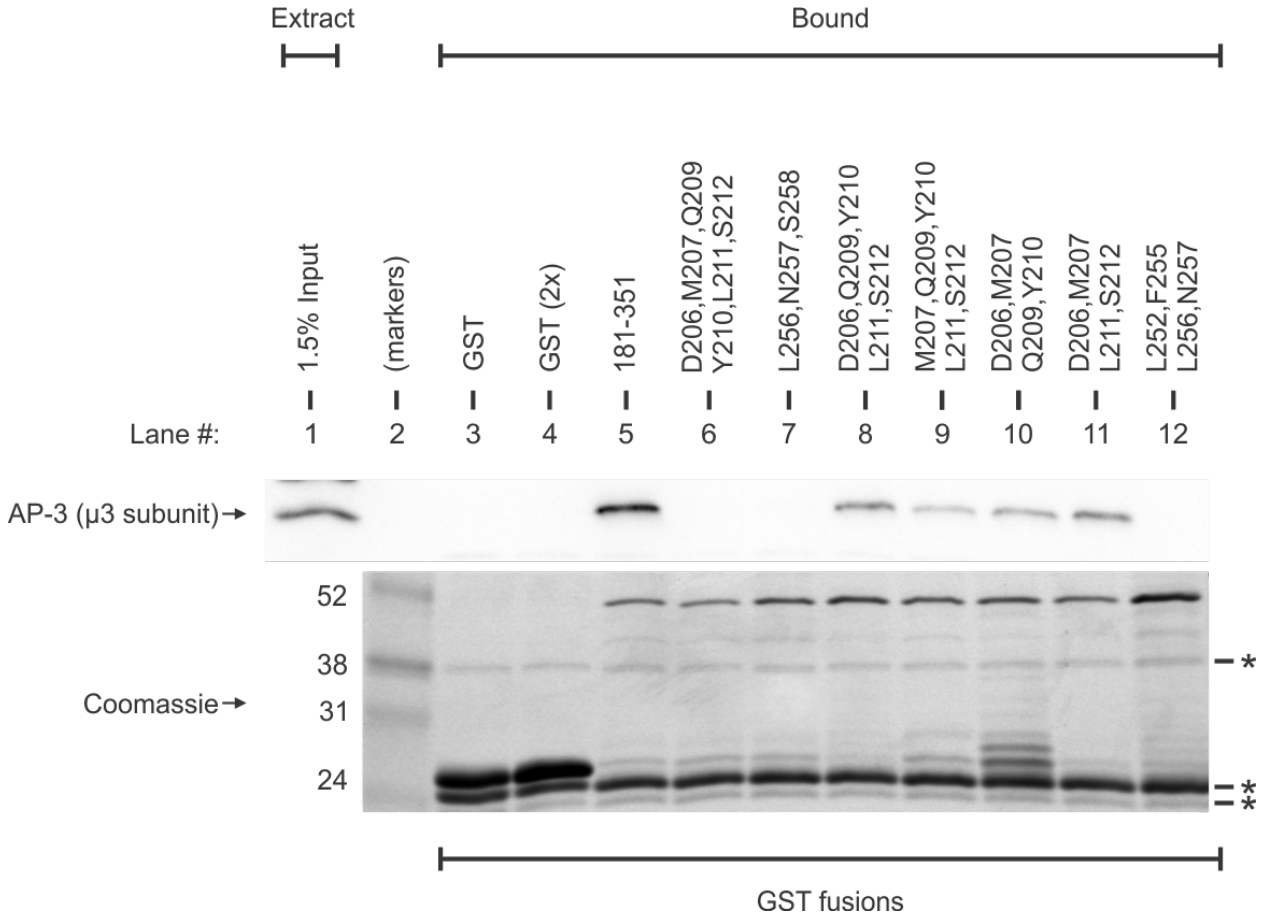

Figure 6.11 Site-directed mutagenesis of residues in the GST-fragment 181-258. Conserved residues were mutated into alanine in GST-dysbindin fragments (181-351). GST-fusion proteins were purified, rebound to glutathione-Sepharose 4 Fast-Flow beads, and incubated with bovine brain cytosol. Beads were washed, and bound proteins were denatured by heating in the presence of SDS and analyzed by SDS-PAGE. AP-3 bound to the GST-fusion proteins was detected by immunoblot analysis using an antibody to its μ3 subunit. GST-fusion proteins bound to the beads were detected by Coomassie staining. The GST-dysbindin fragment in lane 6 is the same fragment that did not bind in Figure 6.6, lane 9. Notice the GST-dysbindin fragments in lanes 8-11 had decreased binding to AP-3, while GST-dysbindin fragments in lanes 7 and 12 were not able to bind AP-3.*proteins from the bovine brain cytosol with affinity to the beads.

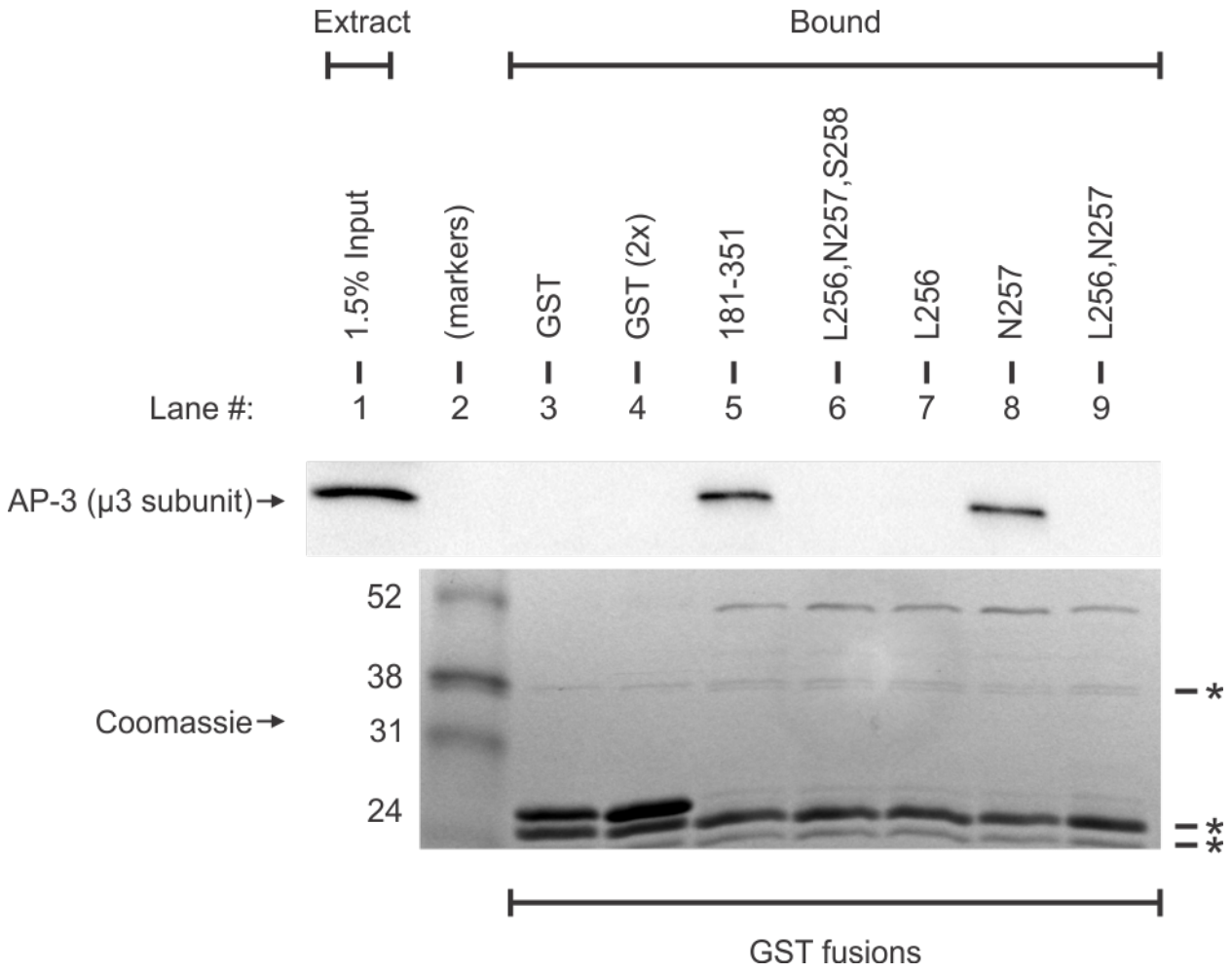

Figure 6.12 Site-directed mutagenesis of residues of GST-fragment 181-258. Residues were mutated into alanine in GST-dysbindin fragments (181-351). GST-fusion proteins were purified, rebound to glutathione-Sepharose 4 Fast-Flow beads, and incubated with bovine brain cytosol. Beads were washed, and bound proteins were denatured by heating in the presence of SDS and analyzed by SDS-PAGE. AP-3 bound to the GST-fusion proteins was detected by immunoblot analysis using an antibody to its μ3 subunit. GST-fusion proteins bound to the beads were detected by Coomassie staining. Notice the GST-dysbindin fragments in lanes 6, 7, and 9 were not able to bind AP-3 and all have a mutation in the leucine 256 residue. *proteins from the bovine brain cytosol with affinity to the beads.

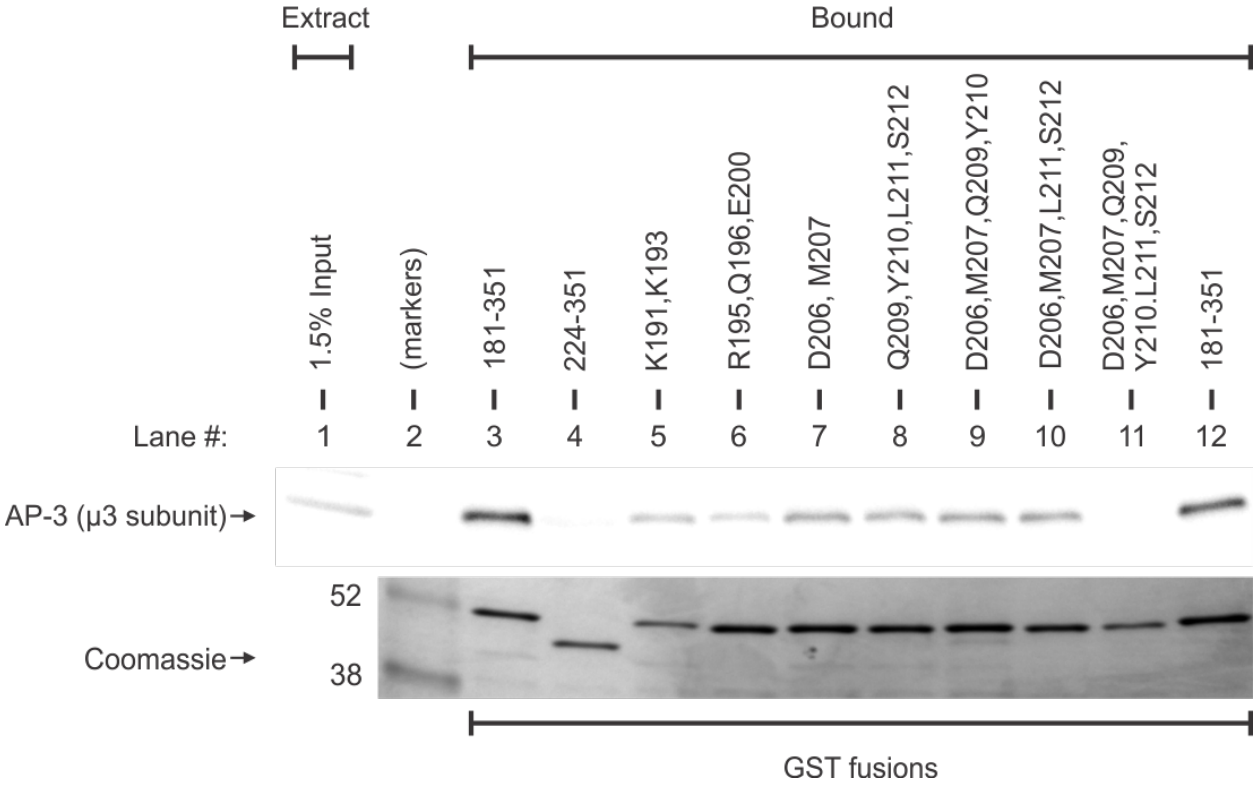

Figure 6.13 Summary of the critical residues of dysbindin fragment 181-258. GST-dysbindin fragments with mutations in the N-terminal were reanalyzed. Previously purified GST-dysbindin fragments were rebound to glutathione-Sepharose 4 Fast-Flow beads, and incubated with bovine brain cytosol. Beads were washed, and bound proteins were denatured by heating in the presence of SDS and analyzed by SDS-PAGE. AP-3 bound to the GST-fusion proteins was detected by immunoblot analysis using an antibody to its μ3 subunit. GST-fusion proteins bound to the beads were detected by Coomassie staining. Notice that the GST-dysbindin fragments in lanes 5-10 had reduced binding to AP-3 and the GST-dysbindin fragment in lane 11 was not able to bind AP-3.

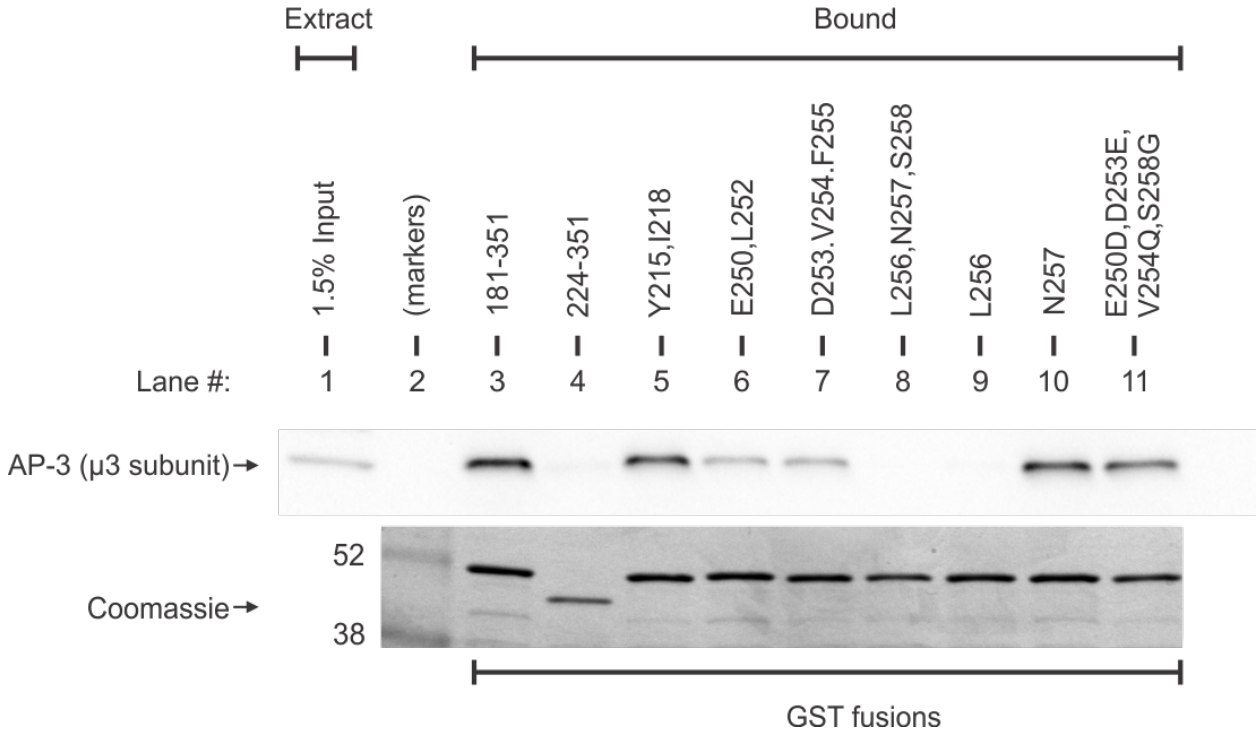

Figure 6.14 Summary of the critical residue of dysbindin fragment 181-258. GST-dysbindin fragments with mutations in the C-terminal were reanalyzed. Previously purified GST-dysbindin fragments were rebound to glutathione-Sepharose 4 Fast-Flow beads, and incubated with bovine brain cytosol. Beads were washed, and bound proteins were denatured by heating in the presence of SDS and analyzed by SDS-PAGE. AP-3 bound to the GST-fusion proteins was detected by immunoblot analysis using an antibody to its μ3 subunit. GST-fusion proteins bound to the beads were detected by Coomassie staining. Notice that the GST-dysbindin fragments in lanes 8 and 9 were not able to bind AP-3 and have a mutation in the leucine 256 residue.

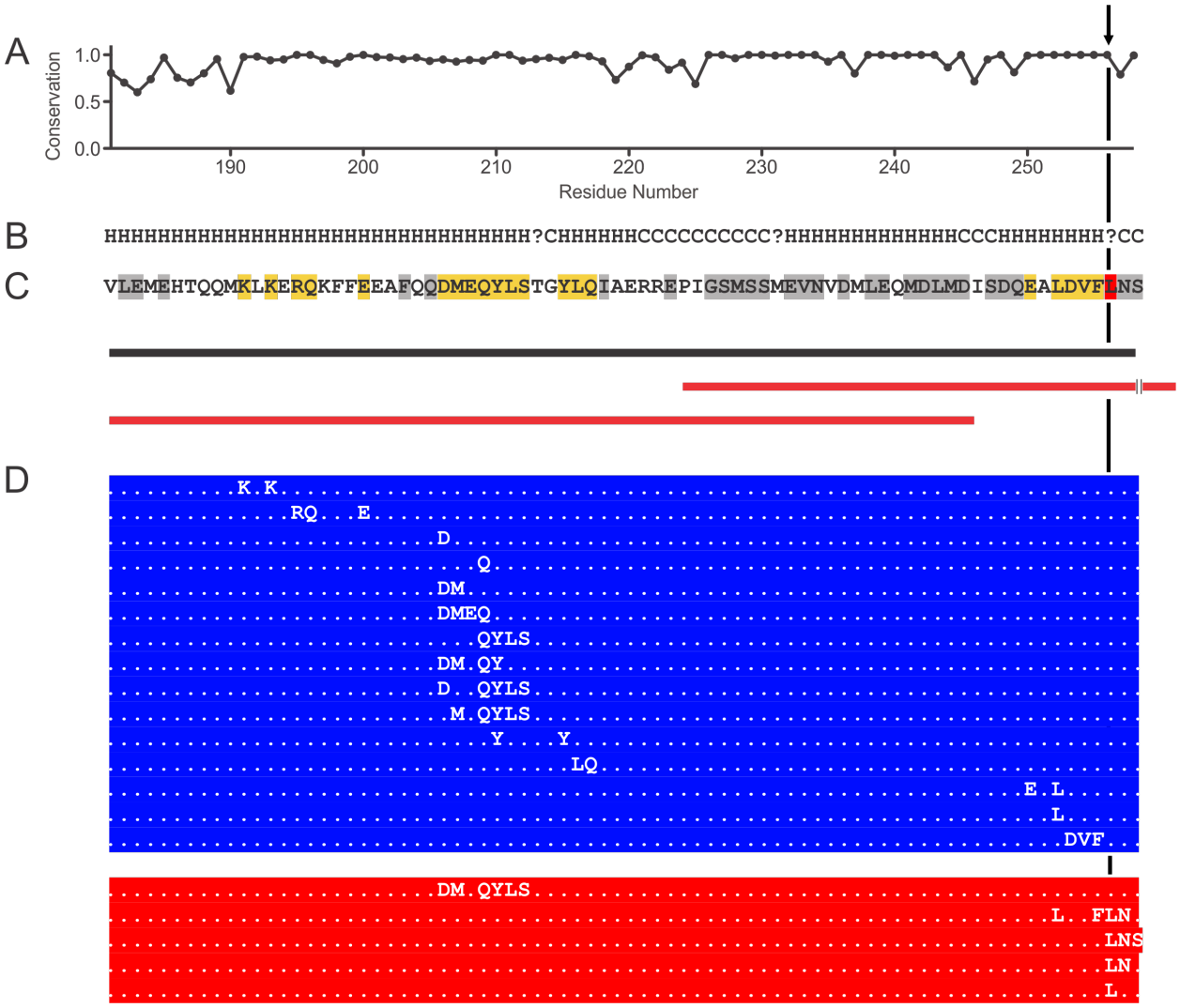

Figure 6.15 Analysis of the dysbindin residues 181-258 and summary of the scanning alanine mutagenesis analysis. (A) Sequence conservation levels of the dysbindin residues 181-258 across mammals. The degree of conservation was calculated as described in Experimental Procedures. (B) The predicted secondary structure of dysbindin residues 181-258. H, Helix. C, coil. ?, undetermined. (C) Summary of the scanning alanine mutagenesis analysis of dysbindin residues 181-258. Letters highlighted in grey represent residues unimportant for binding to AP-3. Letters highlighted in yellow represent residues that affected binding to AP-3, but were not critical. The letter highlighted in red represents the critical residue that when mutated had no binding to AP-3. The letters not highlighted were not tested. The black bar represents the GST-dysbindin fragment (181-258) that is able to bind AP-3. The first red bar represents the GST-dysbindin fragment (224-351) and the second red bar represents the GST-dysbindin fragment (181-246), both of which were not able to bind AP-3. (D) Schematic of constructs that had decreased binding to AP-3 (Blue) or no binding to AP-3 (Red). Dots represent no mutation. Letters present the residues that were mutated into alanine.

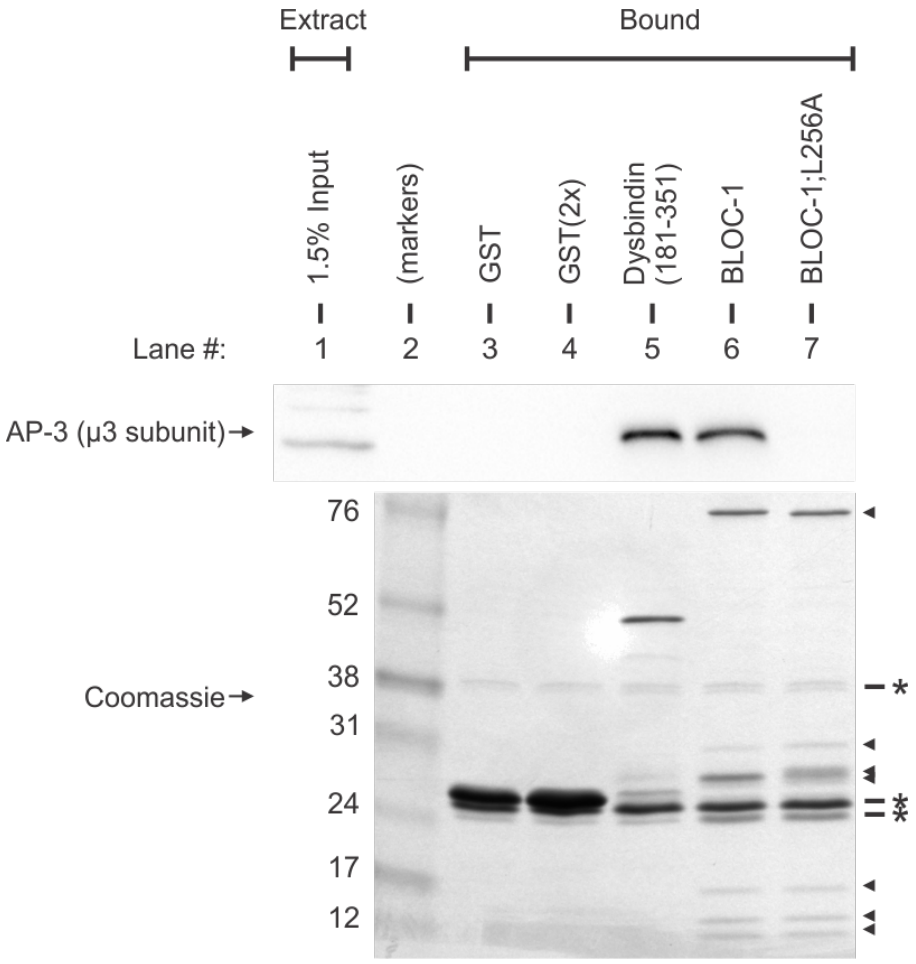

Figure 6.16 Alanine mutagenesis of leucine (residue 256) in recombinant BLOC-1. The leucine residue (256) was mutated to an alanine in the dysbindin subunit of recombinant BLOC-1. Tandem purified recombinant BLOC-1 was rebound to glutathione-Sepharose 4 Fast-Flow beads, and incubated with bovine brain cytosol. Washed beads were denatured by heating in the presence of SDS and analyzed by SDS-PAGE. AP-3 bound to the GST-fusion proteins was detected by immunoblot analysis using an antibody to its μ3 subunits. Proteins bound to the GST beads were detected by Coomassie staining. The subunits of BLOC-1 were detected by Coomassie staining (arrowheads). Notice that the mutated recombinant BLOC-1 in lane 7 was not able to bind AP-3. *proteins from the bovine brain cytosol with affinity to the beads.

REFERENCES

1. Dell'Angelica EC. AP-3-dependent trafficking and disease: the first decade. Curr Opin Cell Biol. 2009 Aug;21(4):552-9.
2. Newell-Litwa K, Seong E, Burmeister M, Faundez V. Neuronal and non-neuronal functions of the AP-3 sorting machinery. J Cell Sci. 2007 Feb 15;120(Pt 4):531-41.
3. Di Pietro SM, Falcón-Pérez JM, Tenza D, Setty SR, Marks MS, Raposo G, Dell'Angelica EC. BLOC-1 interacts with BLOC-2 and the AP-3 complex to facilitate protein trafficking on endosomes. Mol Biol Cell. 2006 Sep;17(9):4027-38.
4. Salazar G, Zlatic S, Craige B, Peden AA, Pohl J, Faundez V. Hermansky-Pudlak syndrome protein complexes associate with phosphatidylinositol 4-kinase type II alpha in neuronal and non-neuronal cells. J Biol Chem. 2009 Jan 16;284(3):1790-802.
5. Mead CL, Kuzyk MA, Moradian A, Wilson GM, Holt RA, Morin GB. Cytosolic protein interactions of the schizophrenia susceptibility gene dysbindin. J Neurochem. 2010 Jun; 113(6):1491-503.
6. Taneichi-Kuroda S, Taya S, Hikita T, Fujino Y, Kaibuchi K. Direct interaction of Dysbindin with the AP-3 complex via its mu subunit. Neurochem Int. 2009 Jun;54(7):431-8.
7. Han MH, Hu Z, Chen CY, Chen Y, Gucek M, Li Z, Markey SP. Dysbindin-associated proteome in the p2 synaptosome fraction of mouse brain. J Proteome Res. 2014 Nov 7;13(11):4567-80.
8. Li W, Zhang Q, Oiso N, Novak EK, Gautam R, O'Brien EP, Tinsley CL, Blake DJ, Spritz RA, Copeland NG, Jenkins NA, Amato D, Roe BA, Starcevic M, Dell'Angelica EC, Elliott RW, Mishra V, Kingsmore SF, Paylor RE, Swank RT. Hermansky-Pudlak syndrome type 7

(HPS-7) results from mutant dysbindin, a member of the biogenesis of lysosome-related organelles complex 1 (BLOC-1). Nat Genet. 2003 Sep;35(1):84-9.

9. Morgan NV, Pasha S, Johnson CA, Ainsworth JR, Eady RA, Dawood B, McKeown C, Trembath RC, Wilde J, Watson SP, Maher ER. A germline mutation in BLOC1S3/reduced pigmentation causes a novel variant of Hermansky-Pudlak syndrome (HPS8). Am J Hum Genet. 2006 Jan;78(1):160-6.
10. Cullinane AR, Curry JA, Carmona-Rivera C, Summers CG, Ciccone C, Cardillo ND, Dorward H, Hess RA, White JG, Adams D, Huizing M, Gahl WA. A BLOC-1 mutation screen reveals that PLDN is mutated in Hermansky-Pudlak Syndrome type 9. Am J Hum Genet. 2011 Jun 10;88(6):778-87.
11. Lowe GC, Sánchez Guiu I, Chapman O, Rivera J, Lordkipanidzé M, Dovlatova N, Wilde J, Watson SP, Morgan NV; UK GAPP collaborative.. Microsatellite markers as a rapid approach for autozygosity mapping in Hermansky-Pudlak syndrome: identification of the second HPS7 mutation in a patient presenting late in life. Thromb Haemost. 2013 Apr; 109(4):766-8.
12. Dell'Angelica EC, Shotelersuk V, Aguilar RC, Gahl WA, Bonifacino JS. Altered trafficking of lysosomal proteins in Hermansky-Pudlak syndrome due to mutations in the β3A subunit of the AP-3 adaptor. Mol Cell. 1999 Jan;3(1):11-21.
13. Shotelersuk V, Dell'Angelica EC, Hartnell L, Bonifacino JS, Gahl WA. A new variant of Hermansky-Pudlak syndrome due to mutations in a gene responsible for vesicle formation. Am J Med. 2000 Apr 1;108(5):423-7.

14. Li W, Rusiniak ME, Chintala S, Gautam R, Novak EK, Swank RT. Murine Hermansky-Pudlak syndrome genes: regulators of lysosome-related organelles. Bioessays. 2004 Jun; 26(6):616-28.
15. Kalthoff C, Groos S, Kohl R, Mahrhold S, Ungewickell EJ. Clint: a novel clathrin-binding ENTH-domain protein at the Golgi. Mol Biol Cell. 2002 Nov;13(11):4060-73.
16. Duncan MC, Costaguta G, Payne GS. Yeast epsin-related proteins required for Golgi-endosome traffic define a gamma-adaptin ear-binding motif. Nat Cell Biol. 2003 Jan;5(1): 77-81. Erratum in: Nat Cell Biol. 2003 Mar;5(3):264.
17. Miller GJ, Mattera R, Bonifacino JS, Hurley JH. Recognition of accessory protein motifs by the gamma-adaptin ear domain of GGA3. Nat Struct Biol. 2003 Aug;10(8):599-606.
18. Wasiak S, Denisov AY, Han Z, Leventis PA, de Heuvel E, Boulianne GL, Kay BK, Gehring K, McPherson PS. Characterization of a gamma-adaptin ear-binding motif in enthoprotin. FEBS Lett. 2003 Dec 18;555(3):437-42.
19. Ritter B, Denisov AY, Philie J, Deprez C, Tung EC, Gehring K, McPherson PS. Two WXXF-based motifs in NECAPs define the specificity of accessory protein binding to AP-1 and AP-2. EMBO J. 2004 Oct 1;23(19):3701-10.
20. Owen DJ, Vallis Y, Noble ME, Hunter JB, Dafforn TR, Evans PR, McMahon HT. A structural explanation for the binding of multiple ligands by the alpha-adaptin appendage domain. Cell. 1999 Jun 11;97(6):805-15.
21. Brett TJ, Traub LM, Fremont DH. Accessory protein recruitment motifs in clathrin-mediated endocytosis. Structure. 2002 Jun;10(6):797-809.

22. Jha A, Agostinelli NR, Mishra SK, Keyel PA, Hawryluk MJ, Traub LM. A novel AP-2 adaptor interaction motif initially identified in the long-splice isoform of synaptojanin 1, SJ170. J Biol Chem. 2004 Jan 16;279(3):2281-90.
23. Mattera R, Guardia CM, Sidhu SS, Bonifacino JS. Bivalent Motif-Ear Interactions Mediate the Association of the Accessory Protein Tepsin with the AP-4 Adaptor Complex. J Biol Chem. 2015 Dec 25;290(52):30736-49.
24. Frazier MN, Davies AK, Voehler M, Kendall AK, Borner GH, Chazin WJ, Robinson MS, Jackson LP. Molecular Basis for the Interaction Between AP4 β4 and its Accessory Protein, Tepsin. Traffic. 2016 Apr;17(4):400-15.
25. Bonifacino JS, Dell'Angelica EC. Molecular bases for the recognition of tyrosine-based sorting signals. J Cell Biol. 1999 May 31;145(5):923-6.
26. Valdar WS. Scoring residue conservation. Proteins. 2002 Aug 1;48(2):227-41.

Chapter 7

CONCLUSIONS

The overall goal of this dissertation was to characterize the possible function(s) of BLOC-1 in the mouse brain (discussed in Chapters 2, 3, and 4) and the interaction with alternative subunit(s) as well as with other similar complexes *in vitro* (discussed in Chapters 4, and 5).

Studies investigating BLOC-1 function in brain have thus far focused on its role in an otherwise normally developed brain. However, my results discussed in Chapters 2 and 3 suggest that BLOC-1-deficient mice present with subtle defects during brain development. I have found that, in these mice, the cell bodies of CA1 hippocampal neurons appeared less compacted and uncharacteristically distributed compared to wild-type mice. By postnatal day 45 this malformation was no longer present, suggesting a delay in this brain area development, which might have profound ramifications in hippocampal adult functions. In a normally developing hippocampus, CA1 develops first and is important that this process occurs in a proper manner, as it will, in turn, influence the development of other hippocampal regions such as the dentate gyrus. I would like to speculate that this early defect elicited by lack of BLOC-1 may prevent the proper delivery of those signals from CA1 necessary for proper development of the dentate gyrus, resulting in the observed defects in dendritic arborization of granule cells. In the long term, such maldevelopment might be the underlie cause of the behavioral abnormalities observed in BLOC-1-deficient mice, particularly the memory defect(s) [1]. Electrophysiological experiments to assess the hippocampal circuit(s) are required to further characterize how this developmental delay affects the internal wiring of the hippocampus as well as its communication with other brain areas.

Sexual dimorphism of the brain is well characterized, but the exact mechanism(s) of these differences is still under investigation. My analysis of the BLOC-1-deficient mice has shown that there are sex differences in these mice whereby female mice appeared to be "protected" from the effects of BLOC-1 deficiency on the brain early postnatal development. As I was completing the experimental work for this dissertation, a paper characterizing another BLOC-1-deficient mouse model reported that an important developmental change in the subunit composition of the N-methyl-D-aspartate (NMDA) receptor was disrupted in the hippocampus of male mice, but not female mice [2], further providing evidence of the females being protected from some of the consequences of BLOC-1 deficiency. Most sex differences in physiology and disease are regulated by sex hormones secreted by the gonads (reviewed in [3]). However, some of the genes on the sex chromosomes independent of the gonads can also cause some sex differences, particularly during development before the emergence of sex-specific patterns from sex hormones (reviewed in [4]). To determine whether the "protective" effects seen in BLOC-1-deficient females derives from the sex hormones or genes on the sex chromosomes, we could consider crossing the BLOC-1-deficient mice with the four-core genotype (FCG) model (reviewed in [54]). There are two critical genetic components in the FCG model: the first is a deletion of the testis-determining gene *Sry* on the Y chromosome [6]; the second is an insertion of the *Sry* transgene onto an autosomal chromosome making the mouse a 'gonadal male' [7]. This model allows XX and XY mice to be gonadal females and males. These manipulations allow for the production of four genotypes: the first two are a XY male, a normal male mouse, and a XY female, which has the deletion in the *Sry* gene making the mouse gonadal female; the second two are a XX female, a normal female mouse, and a XX male, which has the insertion of

the *Sry* transgene making the mouse gonadal male. This cross can be used to isolate the gonadal-determined effects from those due to the sex chromosomes.

Initial studies on dysbindin functions(s) in the brain were largely focused on its role in neurons, in part based on an early paper describing a neuronal-specific expression of dysbindin in human brain [8]. However, other studies have shown that dysbindin, and as extension BLOC-1, is also expressed in glial cells [9,10]; in particular, dysbindin has been found highly enriched in Müller cells [11], which are a subtype of radial glia specifically found in the retina. One of the abnormalities I have observed in the BLOC-1-deficient male brains at P1 was a clear disruption of the radial glial cell processes, which likely caused the anomalous cell distribution observed in the hippocampal cell layer. It appears that BLOC-1 may play an important physiological role in glial cells, not just in neurons, which deserves to be further examined.

In Chapters 4, I reported deficits in the dendritic processes of granule cells in the BLOC-1-deficient dentate gyrus. Similarly, previous work in our lab as well as others [9,12] showed deficits in neurite outgrowth in primary cultures of BLOC-1-deficient hippocampal neurons. These findings altogether strongly suggest a role of BLOC-1 in process elongation. However, the mechanism by which lack of BLOC-1 affects the development of these processes is still largely unknown. Recently, BLOC-1 has been shown to play a role in the formation of recycling endosomes, which diverts cargoes towards the cell surface [13]. It is possible that in certain hippocampal cell types, BLOC-1 is involved in the formation of recycling endosomes that carry small GTPases, such as Rab10 and Rab11, which have been reported to play a role in dendritic arborization [14,15]. Furthermore, in a study that used a data-mining approach to rank

candidate protein-binding partners of BLOC-1, it was reported that Rab11 might be a top candidate among 68 potential binding proteins [16].

Alternatively spliced forms of dysbindin have been reported, and as shown in Chapter 5, the alternatively spliced variant dysbindin isoform B was able to replace the full-length form and assemble into a complex with the other BLOC-1 subunits. The exact biological function of this complex that contains dysbindin isoform B is unclear. Although it is possible that dysbindin isoform B may be able to compensate for the absence of the full-length form of dysbindin, it cannot be ruled out that BLOC-1 with dysbindin isoform B may have novel function(s). The second isoform, dysbindin isoform C, on the other had, was unable to replace the full-length form and assemble into a complex with the other BLOC-1 subunits. At this point, it is still unknown whether dysbindin isoform C even has a biological function independent of BLOC-1. Thus, more work is required to understand the function of these alternatively splice variants. However, it is clear that future studies of dysbindin should take into consideration these alternatively splice variants when interpreting the results.

As mentioned in Chapter 6, binding motifs have been characterized for AP-1 [17-21], AP-2 [21-24], and AP-4 [25,26], where as no binding motif has been identified for AP-3. In an attempt to discover a motif for AP-3, I identified the critical residues for binding between AP-3 and BLOC-1. As described in Chapter 6, I have found two critical regions for binding, but only one critical residue. As a result, it was impossible to characterize a binding motif for AP-3. The question remains whether all other binding partners of AP-3 interact with AP-3 through these two critical regions like BLOC-1, or this method of interaction is unique to BLOC-1. To address this question, the critical residues of other AP-3 binding partners should be analyzed.

REFERENCES

1. Spiegel S, Chiu A, James AS, Jentsch JD, Karlsgodt KH. Recognition deficits in mice carrying mutations of genes encoding BLOC-1 subunits pallidin or dysbindin. Genes Brain Behav. 2015 Nov;14(8):618-24.
2. Sinclair D, Cesare J, McMullen M, Carlson GC, Hahn CG, Borgmann-Winter KE. Effects of sex and DTNBP1 (dysbindin) null gene mutation on the developmental GluN2B-GluN2A switch in the mouse cortex and hippocampus. J Neurodev Disord. 2016 May 1;8:14.
3. Morris JA, Jordan CL, Breedlove SM. Sexual differentiation of the vertebrate nervous system. Nat Neurosci. 2004 Oct;7(10):1034-9.
4. Arnold AP, Rissman EF, De Vries GJ. Two perspectives on the origin of sex differences in the brain. Ann N Y Acad Sci. 2003 Dec;1007:176-88.
5. Arnold AP, Chen X. What does the "four core genotypes" mouse model tell us about sex differences in the brain and other tissues? Front Neuroendocrinol. 2009 Jan;30(1):1-9.
6. Lovell-Badge R, Robertson E. XY female mice resulting from a heritable mutation in the primary testis-determining gene, Tdy. Development. 1990 Jul;109(3):635-46.
7. Mahadevaiah SK, Odorisio T, Elliott DJ, Rattigan A, Szot M, Laval SH, Washburn LL, McCarrey JR, Cattanach BM, Lovell-Badge R, Burgoyne PS. Mouse homologues of the human AZF candidate gene RBM are expressed in spermatogonia and spermatids, and map to a Y chromosome deletion interval associated with a high incidence of sperm abnormalities. Hum Mol Genet. 1998 Apr;7(4):715-27.

8. Talbot K, Eidem WL, Tinsley CL, Benson MA, Thompson EW, Smith RJ, Hahn CG, Siegel SJ, Trojanowski JQ, Gur RE, Blake DJ, Arnold SE. Dysbindin-1 is reduced in intrinsic, glutamatergic terminals of the hippocampal formation in schizophrenia. J Clin Invest. 2004 May;113(9):1353-63.
9. Ghiani CA, Starcevic M, Rodriguez-Fernandez IA, Nazarian R, Cheli VT, Chan LN, Malvar JS, de Vellis J, Sabatti C, Dell'Angelica EC. The dysbindin-containing complex (BLOC-1) in brain: developmental regulation, interaction with SNARE proteins and role in neurite outgrowth. Mol Psychiatry. 2010 Feb;15(2):115, 204-15.
10. Iijima S, Masaki H, Wakayama Y, Inoue M, Jimi T, Hara H, Unaki A, Oniki H, Nakano K, Hirayama Y, Kishimoto K. Immunohistochemical detection of dysbindin at the astroglial endfeet around the capillaries of mouse brain. J Mol Histol. 2009 Apr;40(2):117-21.
11. Matteucci A, Gaddini L, Macchia G, Varano M, Petrucci TC, Macioce P, Malchiodi-Albedi F, Ceccarini M. Developmental expression of dysbindin in Muller cells of rat retina. Exp Eye Res. 2013 Nov;116:1-8.
12. Ma X, Fei E, Fu C, Ren H, Wang G. Dysbindin-1, a schizophrenia-related protein, facilitates neurite outgrowth by promoting the transcriptional activity of p53. Mol Psychiatry. 2011 Nov;16(11):1105-16.
13. Delevoye C, Heiligenstein X, Ripoll L, Gilles-Marsens F, Dennis MK, Linares RA, Derman L, Gokhale A, Morel E, Faundez V, Marks MS, Raposo G. BLOC-1 Brings Together the Actin and Microtubule Cytoskeletons to Generate Recycling Endosomes. Curr Biol. 2016 Jan 11;26(1):1-13.

14. Zou W, Yadav S, DeVault L, Nung Jan Y, Sherwood DR. RAB-10-Dependent Membrane Transport Is Required for Dendrite Arborization. PLoS Genet. 2015 Sep 22;11(9):e1005484.
15. Lazo OM, Gonzalez A, Ascaño M, Kuruvilla R, Couve A, Bronfman FC. BDNF regulates Rab11-mediated recycling endosome dynamics to induce dendritic branching. J Neurosci. 2013 Apr 3;33(14):6112-22.
16. Rodriguez-Fernandez IA, Dell'Angelica EC. A data-mining approach to rank candidate protein-binding partners-The case of biogenesis of lysosome-related organelles complex-1 (BLOC-1). J Inherit Metab Dis. 2009 Apr;32(2):190-203.
17. Kalthoff C, Groos S, Kohl R, Mahrhold S, Ungewickell EJ. Clint: a novel clathrin-binding ENTH-domain protein at the Golgi. Mol Biol Cell. 2002 Nov;13(11):4060-73.
18. Duncan MC, Costaguta G, Payne GS. Yeast epsin-related proteins required for Golgi-endosome traffic define a gamma-adaptin ear-binding motif. Nat Cell Biol. 2003 Jan;5(1): 77-81. Erratum in: Nat Cell Biol. 2003 Mar;5(3):264.
19. Miller GJ, Mattera R, Bonifacino JS, Hurley JH. Recognition of accessory protein motifs by the gamma-adaptin ear domain of GGA3. Nat Struct Biol. 2003 Aug;10(8):599-606.
20. Wasiak S, Denisov AY, Han Z, Leventis PA, de Heuvel E, Boulianne GL, Kay BK, Gehring K, McPherson PS. Characterization of a gamma-adaptin ear-binding motif in enthoprotin. FEBS Lett. 2003 Dec 18;555(3):437-42.
21. Ritter B, Denisov AY, Philie J, Deprez C, Tung EC, Gehring K, McPherson PS. Two WXXF-based motifs in NECAPs define the specificity of accessory protein binding to AP-1 and AP-2. EMBO J. 2004 Oct 1;23(19):3701-10.

22. Owen DJ, Vallis Y, Noble ME, Hunter JB, Dafforn TR, Evans PR, McMahon HT. A structural explanation for the binding of multiple ligands by the alpha-adaptin appendage domain. Cell. 1999 Jun 11;97(6):805-15.
23. Brett TJ, Traub LM, Fremont DH. Accessory protein recruitment motifs in clathrin-mediated endocytosis. Structure. 2002 Jun;10(6):797-809.
24. Jha A, Agostinelli NR, Mishra SK, Keyel PA, Hawryluk MJ, Traub LM. A novel AP-2 adaptor interaction motif initially identified in the long-splice isoform of synaptojanin 1, SJ170. J Biol Chem. 2004 Jan 16;279(3):2281-90.
25. Mattera R, Guardia CM, Sidhu SS, Bonifacino JS. Bivalent Motif-Ear Interactions Mediate the Association of the Accessory Protein Tepsin with the AP-4 Adaptor Complex. J Biol Chem. 2015 Dec 25;290(52):30736-49.
26. Frazier MN, Davies AK, Voehler M, Kendall AK, Borner GH, Chazin WJ, Robinson MS, Jackson LP. Molecular Basis for the Interaction Between AP4 β4 and its Accessory Protein, Tepsin. Traffic. 2016 Apr;17(4):400-15.